2021

Noggin Transport in a Model Human Epiblast

Tiên Phan-Everson

NOGGIN TRANSPORT IN A MODEL HUMAN EPIBLAST

A Thesis Presented to the Faculty of
The Rockefeller University
in Partial Fulfillment of the Requirements for
the degree of Doctor of Philosophy

by
Tiên Phan-Everson
June 2021

NOGGIN TRANSPORT IN A MODEL HUMAN EPIBLAST

Tiên Phan-Everson, Ph.D.
The Rockefeller University 2021

Using self-organizing human models of gastrulation, the Brivanlou/Siggia labs previously showed that (i) BMP4 initiates the cascade of events leading to gastrulation; (ii) BMP4 signal-reception is restricted to the basolateral domain; and (iii) in a human-specific manner, BMP4 directly induces the expression of NOGGIN. In this work, I interrogate the interplay of the morphogen/inhibitor pair BMP4/NOGGIN within our model of the polarized human embryonic disc. Here, I report the surprising discovery that in human epiblasts, NOGGIN and BMP4 were selectively secreted into opposite sides of the polarized epithelium, effectively segregating the ligand and its inhibitor into distinct extracellular spaces. Moreover, utilizing a microfluidic flow chamber, I unambiguously demonstrated the long-distance diffusion of NOGGIN through the extracellular medium at the apical side as well as the short-distance diffusion of BMP4 over few direct neighbors. Surprisingly, I further demonstrate that apically-applied NOGGIN can inhibit basally-applied BMP4 across a tight hESC epithelium, which points to mechanisms of trans-epithelial transport. And finally, I trace the transcytosis route of apical NOGGIN through the endosomal system. Overall, I highlight a complex mechanism where apically-secreted NOGGIN diffuses over long distance in the apical compartment; NOGGIN is then internalized, transcytosed, and trafficked to the basal-lateral surface close to the subcellular locus where BMP receptors are located. This apical-to-basal transcytosis was indispensable for NOGGIN inhibition. Taken together, the segregation of activator/inhibitor into distinct extracellular spaces challenges classical views of morphogen movement.

This discovery challenges current dogma which assumes that the morphogen activator and inhibitor diffuse in the same compartment. I propose that the transport of morphogen inhibitors regulates the spatial availability of morphogens during embryogenesis. My study shed light on an important and unexpected level of regulation for the transport of morphogen inhibitors whose role in spatially restricting the spread of morphogen signaling ultimately shapes the embryonic body plan.

This thesis is dedicated to my grandparents, whom I love dearly.

Bé đề tặng Luận án Tiến sĩ này cho ông bà nội thương yêu.

ACKNOWLEDGMENTS (English and Vietnamese)

I would like to extend my most sincere gratitude and appreciation to my thesis co-advisors, Dr. Eric Siggia and Dr. Ali Brivanlou, who directly guided and supported me in my research endeavors. It truly was an honor and privilege to be under the tutelage of not one, but two amazing scientists. On the one hand, Dr. Brivanlou always pushes me to ask the big scientific questions. He generously provides the encouragement and resources for me to pursue ambitious experiments. His enthusiasm, positivity, and vibrant personality rallied me through many stumbling blocks. On the other hand, Dr. Siggia's composure and discipline kept me grounded and focused. His analytical approach to biology fostered my critical thinking and scientific reasoning. He teaches me to approach scientific questions holistically and systematically. I consider myself extremely fortunate to have been under the guidance of my two advisors who, despite their differences, have both been exceedingly kind and supportive towards me.

I would like to sincerely thank the remaining members of my thesis committee - Dr. Hermann Steller and Dr. Anna-Katerina Hadjantonakis. Thank you for your invaluable inputs and guidance over the years. Your constructive criticisms prompted me to stay focused and do better. I would also like to thank Dr. Richard Harland from the University of California – Berkeley for kindly accepting to be my external examiner. It is a special privilege to have my thesis work, which revolves around the protein NOGGIN, to be evaluated by the scientist who discovered NOGGIN nearly 30 years ago.

I consider myself extremely fortunate to be able to work alongside my friends and colleagues from the Brivanlou and Siggia groups. I want to specially thank Fred Etoc, Zeeshan Ozair, Tatiane Kanno, Riccardo De Santis, Tomomi Haremaki, Min Yang, Shu Li, Anna Yoney, Iain Martyn, Tiago Laundos, Edwin Rosado-Olivieri, Manon Valet, Jakob Metzger, and Mijo Simunovic. I am grateful for your intellectual stimulation as well as moral support. You all patiently answered my questions and shared your knowledge without reservation. I learned a lot from your creative ideas and helpful criticisms. I feel so fortunate to have such enthusiastic, smart, and kind coworkers. I learned a lot from all of you in the past 4 years.

My graduate school journey was made possible thanks to a village of support from various departments. I am indebted to the administrative staff of the graduate program, who facilitated the optimal working condition and allowed me to make scientific research my sole focus of attention. Thanks to the administrative managers and assistants from both the Brivanlou and Siggia labs, including Peter Ingrassia, Adam Souza, Jean-Marx Santel, and Melanie Lee. I would also like to thank staff members of the Bio-Imaging Resource Center (BIRC) and Precision Instrumentation Technologies (PIT) at the Rockefeller University for providing the resources necessary for me to advance my research. I am also indebted to the 2019 Center for the Physics of Living Cells Summer School program for giving me inspirations for the creation of the microfluidic device which became one of the highlights of my thesis project.

I would like to extend my deep appreciation for my past teachers. I would like to thank Mr. Hiền, my first English teacher, who laid the foundation for my English proficiency. He would be happy to know that 20 years after he taught me the first English words, I am now completing a 100+ page PhD dissertation. I would also like to thank my undergraduate research advisor, Dr. Karen

Lyons, whose Developmental Biology lectures instilled in me the original curiosity for embryogenesis and compelled me to explore more. I would like to especially thank Dr. Cron, Dr. Mickey Laux, and Dr. Farah Sogo – if it weren't for your encouragement and support in the last decade, my aspirations to pursue higher education might not have been realized now.

I want to thank my friends who have been by my side through college and graduate school. Sharon and Leah shared this graduate school journey with me from a distance. I am glad to have been able to share with you both the frustrations and joys of research. From the West Coast, you stayed up late to proofread my scientific writing and woke up early to attend my presentation practice sessions. Your feedback helped improve my writing and presentation skills tremendously, and for that, I am grateful.

Thank you to the friends whom I have been fortunate to get acquainted with when I moved to New York City. Tati Kanno, Kevin Gonzales, Tiago Laundos, Tiago Rito, David Requena, and James Knox shared with me new experiences in New York City. In addition, we had many interesting discussions about science, careers, and more. Your enthusiasm and positive energy have made my graduate journey more enjoyable and effective over the years. Thank you for your brains, inspiration, thoughtfulness, cheer, hope, empathy, and solidarity.

I would like to thank my grandparent, my parents, aunts, uncles, and siblings from both the Phan and Everson families in Vietnam and the States. I am indebted to my Aunt Hồng and Uncle Hà, who sponsored my family's immigration to the States in 2009. From a distance, you all supported and encouraged me throughout my time in graduate school.

Last but absolutely not least, I would like to thank my husband, my bestest life companion, Zachary. You constantly supported and motivated me in life as well as in my graduate work. My husband Zachary and my cat Carbon bring me so much joy and laughter every single day. Without you, I probably would still have finished this dissertation, but the journey wouldn't have been nearly as enjoyable.

LỜI CẢM ƠN

Tôi xin bày tỏ lòng biết ơn sâu sắc tới Giáo sư Tiến sĩ Ali Brivanlou và Giáo sư Tiến sĩ Eric Siggia, là hai người thầy đã trực tiếp dẫn dắt và cố vấn cho tôi trong suốt thời gian thực hiện đề án nghiên cứu khoa học này. Tôi cảm thấy rất vinh dự và may mắn khi được dạy bởi hai nhà khoa học danh tiếng. Thầy Ali luôn khuyến khích tôi tìm hiểu về những đề tài nghiên cứu táo bạo, có phạm vi rảnh hưởng rộng. Thầy khuyến khích và ưu tiên hỗ trợ cho tôi tự do theo đuổi tham vọng về những thí nghiệm khó, mà không màng tới chi phí. Tính cách nhiệt tình và năng động của thầy là sự tích cực lan tỏa giúp tôi vượt qua nhiều lần vấp ngã. Trong khí đó, sự điềm tĩnh và tính kỷ luật của Tiến sĩ Siggia giúp tôi có được điểm tựa và sự tập trong. Cách thầy Eric phân tích những đề tài sinh học đã nuôi dưỡng tư duy phản biện và lý luận khoa học trong tôi. Thầy đã dạy tôi cách tiếp cận các câu hỏi khoa học một cách tổng thể và có hệ thống. Tôi cảm thấy bản thân vô cùng may mắn khi được dẫn dắt bởi hai thầy. Tính cách hai thầy cố vấn của tôi rất khác nhau, nhưng cả hai nguoiwf đều vô cùng tốt bụng và ủng hộ tôi.

Tôi xin gửi lời cảm ơn chân thành đến các thành viên còn lại trong hội đồng cố vấn của tôi - GS TS Hermann Steller và GS TS Anna-Katerina Hadjantonakis. Cám ơn thầy cô đã nhiệt tình hướng dẫn tôi trong suốt những năm qua. Hai thầy cô luôn đưa ra những nhận định sắc sảo, hữu ích. Những lời phê bình mang tính xây dựng của thầy cô đã thúc đẩy tôi tập trung và làm tốt hơn. Tôi cũng xin cám ơn GS TS Richard Harland từ Đại học California – Berkeley đã vui lòng nhận lời làm giám định viên cho buổi bảo vệ luận án của tôi. Thật là một vinh hạnh đặc biệt khi công trình luận án của tôi, xoay quanh protein NOGGIN, được đánh giá bởi nhà khoa học đã phát hiện ra NOGGIN gần 30 năm trước.

Cám ơn những người bạn và những người đồng nghiệp từ nhóm Brivanlou và Siggia mà tôi đã may mắn được làm việc cùng. Tôi muốn gửi lời cảm ơn đặc biết tới Fred Etoc, Zeeshan Ozair, Tatiane Kanno, Riccardo De Santis, Tomomi Haremaki, Min Yang, Shu Li, Anna Yoney, Iain Martyn, Tiago Laundos, Edwin Rosado-Olivieri, Manon Valet, Jakob Metzger, và Mijo Simunovic. Tôi rất cảm kích sự tất cả sự trợ giúp về tinh thần và trí tuệ. Các anh chị đã kiên nhẫn trả lời mọi câu hỏi của tôi cũng như đã không ngần ngại chia sẻ kinh nghiệm cho tôi. Tôi đã học rất nhiều từ những ý tưởng mới và những lời phê bình hữu ích. Tôi cảm thấy thật sự may mắn khi được làm việc với những người đồng nghiệp vô cùng nhiệt tình, tốt bụng, và thông minh như các bạn. Tôi đã học được rất nhiều điều thú vị và mới mẻ từ mọi người trong suốt 4 năm qua.

Hành trình học tập và đào tạo của tôi trong 4 năm qua đã khá suôn sẻ, nhờ vào sự hỗ trợ từ nhiều khía cạnh. Cám ơn các thành viên hành chính của khoa và của chương trình đào tạo Tiến sĩ đã tạo điều kiện tốt nhất để tôi có thể chuyên tâm nghiên cứu. Cám ơn những người quản lý hành chính và trợ lý từ nhóm Brivanlou và Siggia như Peter Ingrassia, Adam Souza, Jean-Marx Santel, và Melanie Lee; mọi người đã giúp công việc nghiên cứu của tôi dễ dàng và thuận tiện hơn. Và cũng cám ơn các nhân viên từ Trung tâm Sinh học Hiển vi (BIRC) và Cơ sở Chế tạo Máy móc (PIT) tại trường ĐH Rockefeller vì đã cung cấp những dụng cụ nghiên cứu cần thiết cho công trình nghiên cứu của tôi. Tôi cũng rất biết ơn chương trình hè 2019 của Trung tâm Vật lý về Tế Bào Sống đã cho tôi nguồn cảm hứng để tạo ra thiết bị vi lỏng; thiết bị này đã trở thành một trong những điểm sáng trong dự án luận văn của tôi.

Tôi muốn đặc biệt cám ơn những thầy cô cũ của tôi. Trong số đó là thầy Hiền – người thầy tiếng Anh đầu tiên của tôi. Nếu thầy biết học trò 20 năm trước của thầy bây giờ đã viết được bài luận án Tiến sĩ hơn 100 trang, chắc thầy sẽ vui. Tôi cũng muốn cảm ơn cố vấn nghiên cứu của tôi thời Đại học, GS TS Karen Lyons. Chính những bào giảng của cô về sinh học phát triển đã truyền cho tôi sự tò mò về quá trình hình thành phôi và thúc đẩy tôi khám phá nhiều hơn. Tôi muốn đặc biệt cảm ơn các thầy cô đã truyền cho tôi niềm đam mê cho khoa học nói chung, và cho bộ môn sinh học nói riêng. Cám ơn TS Cron, GS TS Mickey Laux, và GS TS Farah Sogo, nếu không có sự động viên và khuyến khích của các thầy cô hơn 10 năm trước, nguyện vọng học lên cao học của tôi có thể đã không thành hiện thực.

Tôi muốn cảm ơn những người bạn của tôi, những người đã sát cánh cùng tôi trong suốt thời gian học đại học và tiến sĩ. Sharon và Leah đã chia sẻ hành trình này với tôi từ xa. Tôi rất vui vì đã có thể chia sẻ với bạn cả những niềm vui và thất vọng khi nghiên cứu. Từ bờ Tây của đất nước, các bạn chịu khó thức khuya dậy sớm để đọc các văn bản khoa học của tôi, tham dự những buổi luyện tập thuyết trình của tôi, cho tôi nhiều phản hồi để cải thiện kỹ năng viết và thuyết trình. Phản hồi của bạn đã giúp tôi cải thiện kỹ năng viết và trình bày rất nhiều, và vì điều đó, tôi rất biết ơn.

Cám ơn những anh, chị mà tôi đã may mắn được kết thân khi chuyển đến thành phố New York này. Cám ơn Tati Kanno, Kevin Gonzales, Tiago Laundos, Tiago Rito, David Requena, và James Knox. Các anh chị đã cùng tôi khám phá những trải nghiệm mới mẻ ở Thành phố New York. Ngoài ra, các anh chị cũng cùng tôi trao đổi về những đề tài khoa học, nghề nghiệp, và nhiều đề tài khác. Sự nhiệt tình và năng lượng tích cực từ các anh chị đã giúp hành trình học tập, nghiên cứu của tôi trong những năm qua thêm phần thú vị và hiệu quả. Cám ơn các anh chị đã chỉ dẫn tôi và truyền cho tôi nhiều cảm hứng, sự chín chắn, cổ vũ, hy vọng, đồng cảm, và đoàn kết.

Tôi xin tỏ lòng biết ơn tới ông bà nội, ba mẹ, cô chú bác, anh chị em từ cả dòng họ Phan và Everson ở Mỹ và Việt Nam. Cám ơn bác Hồng và bác Hà, là hai người đã bảo lãnh gia đình tôi sang Mỹ vào năm 2009. Cám ơn mọi người đã luôn ủng hộ, động viên tôi trong cuộc sống cũng như trong thời gian tôi hoàn thành luận án tiến sĩ mặc dù mọi người đều ở xa.

Đặc biệt, tôi cảm ơn người chồng và người bạn đồng hành thân thiết nhất của tôi, Zachary. Chồng tôi và mèo Carbon đã liên tục đem lại cho tôi nhiều niềm vui và tiếng cười trong cuộc sống hằng ngày. Chồng tôi đã không ngừng ủng hộ và tạo động lực cho tôi cả trong cuộc sống và khi tôi hoàn thành đề án. Nếu không có Zachary thì có lẽ tôi cũng sẽ hoàn thành được luận án này thôi, nhưng cuộc hành tình đó chắc chắn sẽ kém vui hơn nhiều lần.

STATEMENT OF CONTRIBUTIONS

Parts of this thesis were modified from a published manuscript that was co-written with Dr. Ali Brivanlou and Dr. Eric Siggia.

The transgene constructs for the TRE:BMP4-my and TRE::NOGGIN-V5 were generated by Fred Etoc. Shu Li assisted with the secreted NOGGIN western blot. Samuel Khodursky assisted with BMP receptor immunostaining. Anna Yoney for generated the BMP4-KO hESC lines.

TABLE OF CONTENTS

LIST OF FIGURES

LIST OF TABLES

LIST OF ABBREVIATIONS

BMP4	Bone morphogenetic protein 4
DOX	Doxycycline
IF	Immunofluorescence
kDA	kilodalton
MEF-CM	Mouse embryonic fibroblast conditioned media
PBS	Phosphate-buffered saline
qPCR	Quantitative polymerase chain reaction
ROCK	Rho Kinase
RUES2	Rockefeller university embryonic stem cell line 2
SMAD1/5/8	Mothers against decapentaplegic homolog 1/5/8

CHAPTER 1. INTRODUCTION

1.1 Morphogens in a Developmental Context

Understanding the mechanisms that give rise to spatial patterns in development is a challenge that has intrigued scientists for over a century (Morgan, 1901, Stumpf, 1966, Crick, 1970, Lawrence, 1988, Wolpert, 1986). A morphogen is defined as a molecule whose non-uniform distribution across a field of cells differentially determines the fates and phenotypes of those cells (Gurdon and Bourillot, 2001). A morphogenetic gradient is thought to provide positional information that directs cell fate specification in developing tissues (Rogers and Schier, 2011).The emergence of distinct cell types that instigates a broad variety of tissue shapes and functions is the pillars of embryonic development. Multiple morphogenetic gradients working in synchrony effectively serve as a coordinate system guiding the patterning of various tissue types over a complex, multi-dimensional landscape that is the developing embryo. Therefore, it is critical for morphogenetic cues to be correctly modulated, positioned, and interpreted by the target tissues.

Historically, morphogens were identified and researched in the *Drosophila melanogaster*'s appendages to a great extent. More recently, morphogens directing vertebrate development have been identified. Examples of morphogens include members of the Hedgehog (HH) family, Wnt family, transforming growth factor beta (TGF-β) family, and more recently the retinoic acid (RA) family. The secreted protein Hedgehog was found to transmit a signal from posterior to anterior cells and forms a concentration gradient that patterns the wing disc (Mullor et al., 1997, Strigini and Cohen, 1997). Its mammalian ortholog Sonic hedgehog (Shh) acts in a graded fashion to pattern the dorsal–ventral axis of the vertebrate neural tube (Briscoe et al., 2001,

Huangfu and Anderson, 2006, Briscoe and Therond, 2013, Lee et al., 2016, Kong et al., 2019, Liu, 2019). The Wnt family member Wingless (Wg) was found to regulate *Drosophila* appendage development (Zecca et al., 1996, Neumann and Cohen, 1997). In vertebrates, Wnt signaling specifies the dorso-ventral axis by establishing the dorsal region while Shh signaling patterns the ventral region (Sokol, 1999, Ulloa and Marti, 2010, Hikasa and Sokol, 2013, Kozmikova and Kozmik, 2020). In addition, recent studies indicate that RA demonstrates morphogen-like diffusion gradients and its metabolism establishes posteriorizing signaling boundaries (Begemann et al., 2001, Grandel et al., 2002, White et al., 2007, Pennimpede et al., 2010, Rhinn and Dolle, 2012).

Since morphogens act as long-range signaling ligands that control cell fate specification in a concentration-dependent manner, the mechanism by which morphogenetic concentration gradients form is of great interest. The two archetypal models that attempt at explaining the emergence of tissue patterns in response to morphogens are Wolpert's French Flag Model/Positional Information Model and Turing's Reaction-Diffusion Model (Figure 1.1). In 1952, Turing proposed the reaction-diffusion model in which he postulated that diffusive, interacting morphogens could spontaneously produce a differentiated pattern from a homogenous field of cells (Turing, 1990). Turing described different types of spatial patterns that could arise due to two diffusing chemicals, the interaction of which could lead to travelling waves, oscillation motions, or stable periodic patterns. Most notably and possibly most relevant to embryological development, the presence of a slow diffusing activator that induces its own expression as well as the expression of its fast diffusion inhibitor could generate patterns of spots or stripes with regular periodicity (Turing, 1990, Gierer and Meinhardt, 1972, Kondo and Miura,

2010, Green and Sharpe, 2015). On the other hand, the French flag/positional information model was proposed by Wolpert in 1969. In Wolpert's positional information model, a pre-existing concentration of a morphogen serves as a coordinate for the cell fate position within a tissue. In response to different morphogenetic concentrations, cells make different fate choices based on their interpretation of the concentration. This interpretation step permits a smooth, monotonic morphogenetic concentration gradient to give rise to an arbitrary pattern (Wolpert, 1969, Wolpert, 1971). Well-known *in vivo* demonstrations of Wolpert's positional information model include the development of Drosophila segments modulated by the gap gene system and the patterning of the vertebrate neural tube modulated by Shh (St Johnston and Nusslein-Volhard, 1992, Briscoe and Small, 2015).

While Turing's model suggests an initially homogeneous reaction-diffusion system that causes a *de novo* symmetry breaking and produces repetitive structures of defined wavelengths, Wolpert's model implies that a pre-existing morphogen gradient already exists and such a gradient is interpreted by the cells in a threshold-dependent manner, creating distinct tissue regions with sharp borders. Historically, these two models were considered mutually exclusive. However, recent hypotheses have suggested that these two proposed patterning mechanisms work together to shape biological forms (Green and Sharpe, 2015, Rulands et al., 2013, Quininao et al., 2015).

Figure 1.1: The Principles of Turing's Reaction-Diffusion Model vs. Wolpert's Positional Information Model

(A) Within Turing's reaction-diffusion model, the activator-inhibitor system involves two molecular concentrations generate periodic patterns that are in phase with each other. The premises of Turing's reaction-diffusion system are 1) the diffusion rate of the inhibitor is significantly greater than that of the activator; 2) the activator induces itself and its inhibitor. This, small molecular fluctuations across a seemingly homogeneous landscape will self-enhance (i). Increased levels of the activator lead to increased levels of the inhibitor (ii). Since the inhibitor diffuse faster than the activator, the levels of inhibitor drop off at the original peak, allowing the levels of activator there to stabilize. In addition, the spread of the inhibitor to neighboring cells prevents the levels of activator to rise from either side of the first peak (iii). However, further away from these regions of lateral inhibition, new peaks can form (iv). As such, the system modulates itself dynamically, and eventually forms a regular array of peaks and valleys across the field of cells (v).
(B) Within Wolpert's positional information model, a prior asymmetry results in a graded concentration distribution of a morphogen. Cells can interpret this distribution to make fate choices. The French Flag Problem is popular representation of this model: a homogenous field of cells can interpret morphogenetic concentration and differentiate into three different cell fates (represented by red, white, and blue colors) (i). Depending how the cells interpret morphogenetic concentrations, define threshold levels (T1 – T7), and assign fates to different concentration ranges, different patterns can arise (ii).

Graphic modified from (Green and Sharpe, 2015).

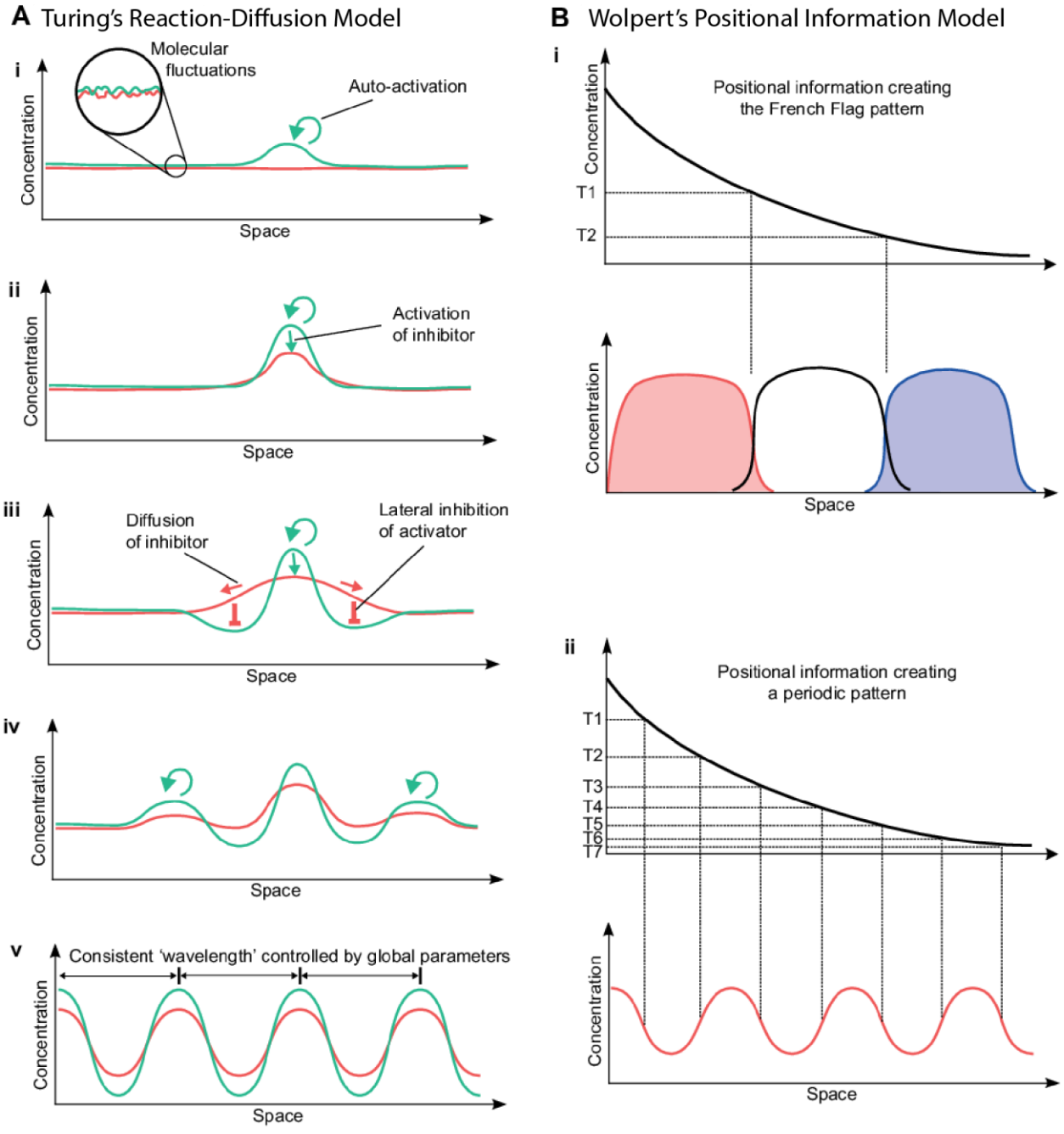
A Turing's Reaction-Diffusion Model
i
Molecular fluctuations
Auto-activation
Concentration
Space
ii
Activation of inhibitor
Concentration
Space
iii
Diffusion of inhibitor
Lateral inhibition of activator
Concentration
Space
iv
Concentration
Space
v
Consistent 'wavelength' controlled by global parameters
Concentration
Space
B Wolpert's Positional Information Model
i
Positional information creating the French Flag pattern
Concentration
T1
T2
Concentration
Space
ii
Positional information creating a periodic pattern
T1
T2
T3
T4
T5
T6
T7
Concentration
Space

1.2 Dynamic Modes of Morphogen Transport

In both positional information and reaction-diffusion models, long-range extracellular signaling molecules form a concentration radiating from a localized source. Cellular perception of different morphogenetic concentration instigates the configuration of various developmental fates in a correct spatial relationship to each other. As such, morphogen action is intimately linked to positional information. Even for the prominent morphogens described above in Chapter 1.1, we still do not have a comprehensive understanding as to how morphogen gradients are established and maintained in a tissue.

It is often implicitly assumed that morphogens and their secreted inhibitors can freely spread from a source to their point of action. Morphogen spreading is traditionally conceptualized and modeled as simple diffusion with decay, though the actual molecular mechanisms are likely to be much more complicated and highly dynamic (Sorre et al., 2014, Kornberg, 2017, Muller et al., 2013, Hidalgo, 2019). Contemporary transport models can be categorized into two different groups: (1) extracellular diffusion-based mechanisms and (2) cell-based mechanisms. Extracellular diffusion-based mechanisms can comprise of free, hindered, and facilitated diffusion. Cell-based mechanisms include transcytosis and cytoneme-mediated transport, where morphogens move through cells or via cellular extensions (Muller et al., 2013) (Figure 1.2).

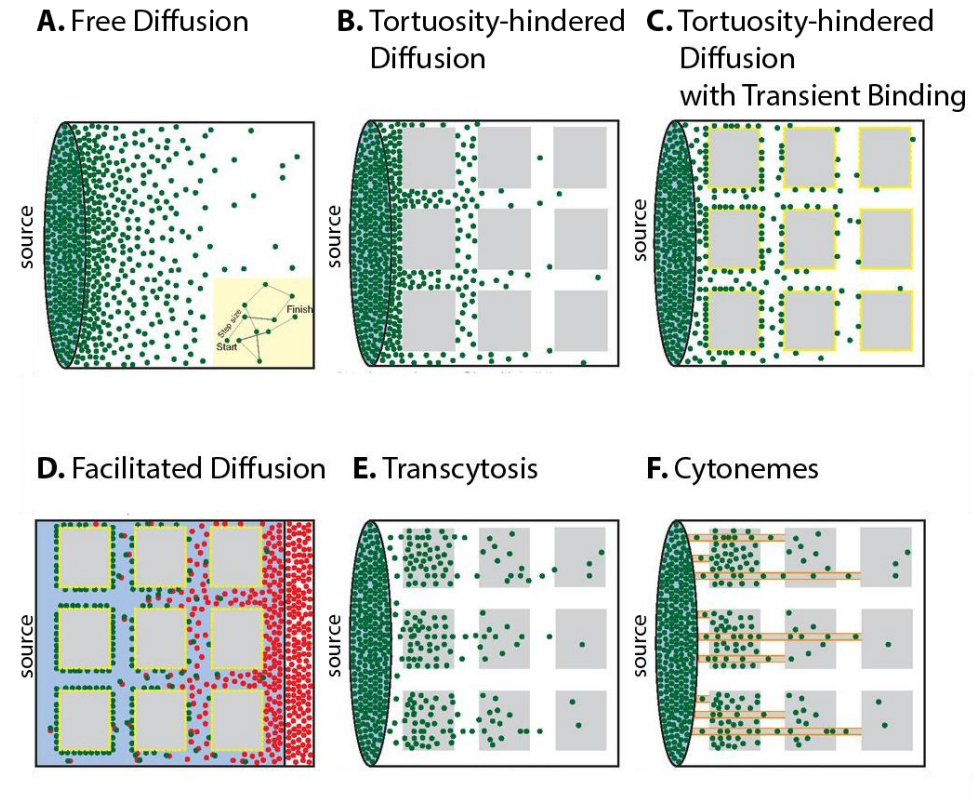

Figure 1.2: Some Models of Morphogen Transport

(A) In the Free Diffusion model, morphogens (green dots) originate from the source, undergo random walks, and disperse away from the source. In this model, morphogen's movement is not restricted by cells or interrupted by extracellular binding interactions. (B) In the Tortuosity-hindered Diffusion model, extracellular morphogen's diffusion is restricted by cells. (C) In the Tortuosity-hindered Diffusion with Transient Binding, extracellular morphogen's diffusion is restricted by tissue architecture and by transient interactions to extracellular matrix components. (D) In the Facilitated Diffusion model, the morphogen's diffusion is regulated by diffusion regulators (red dots). An example of a diffusion regulator is a molecule having hind affinity for extracellular matrix components which would otherwise impede morphogen movement. (E) In the Transcytosis model, the morphogens travel through the cells (F). In the Cytoneme model, morphogens undergo directed transport via fidopodial structures called cytonemes. These cytonemes establish contact between the morphogen-producing cells and the targe cells; morphogens are then transported along these cytonemes.

Graphic modified from (Muller et al., 2013)

The transport mechanisms of various morphogens, including BMP, NODAL, FGF, as well as Bicoid have been investigated in recent years. However, some of these studies arrived at different conclusions: these morphogens have been experimentally demonstrated to employ a variety of transport modes as well as a combination of transport modes (Muller et al., 2013).

The focus of this dissertation is the BMP ligand in the secreted TGFβ superfamily member. The transport modes of BMP have been most extensively studied in the *Drosophila* wing discs. Data on the kinetics of gradient formation suggest that BMP exhibit diffusion. Contemporary methods are unable to determine whether BMP undergoes free or hindered diffusion (Teleman and Cohen, 2000, Entchev et al., 2000, Zhou et al., 2012). BMP diffusion could be hindered by binding to receptor or other immobilizing extracellular molecules (Lander et al., 2002, Sawala et al., 2012). Heparan sulfate proteoglycans (HSPGs) have been implicated in slowing BMP diffusion by transiently binding BMP (Fujise et al., 2003, Belenkaya et al., 2004, Han et al., 2004, Takei et al., 2004, Akiyama et al., 2008, Dejima et al., 2011). In addition, BMP has been suggested to utilize transytosis as a transport mode via endocytosis inhibition experiment (Gallet et al., 2008, Bollenbach et al., 2007, Entchev et al., 2000, Kruse et al., 2004). However, direct evidence for the transcytosis of BMP (or any morphogen) such as cellular uptake and release has not been demonstrated. Furthermore, there exists conflicting evidence supporting and refuting cytonemes as having a role in BMP gradient formation (Ramirez-Weber and Kornberg, 1999, Hsiung et al., 2005, Roy et al., 2011, Demontis and Dahmann, 2007). Lastly, the formation of a gradient in the absence of a localized source can be caused by shuttling of BMP by cell-surface factors (Wang and Ferguson, 2005). In short, strong evidence support the diffusion-based (free or hindered)

models of BMP transport. Further studies are required to elucidate the factors that regulate BMP movement in different tissue types.

Surprisingly, how morphogen signaling integrates within tissue components is mostly unknown. In addition, the extracellular micro-environment that contains these diffusive molecules is less well-understood (Yan and Lin, 2009). The behavior of morphogen transport is further complicated by the fact that morphogens can be secreted either apically or basally (Harmansa et al., 2017). For example, the morphogen *Wingless,* the main *Drosophila* Wnt, is secreted apically and then undergoes apical-to-basolateral trafficking in the wing imaginal disc epithelium (Yamazaki et al., 2016); the diffusion rate of Wnt is modulated through binding with extracellular glypicans (McGough et al., 2020). How complex patterns of morphogen secretion, transport, and diffusion work together synergistically to shape gradient is an exciting area for future studies.

Epithelial tissues, which play key roles in shaping human's basic embryonic body plan, consist of a laterally cohesive sheet of cells whose epithelial integrity is maintained by adherens and tight junctions, hence presenting a diffusion barrier (Gilmour et al., 2017). Another defining characteristic of epithelia is a distinct apicobasal polarity which enables apical and basolateral domains to adopt distinct features. As such, signaling is coupled to global embryo as well as local tissue geometry. Although a number of morphogens responsible for embryonic patterning have been identified, we are very far from a quantitative understanding of the dynamics of signaling by these morphogens, which are collectively responsible for transforming a zygote into

an embryo. More cell biological and biochemical studies are required to evaluate how morphogenetic gradients are regulated.

1.3 BMP4 Signaling in Embryogenesis

The TGF-β morphogen family is the emphasis of this dissertation (Figure 1.1). The TGF-β superfamily of growth factors contains 33 members including TGF-βs, bone morphogenetic proteins (BMPs), growth and differentiation factors (GDFs), Activins, and Nodal (Feng and Derynck, 2005, Morikawa et al., 2016). These various TGF-β family members act as positional cues that direct the patterning of developing tissues during embryogenesis. For example, Squint was found to be required for mesoderm formation and patterning in zebrafish (Chen and Schier, 2001). An important member of the TGF-β family is Activin, whose role in mesoderm induction has been demonstrated (Mitrani et al., 1990, Gurdon and Bourillot, 2001). Another significant member is Decapentaplegic (Dpp), which is involved in *Drosophila* appendage development, specifically in anterior-posterior and dorsal-ventral axis formation (Lecuit et al., 1996, Nellen et al., 1996). This dissertation will focus on Dpp's vertebrate ortholog Bone Morphogenetic Protein (BMP). BMP plays crucial roles in several aspects of development including ventral mesoderm patterning (Jones et al., 1992, Dale et al., 1992, Jones et al., 1996). Details about the roles and mechanism of BMP signaling in various aspects of embryonic development is discussed in a subsequent chapter.

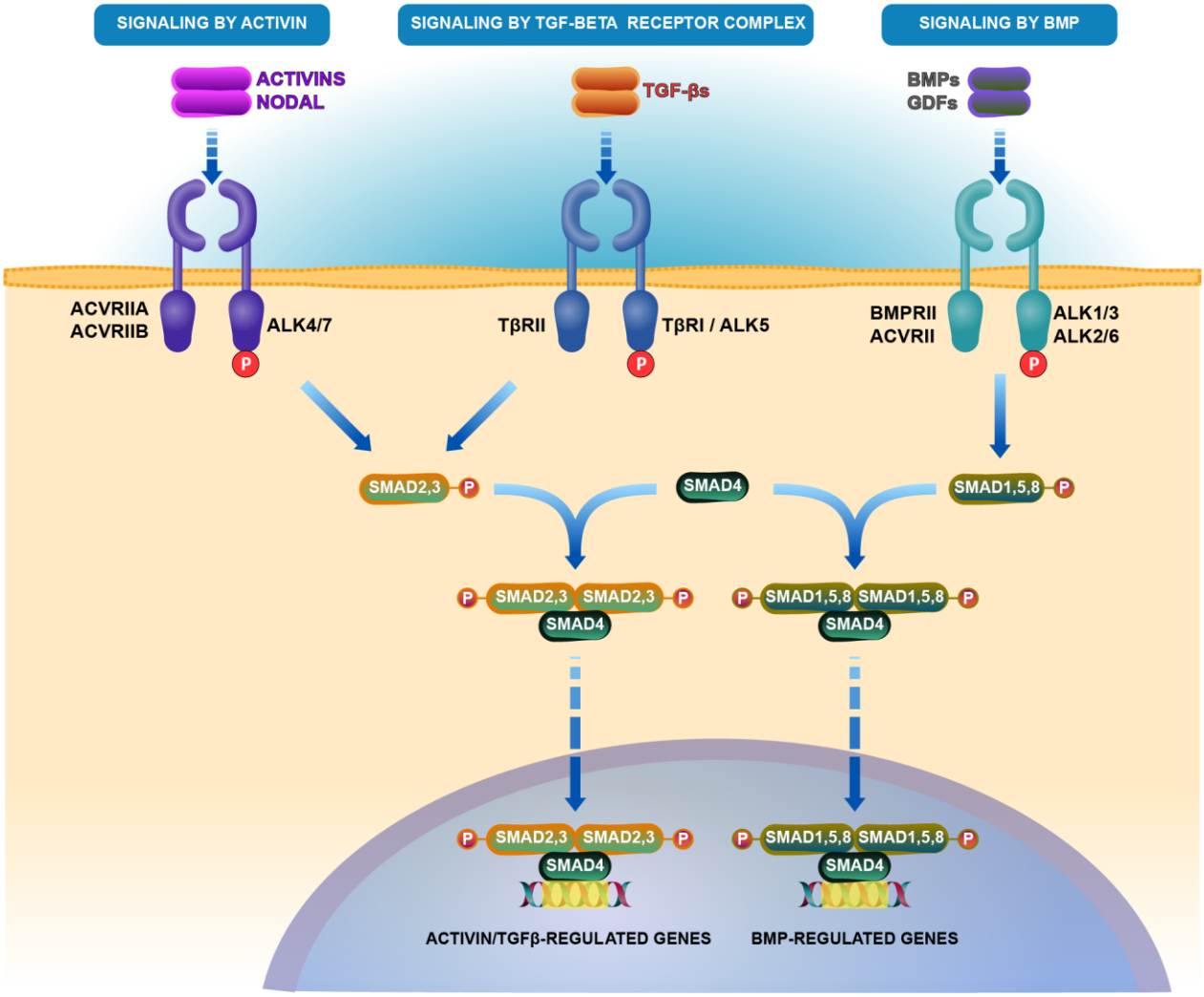

Figure 1.3: Signaling by Major TGF-β Family Members

Extracellular ligands Activin or Nodal bind to type II transmembrane receptor (ACVRIIA/ACVRIIB) and type I transmembrane receptor (ALK4/7). (Nodal binding requires the additional binding of the transmembrane co-receptor CRIPTO1). TGF-β growth factors bind to type II receptor TβRII and type I receptor TβRII/ALK5. The type II receptor for BMPs are BMPRII and ACVRII; the type I receptor for BMPs are ALK1/3 and ALK2/6.
The activated receptor complex phosphorylates their respective Smad proteins (Smad2 and Smad3 for Activin/Nodal and TGFβ pathways; Smad1, Smad5, and Smad8 for BMP pathway). Phosphorylated Smads form a complex with Smad4. These trimer complexes most likely contain two R-Smads that are identical or different and one Smad4 subunit. Together they enter the nucleus, bind to chromatins, and regulate target gene expression (Massague et al., 2005, Schmierer and Hill, 2007, Moustakas and Heldin, 2009).

Graphic modified from Reactome Diagram (Fabregat et al., 2018).

BMPs are extracellular ligands that regulate growth, patterning, as well as morphpgenesis (Wu and Hill, 2009, Affolter and Basler, 2007). BMPs signal as a homodimer or a heterodimer with another BMP-subfamily ligand. Class I BMPs, which include BMP2 and BMP4, can heterodimerize with class II BMPs, which include BMP5, BMP6, BMP7, BMP8 (Guo and Wu, 2012). Compared to homodimers, heterodimers composed of different BMP family members are demonstrated to have higher signaling efficacy *in vivo* and *in vitro*. For example, heterodimers of BMP2/BMP7 or BMP4/BMP7 can induce patterning and downstream gene expression more potently than homodimers of BMP2, BMP4, or BMP7 (Aono et al., 1995, Hazama et al., 1995, Israel et al., 1996, Nishimatsu and Thomsen, 1998, Schmid et al., 2000, Suzuki et al., 1997, Little and Mullins, 2009). It is speculated that the reason BMP heterodimers signal more actively is because BMP heterodimers form a more stable receptor-ligand complex, although the exact mechanism is unknown.

BMPs are synthesized as inactive precursor proteins (proBMPs). These precursor proteins are then cleaved to produce the active mature ligand and the prodomain fragments (Bragdon et al., 2011). The prodomain fragment has not been shown to facilitate dimerization, folding, and secretion of the active ligand (Gray and Mason, 1990).

The active mature BMP ligands bind to and activate BMP receptor complexes which compise of transmembrane serine/threonine kinases. Specifically, BMP binding causes the phosphorylation of te type I receptor by the type II receptor. This activated heteromeric complex triggers intracellular signaling that is specific for the BMP pathway. Namely, SMAD1, SMAD5, and SMAD8 are phosphorylated. Phosphorylated SMAD1/5/8 then forms a heteromeric complex

with SMAD4. This complex translocates to the nucleus where it binds to BMP response elements and activates transcription of BMP target genes (Bragdon et al., 2011) (Figure1.3).

BMPs are essential during embryogenesis. BMP4 is among the early embryonic morphogens that play critical roles in the early patterning (Arnold and Robertson, 2009, Ben-Haim et al., 2006, Wilson et al., 1997). Most prominently, BMPs are crucial for medoderm formation. Shortly after implantation (E5.5), upregulated levels of BMP4 in the extraembryonic ectoderm are required to pattern the proximal epiblast and the adjacent visceral endoderm. By E6.0, the embryo is pre-patterned by regional differences in gene expression. Removal of the BMP4-rich extraembryonic ectoderm in pre-gastrulation embryos leads to expansion of DVE markers throughout the VE and the loss of proximal epiblast marker gene expression (Rodriguez et al., 2005). In the HH stage 6 of the chick epiblast, which shares a similar morphology to the human epiblast, BMP4 is expressed in the margins of the neural plate and in the caudal third of the primitive streak (Chapman et al., 2002). Knocking-out different components of BMP signaling pathways such as BMP ligands, BMP receptors, or SMAD factors generally results in embryonic lethality and defects in mesoderm formation (Mishina et al., 1995, Wang et al., 2014).

We have previously shown that BMP4 alone is sufficient to initiate germ layer self-organization in a gastrulation-like process either in flat 2D micropatterned epiblast model (Etoc et al., 2016), or in a 3D model for primitive streak formation and anterior-posterior symmetry-breaking (Simunovic et al., 2019). Strikingly, our *in vitro* models have revealed that BMP4 reception in the polarized epithelium is restricted to the basolateral cell domain, due to BMP receptors' basolateral localization below the junctional diffusion barrier (Etoc et al., 2016, Zhang et al.,

2019, Nallet-Staub et al., 2015). A similar pattern of basolateral receptor localization has also been observed *in vivo* in the developing mouse embryo (Zhang et al., 2019). LTA amino acid motif suggests that this basolateral localization of TGF-β family receptors may be evolutionarily conserved (Zhang et al., 2019).

1.4 NOGGIN-Mediated Antagonism of BMP Signaling

The roles of BMP4 extracellular antagonists including NOGGIN, CHORDIN, CERBERUS, and FOLLISTATIN have been illustrated in neural induction and differentiation (Canalis et al., 2003). Much of our knowledge about BMP antagonists is derived from the developmental studies of the Spemann organizer. NOGGIN is the first molecule reported to have the properties of a Spemann organizer, inducing dorsal structures (Smith and Harland, 1992).

The human NOGGIN gene consists of a single exon and encodes a secreted homodimeric glycoprotein protein. NOGGIN's functions as a dorsalizing factor promoting neural tissue formation is well-conserved (Valenzuela et al., 1995). Furthermore, it is well-established that NOGGIN antagonizes BMP4 by binding tightly to BMP4, preventing binding to BMP receptors (Zimmerman et al., 1996). Crystal structures of the antagonist Noggin homodimer bound to BMP7 homodimer reveal that NOGGIN inhibits BMP signaling by blocking the binding sites of both BMPR types 1 and 2, thereby preventing BMP from interacting with its receptors (Groppe et al., 2002). Thus, NOGGIN functions by sequestering its ligand in an inactive complex. NOGGIN binds BMP2, BMP 4, BMP 5, BMP 6, BMP 7, GDF5, GDF6, and Vg1, with various degrees of affinity; however, NOGGIN does not bind other members of the TGF-β family of peptides (Zimmerman et al., 1996, Aspenberg et al., 2001).

While BMP4 direct ventralization and non-neural ectoderm development, BMP-antagonizing signals NOGGIN from the node/Spemann organizer direct dorsalization and neural formation (Re'em-Kalma et al., 1995, Graff, 1997). In the HH stage 6 of the chick epiblast, which shares a similar morphology to the human epiblast, NOGGIN is expressed only in the first axial mesendoderm cells to ingress through Hensen's node (Chapman et al., 2002). Knocking out NOGGIN results in severe developmental defects leading to fetal lethality (Brunet et al., 1998). As a human-specific trait, BMP4 induces the direct expression of its own inhibitor NOGGIN, which is required for germ-layer patterning in human models of gastrulation (Etoc et al., 2016).

In contrast to the detailed characterization of morphogens' signaling pathways, the movement of the morphogens' inhibitors has received less attention. The mechanisms for NOGGIN spreading and its associated kinetics in embryonic tissue have not been investigated.

1.5 Models of the Human Embryos

Human development starts with the union of male and female gametes to give rise to a new, genetically-distinct organism. A sperm fertilizes an oocyte and together they form a zygote. This single-cell zygote undergoes repeated cell division and trophoblast differentiation to generate a multi-cellular blastocyst. At approximately five days after fertilization, the embryo hatches from the zona pellucida and can directly interact with the endometrium. Upon implantation into the uterine wall, the blastocyst further undertakes considerable cell division, cell rearrangements, and cellular differentiation into complex, three-dimensional embryo and fetus that change its shape as it develops over time. Early human development is a dynamic, heterogeneous, complex and multidimensional process (Petropoulos et al., 2016).

This complex, multi-dimensional process is not well understood because the study of early human embryonic development suffers from both technical and ethical problems. The paucity of biological samples as well as regulations by international guidelines make the study of early human embryology extremely challenging (Rivron et al., 2018a) (Council, 2010). For this reason, *in vitro* methods to culture human embryos beyond the blastocyst stage remain suboptimal (Deglincerti et al., 2016a, Shahbazi et al., 2016). In addition, international bioethical guidelines condemn the *in vitro* culture of human embryos beyond 14 days post fertilization (Daley et al., 2016, Hyun et al., 2016).

While model organisms have been instrumental in the dissection of early developmental processes, there are human-specific differences which may render these animal models irrelevant (Davidson et al., 2015, Rossant, 2015). For example, the early human embryos have a geometry different from most other model organisms. (Muller et al., 2013, Rogers and Schier, 2011, Wartlick et al., 2009, Wartlick et al., 2014, Zhang et al., 2019). The epithelialized epiblast morphology inherent to the human bilaminar embryonic disc is distinct from the tissue shape of a stage-matched mouse embryo (O'Rahilly and Muller, 2010, Shahbazi and Zernicka-Goetz, 2018, Shahbazi, 2020).

Thus, for these various reasons, human models based on human embryonic stem cells are an ethical alternative to gain insights about early human development, especially in the post-implantation stages when human embryonic development remains largely unexplored. Many existing embryoid-based models lack efficiency and reproducibility, and thus are less suitable for

rigorous quantitative applications (ten Berge et al., 2008, van den Brink et al., 2014, Harrison et al., 2017, Shao et al., 2017, Simunovic et al., 2019). For analytical studies, more recent applications such as micropattterned surfaces, microwell structures, and microfluidic platforms are preferred as more controllable, scalable, and robust new means to study human embryology (Deglincerti et al., 2016b, Xue et al., 2018, Beccari et al., 2018, Rivron et al., 2018b, Zheng et al., 2019). These new methods serve as effective platforms to study lineage diversification, cell-fate specification, and tissue patterning that occurs during early human embryonic development.

1.6 Motivation for the Study of Human Embryology

Human embryology sheds light about our prenatal origins, which is fascinating in itself. It tells us the commonalities among all humans: fertilization, cleavage, gastrulation, formation of the tube-within-a-tube body plan, and organogenesis. Despite our unique thoughts and behaviors, all human beings we will encounter throughout our lives will have shared the same prenatal experiences. Although we have learned a lot about how embryos develop, there are still many mysteries to unravel. Our knowledge and understanding of human embryology are always evolving.

Besides, the study of human embryology also elucidates birth defects, or congenital anomalies, that occur during embryonic stages. Generally, congenital anomalies include functional and structural deviations which have considerable effects on the individual's physical, intellectual, and social wellbeing ((WHO), 2010). Major birth defects occur in one in 33 births, which translates to 7.8 million babies worldwide (Centers for Disease and Prevention, 2008, Christianson A, 2006). The financial, personal, and society costs are immense. Due to their

global impact on human health, congenital anomalies represent an increasing public health issue. Focused research initiatives to investigate common developmental pathways among birth defects will contribute towards the discovery of modifiable causes of birth defects. To grasp why and how embryology goes amiss requires a detailed understanding of the molecular and cellular events underlying normal human embryology.

In short, human embryology research will provide not only a biological understanding of the cell and molecular basis of human life, but also the potential foundation for therapies to overcome congenital anomalies. As such, the study of human embryology, spearheaded by George Linius Streeter in the early 20th century in New York, continues to be fascinating and relevant, attracting a strong following in New York and worldwide (Corner, 1954).

CHAPTER 2. DIFFERENTIAL COMPARTMENTALIZATION OF NOGGIN & BMP4

2.1 BMP4 is Secreted Basally and Spreads Locally

In this study, human embryonic stem cells (hESCs) are cultured on transwell filters, resembling the embryonic disc. The apical and basal compartments can be independently accessed. The transwell culture system recapitulate the Carnegie stage 6 human epiblast, where each side of the epiblast is exposed to a different cocktail of signals (amniotic cavity on the apical side; hypoblasts and yolk sac on the basal side). Under culture conditions designed for pluripotency maintenance, confluent hESCs form a pseudostratified, apico-basal polarized epithelium reminiscent of the organization of the embryonic epiblast with tight junctions separating the apical and the baso-lateral cell membranes (Figure 2.2).

As previously shown, hESCs localize their BMP receptors to the basolateral domain just below the tight junctions, making them non-responsive to apically applied BMP4 (Figure 2.2) (Etoc et al., 2016). In order to study the signaling dynamics of BMP4 within our model epiblast, we used our own hESC line, RUES2 (NIH# 00012), to stably express transgenes for doxycycline (DOX)-dependent induction of epitope-tagged BMP4 (Figure 2.1). We confirmed that these BMP4-secreting cells could induce the expected patterning of various germ layers in a foci-specific manner (Figure 2.4). BMP4-secreting cells were then transfected with a constitutively expressed nuclear marker, H2B-mCitrine, to allow tracing (Figure 2.1). Since secretion can potentially take place from both sides of the polarized epithelium, we cultured the cells on transwell filters, allowing easy access to both apical and basal compartments. At a starting seeding density of ~4,000 cells/mm^2; the cells form a confluent, polarized epithelium on the filters after 22 hrs in

culture (Figure 2.2). This defines our set of standard conditions for the culture of our model epiblasts.

We used DOX to induce RUES2 on transwell filters to produce BMP4 then probed for secreted BMP4 in the apical and basal compartments. BMP4 was found nearly exclusively in the basal media for up to 24 hrs (Figure 2.3). We then characterized BMP4 lateral spreading dynamics by mixing a low proportion (1:200) of BMP4-producing hESCs within a WT hESCs background. This allowed us to quantify the spatial range of BMP4 propagation in the WT "receiving" cells by quantifying nuclear phosphorylated SMAD1/5/8. Starting at 8 hrs post-induction, basally-secreted BMP4 activated nuclear pSMAD1/5/8, first in an autocrine manner in the secreting cells. At later time-points, a paracrine signal – which could be fitted by an exponential decay function – spread through the epithelium and reached a characteristic length of 20 μm from the closest secreting cells after 24 hrs (Figure 2.3).

To further characterize the contribution of WT "receiving" cells to BMP4-dependent pSMAD1/5/8 propagation, we generated a stable line of BMP4-KO hESCs (Figure 2.5). We mixed a low proportion (1:200) of BMP4-producing hESCs within a background of BMP4-KO or WT hESCs. We observed that the spatial range of pSMAD1/5/8 propagation was similar in WT and BMP4-KO hESCs (Figure 2.6). Our result suggests that the observed pSMAD1/5/8 signal propagation was driven by BMP4 ligands overexpressed by the BMP4-producing hESCs and not by endogenous BMP4 secreted by "receiving" cells.

Figure 2.4: Generation of BMP4-myc and NOGGIN-V5 hESC Cell Lines

(A) Schematics of the doxycycline-inducible constructs for the generation of the xBMP4-overexpressing hESC line. A Myc tag was inserted near the C-terminal of the coding sequence of the precursor protein (N-terminal of the mature protein) (Degnin et al., 2004, Cui et al., 2001), so that both precursor and mature forms of exogenously expressed BMP4 can be detected by the Myc epitope. A constitutive mCitrine nuclear reporter was added subsequently. Sequence integrity of our engineered TRE::BMP4-myc; H2B-mCitrine cell line showing the location of the Myc tag. (B) Schematics of the doxycycline-inducible constructs for the generation of the hNOGGIN-overexpressing hESC line. A V5 tag was inserted at the N-terminal of the protein-coding sequence (Etoc et al., 2016). A constitutive mCherry nuclear reporter was subsequent added. Sequence integrity of our engineered TRE::NOGGIN-V5; H2B-mCherry cell line showing the location of the V5 tags (C) G-band karyotyping results of our engineered hESC lines show normal human female karyotypes.

A

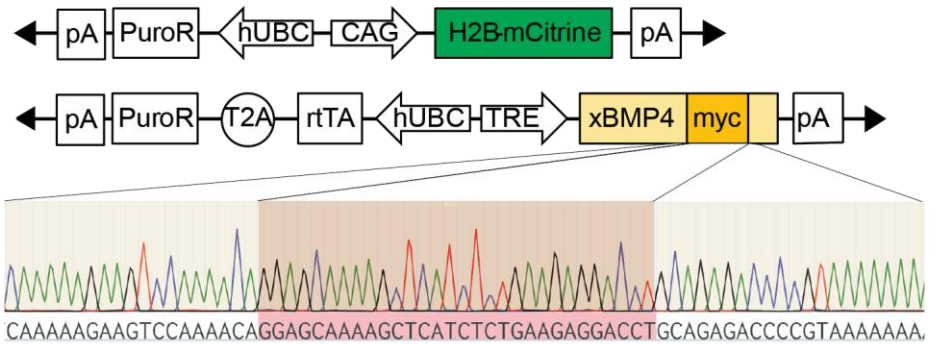

B

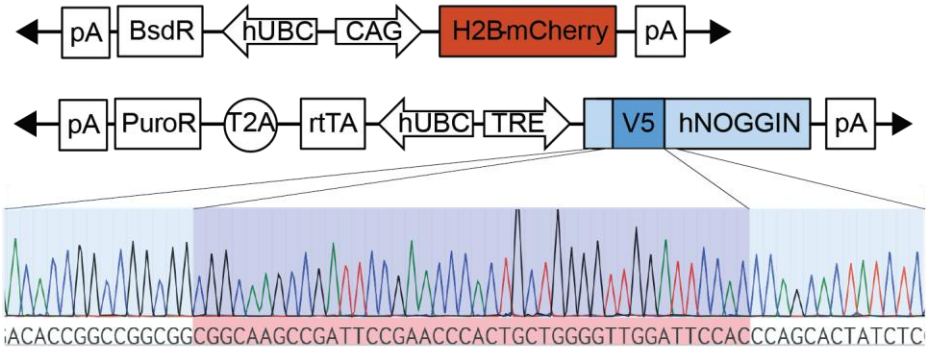

C

TRE::xBMP4-myc; H2B-mCitrine

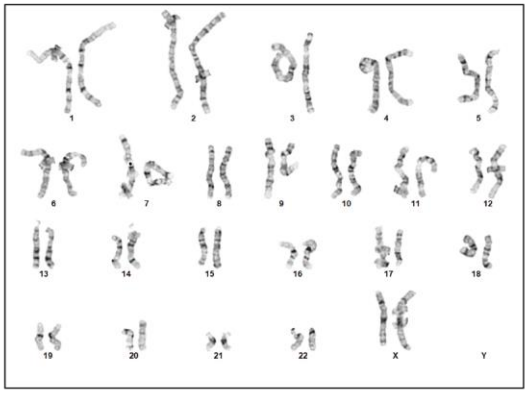

TRE::NOGGIN-V5; H2B-mCherry

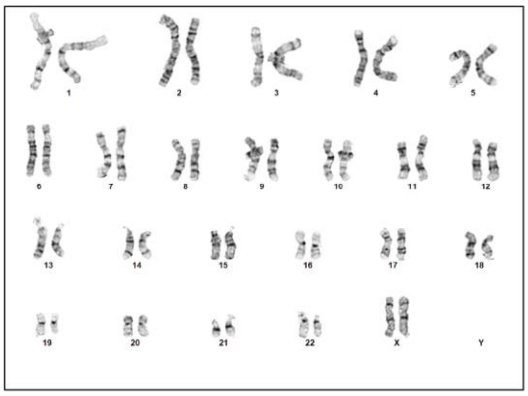

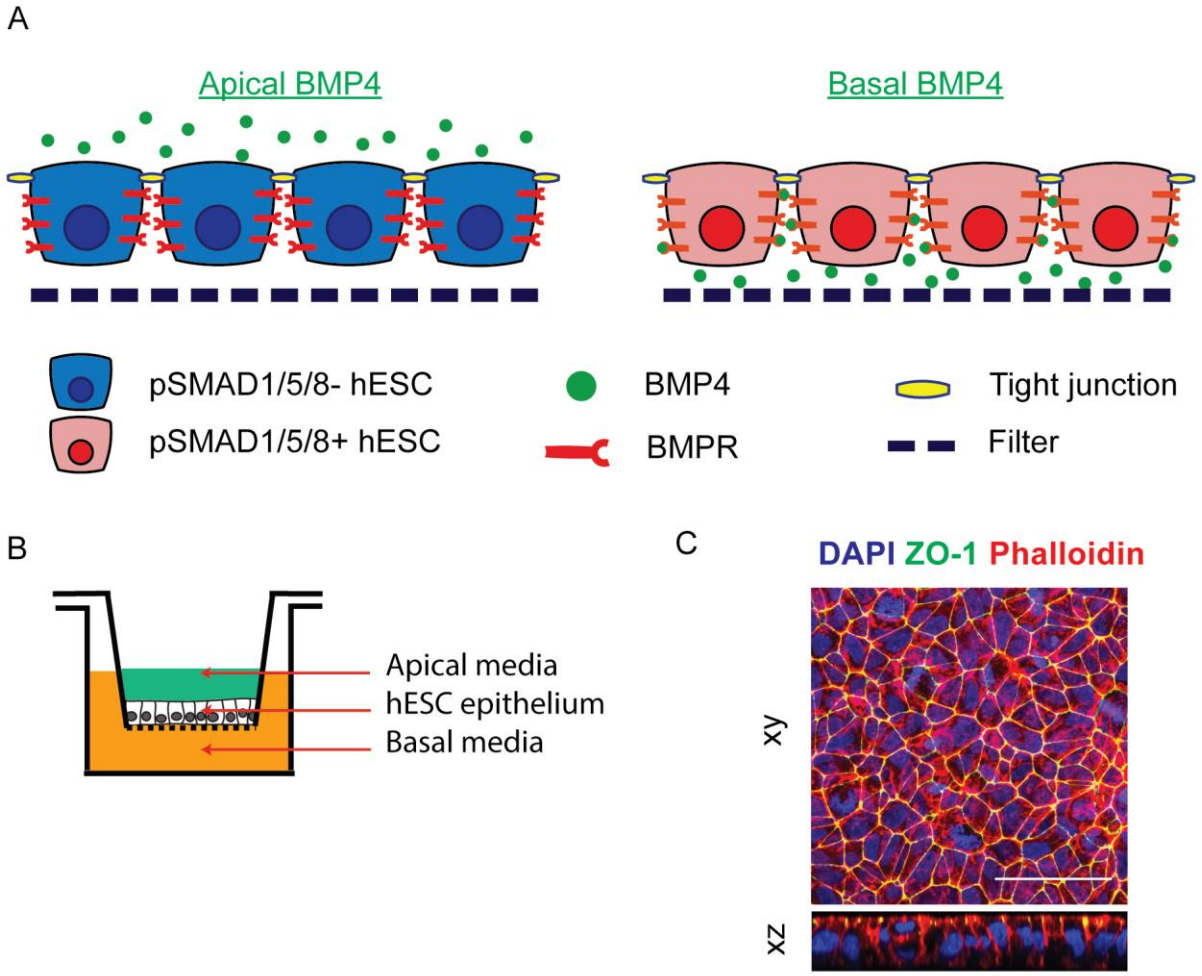

Figure 2.5: *in vitro* Model of Human Epiblast

(A) Schematics of polarized hESC epithelium. BMPR localization restricts hESC response to BMP4 to the basolateral domain. (B) The transwell culture allows the *in vitro* recapitulation of a Carnergie stage 6 human embryo. hESCs are plated and cultured as a polarized epithelium on the filter, resembling the embryonic disc. The apical and basal compartments can be independently accessed. (C) WT-RUES2 cultured as a confluent, pseudostratified, polarized epithelium. Cells were seeded with a starting seeding density of ~4,000 cells/mm^2. 24 hrs after seeding, cells were fixed and stained for markers of tight junctions (ZO-1) and actin (Phalloidin). Scale bars = 50 μm.

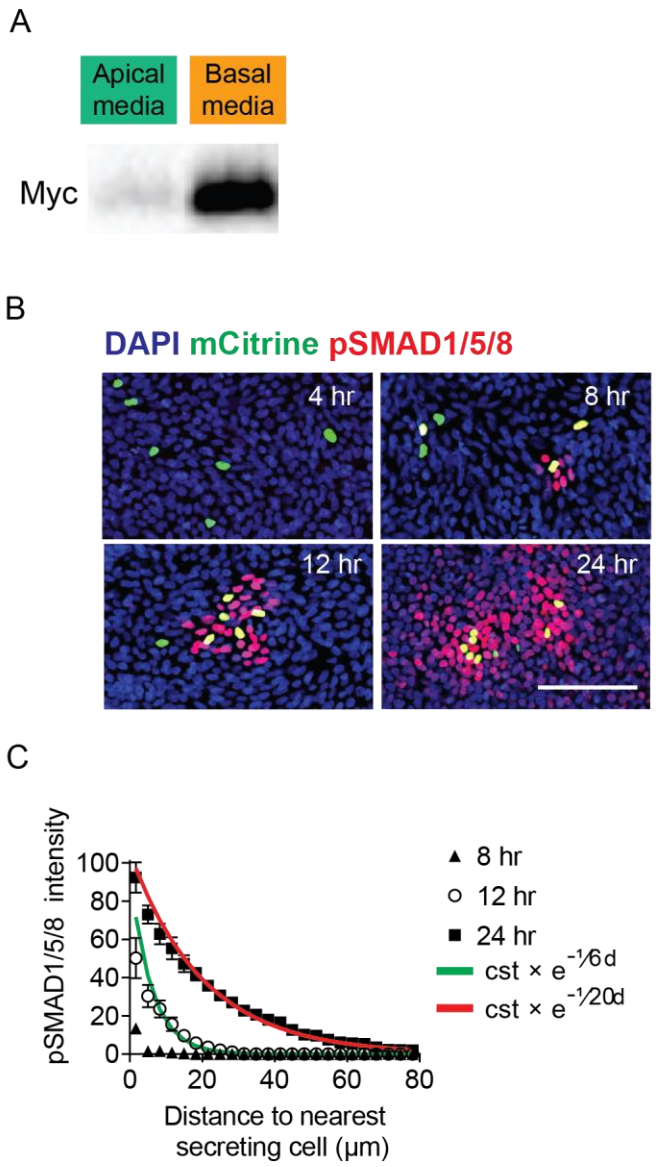

Figure 2.6: BMP4 Is Secreted Basally and Spreads from a Local Source

(A) BMP4 was secreted to the basolateral media. (B) TRE::xBMP4-myc hESCs were cultured to form a tight epithelium on filter and induced to produce BMP4. After 24 hrs, culture media collected from the apical (green) or basal (orange) chambers were analyzed with Western blot. (D) BMP4 signaling propagated in the epithelium as a function of time. pSMAD1/5/8 signaling originated from TRE::BMP4-myc; CAG::H2B-mCitrine cells and propagated to adjacent cells. TRE::xBMP4-myc; CAG::H2B-mCitrine were diluted in wildtype (WT) hESCs (ratio 1:200) and induced to produce BMP4. pSMAD1/5/8 signal intensity was used as a read-out for BMP4 reception in time-course analysis. Scale bar = 100 μm. (C) Quantification of BMP4 signal propagation as a function of time. Exponential curves were fitted to the datapoints. The exponential function is described by the constant "cst" which is the prefactor of the exponential function and the spreading length (in μm) which characterizes the function's rate of decay. Error bars = SEM (standard error of mean).

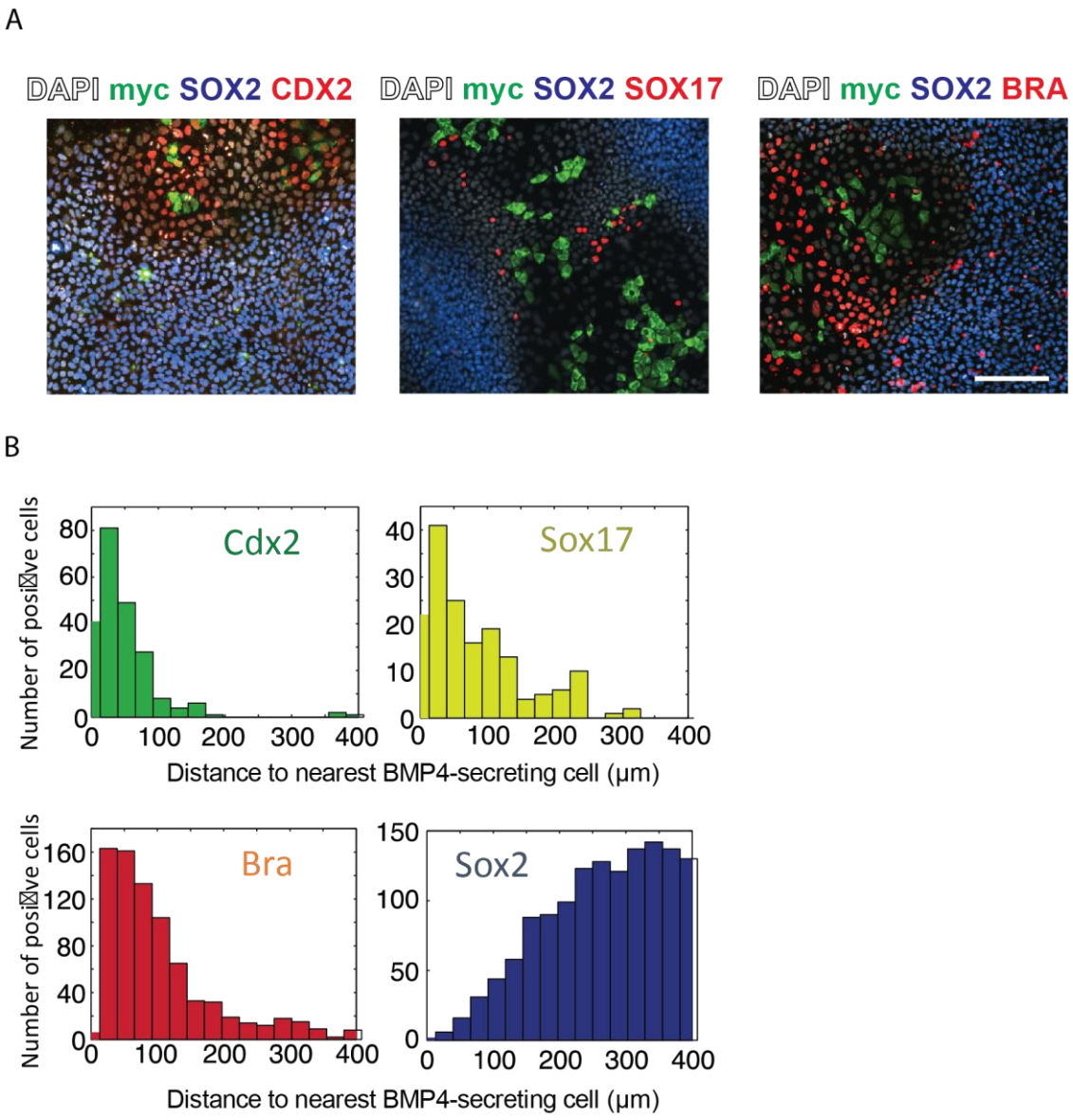

Figure 2.7: BMP4-Secreting Cells Induce the Expected Pattern of Germ Layer Markers

(A) TRE::xBMP4-myc cells were co-cultured with WT hESCs on glass surface. TRE::xBMP4-myc cells were induced with 0.2 μg ml^{-1} doxycycline to produce BMP4. The cells were stained for embryonic germ layer markers (SOX2 = epiblast/ectodermal fate; BRA = mesodermal fate; SOX17 = definitive endodermal fate; CDX2 = extraembryonic fate). Scale bars = 100 μm. (B) Quantification of embryonic germ layer markers as a function of distance from the nearest TRE::xBMP4-myc cell.

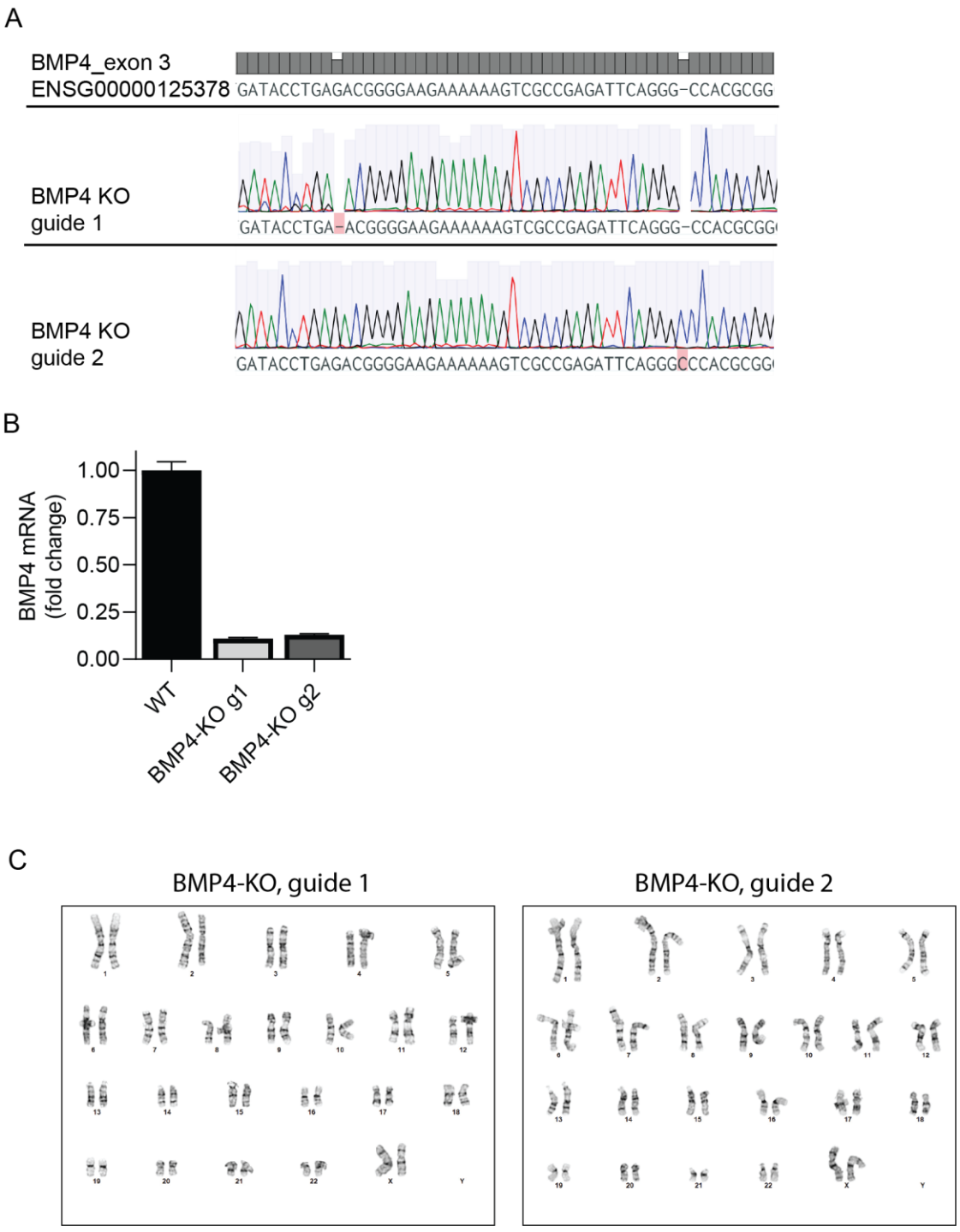

Figure 2.8: Generation of BMP4-KO Cell Lines

(A) Generation of two BMP4-KO hESC lines: Genomic sequencing demonstrates the location of the deletion (BMP4-KO guide 1) and insertion (BMP4-KO guide 2) point mutations at exon 3 of the BMP4 gene as a result of CRSPR/Cas9-mediated non-homologous end joining. (B) qPCR quantification of BMP4 mRNA in the BMP4-KO lines suggests homogeneous BMP4 knockout has occurred in both BMP4-KO lines. n = 3. Error bars = SD. (C) G-band karyotyping results of our engineered hESC lines show normal human female karyotypes.

A

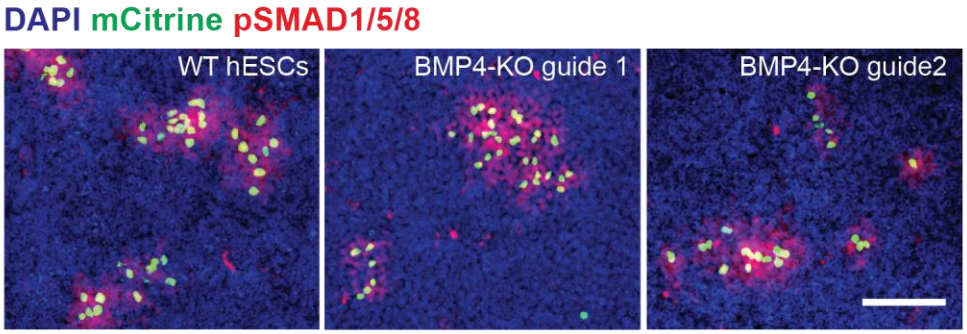

B

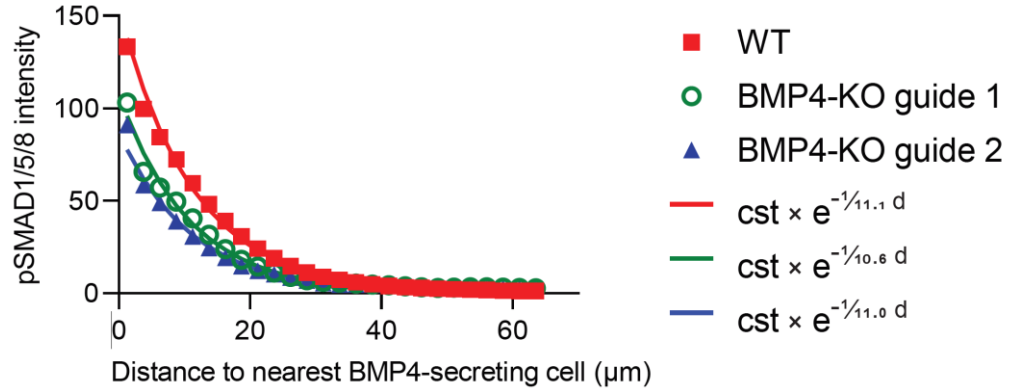

Figure 2.9: Dynamics of BMP4 Signaling

(A) pSMAD1/5/8 signaling propagation was similar in WT and BMP4-KO hESCs. TRE::xBMP4-myc; CAG::H2B-mCitrine cells were co-cultured with WT hESCs or BMP4-KO hESCs on filters. Doxycycline was added for 12 hrs. (B) Quantification of BMP4 signal propagation as a function of distance to the nearest BMP4-secreting cells. There was no significant difference between the range of pSMAD1/5/8 activation in BMP4-KO hESCs and WT hESCs. Exponential curves were fitted to the datapoints. The exponential function is described by the constant "cst" which is the prefactor of the exponent function and the spreading length (in μm) which characterizes the function's rate of decay. Error bars = SEM.

2.2 NOGGIN is Secreted Apically and Forms a Concentration Gradient

Since NOGGIN is expressed as a response to BMP4 (Etoc et al., 2016), we then asked whether NOGGIN propagated with the same characteristics as BMP4, i.e. basal secretion with short-ranged lateral propagation. Similar to the strategy we employed for studying BMP4 propagation, we generated an RUES2 line stably incorporating a transgene for doxycycline-dependent induction of epitope-tagged NOGGIN together with a constitutively expressed H2B-mCherry nuclear marker (Figure 2.1). The level of NOGGIN produced by these inducible NOGGIN-secreting cells was higher than that produced as a response to BMP4 stimulation (Etoc et al., 2016) (Figure 2.7). Compared to BMP4, in our induction assay on transwells, secreted NOGGIN could be detected at earlier time points. To our surprise, we found that V5-tagged NOGGIN was exclusively secreted to the apical media after 2-, 4- and 8-hr induction (Figure 2.8). As such, the ligand BMP4 and its inhibitor NOGGIN were secreted into opposite extracellular spaces.

We next examined the dynamics of NOGGIN transport within our model epiblast by seeding a low dilution of NOGGIN-producing cells in a background of WT-RUES2. We applied DOX for different durations to induce secretion of NOGGIN, followed by a brief 1 hr pulse of BMP4 presented to the basal media. Spatial domains of BMP4 activity were highlighted by pSMAD1/5/8 staining. As expected, NOGGIN-producing cells effectively prevented BMP4-dependent initiation of pSMAD1/5/8 autonomously and non-autonomously. The spatiotemporal range of NOGGIN inhibition was defined by the area of pSMAD1/5/8-negative hESCs surrounding the NOGGIN-producing cells (Figure 2.8). The range of inhibition extended from 13 μm (at 4 hrs) to 150 μm (at 24 hrs) (Figure 2.8).

Finally, we probed the concentration profile of NOGGIN away from a secreting source. To this end, we induced diluted NOGGIN-producing cells for a defined period of time (6 hrs) and then challenged the tissue globally via basal application of different concentrations of BMP4. As expected, NOGGIN's efficiency in counteracting pSMAD1/5/8 induced by basally-applied BMP4 was inversely proportional to BMP4 concentration: the inhibition rings around the NOGGIN-producing cells had decreasing radii as BMP4 concentration increased (Figure 2.9). This result demonstrates that the activity of NOGGIN away from a source was indeed graded.

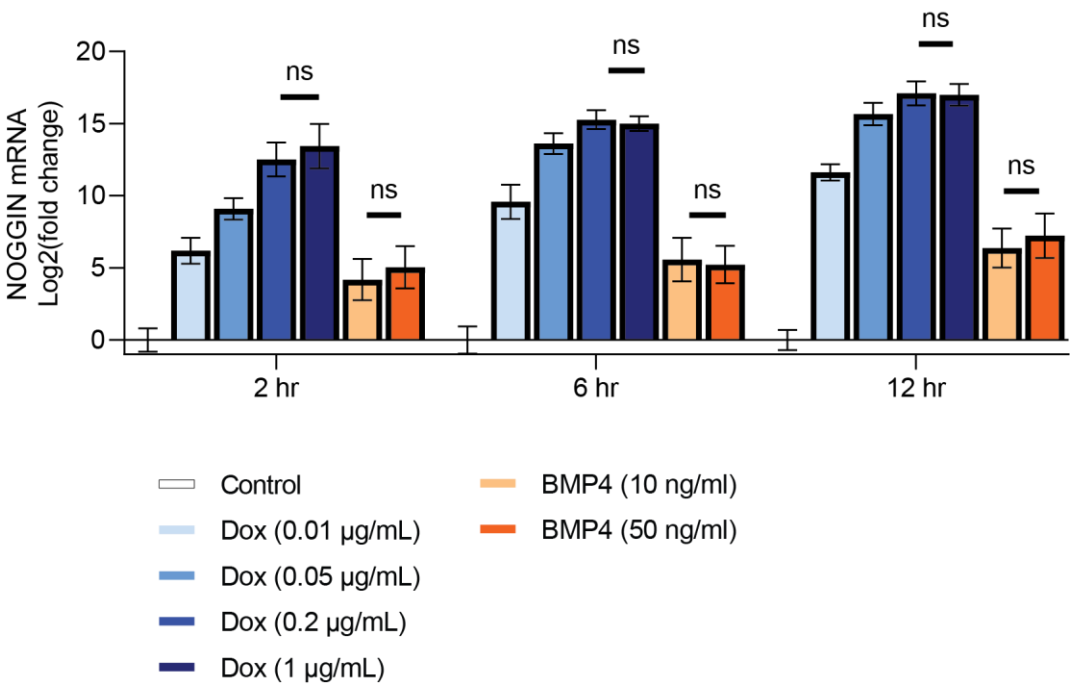

Figure 2.10: Comparison of NOGGIN mRNA Levels Induced by Dox Relative to Normal Physiological Levels Induced by BMP4

TRE::NOGGIN-V5 hESCs were cultured on filters and induced with varying concentrations of doxycycline or with recombinant BMP4. After indicated amounts of induction time, cells were collected for qPCR quantifying levels of NOGGIN mRNA. The level of NOGGIN mRNA produced was saturated at 0.2 µg ml^{-1} Doxycycline. n = 3. Error bars = SD.

Figure 2.11: NOGGIN Is Secreted Apically and Spreads from a Local Source

(A) NOGGIN was secreted to the apical media. TRE::V5-NOGGIN hESCs were cultured on filters to form confluent epithelia and induced to produce NOGGIN for 2, 4, 8, or 24 hrs. Media collected from the apical (AP) or basolateral (BL) chambers were collected and analyzed with Western blot. (B) The range of NOGGIN's inhibitory effects extended as a function of time. TRE::V5-NOGGIN hESCs; CAG::H2B-mCherry were diluted in a background of WT hESCs (ratio 1:200) and induced to secret NOGGIN for the specified times. Then, BMP4 (10 ng ml^{-1}) was applied basally for 1 hr. pSMAD1/5/8 labeling demarcated the range of NOGGIN inhibition. The yellow cells one seen in the panel at 0 hrs are NOGGIN secreting cells (nuclear label green) that are pSMAD-positive (red). Scale bars = 100 μm. (C) Quantification of NOGGIN inhibitory range as a function of time. The black vertical dashed lines indicate the point where the local slope of the fit changes (maximum of second derivative). Error bars = SEM.

A

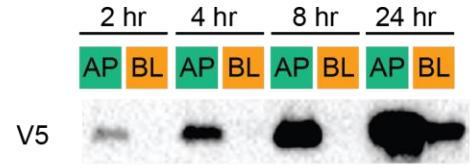
2 hr
4 hr
8 hr
24 hr
AP
BL
AP
BL
AP
BL
AP
BL
V5

B

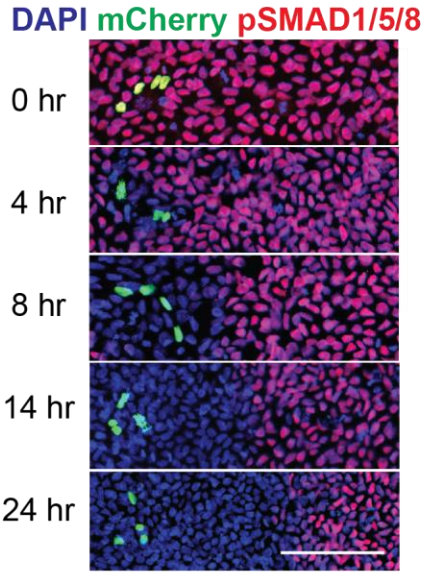
DAPI mCherry pSMAD1/5/8
0 hr
4 hr
8 hr
14 hr
24 hr

C

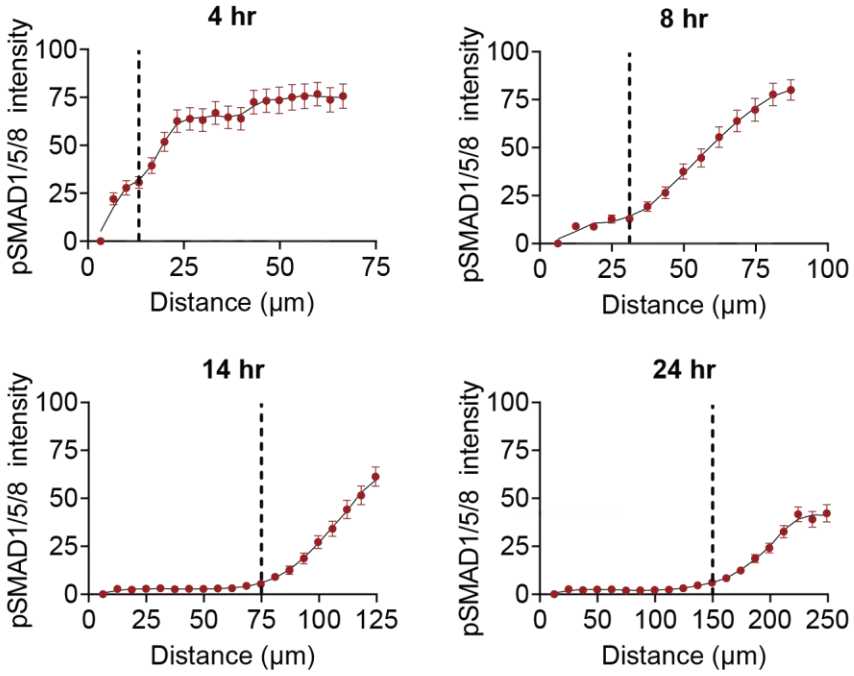
4 hr
8 hr
14 hr
24 hr
pSMAD1/5/8 intensity
Distance (μm)
0
25
50
75
100
125
150
200
250

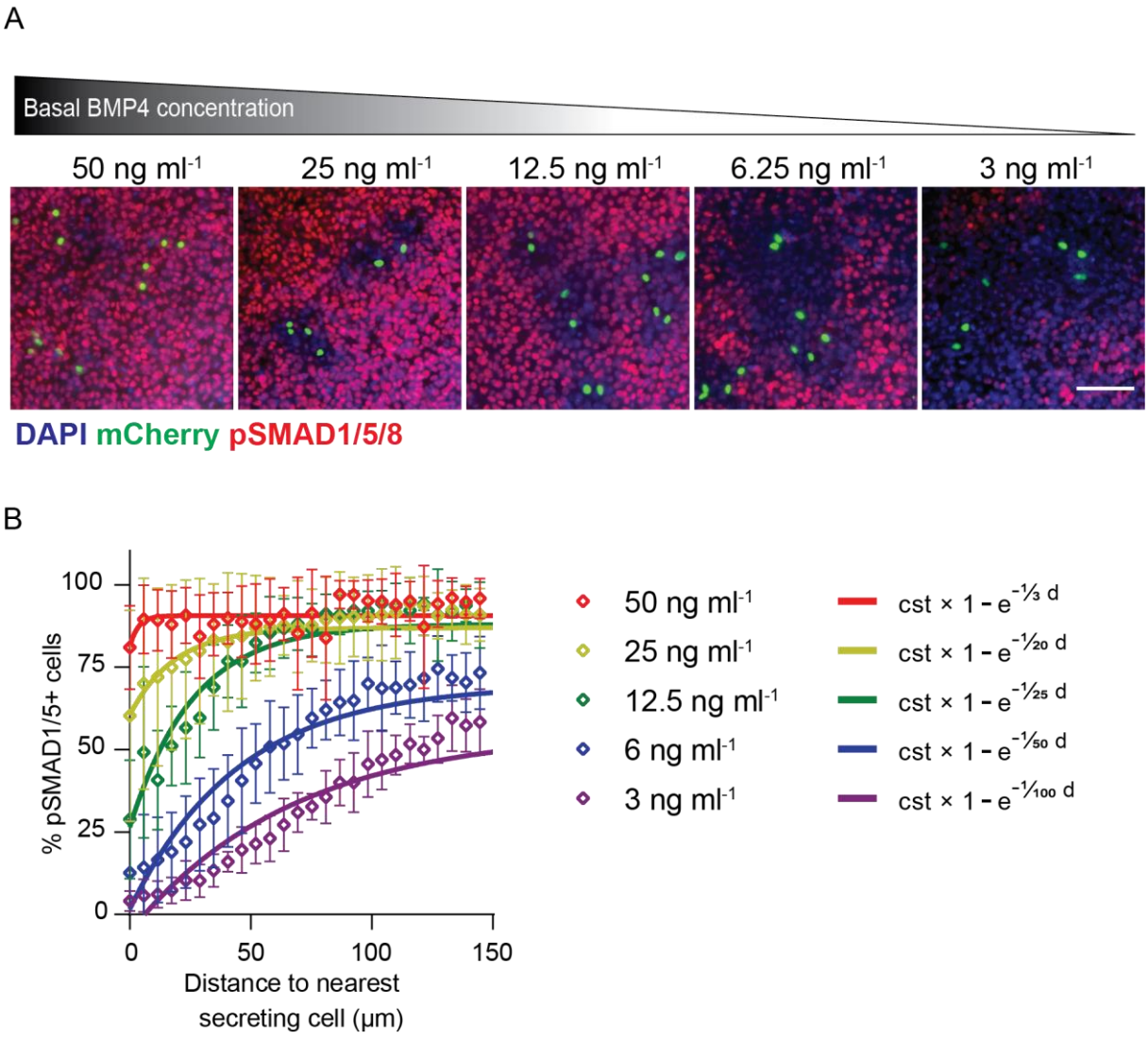

Figure 2.12: NOGGIN Activity away from the Source Is Graded

(A) NOGGIN inhibitory range as a function of BMP4 concentration. TRE::V5-NOGGIN hESCs were diluted in a background of WT hESCs (ratio 1:200) and induced to secret NOGGIN (8 hrs). Then, different concentrations of recombinant BMP4 was applied basally for 1 hr. The range of NOGGIN inhibition was inversely correlated with the concentration of BMP4. Scale bars = 100 µm. (B) Quantification of NOGGIN's efficacy in inhibiting pSMAD1/5/8 BMP4 concentration as a function of BMP4 concentration. Exponential curves were fitted to the datapoints. The exponential function is described by the constant "cst" which is the prefactor of the exponential function and the exclusion length (in µm). Error bars = SEM.

CHAPTER 3. INHIBITION OF BASAL BMP4 BY APICAL NOGGIN

3.1 Apically-Applied NOGGIN Can Inhibit Basally-Applied BMP4

That BMP4 and NOGGIN are secreted into different extracellular spaces is surprising since NOGGIN has to directly bind BMP4 in order to prevent its interaction with BMP receptors and block signaling. Where and how can two proteins, in different compartments separated by a diffusion barrier - the tight junctions, meet and interact? In order to address this question, we first set up a series of time-course Western blot analysis of cell lysates probing for pSMAD1/5/8 activation under different signaling conditions. Specifically, we recorded the level of pSMAD1/5/8 following a pulse or a sustained application of BMP4. The efficacy of apically-applied NOGGIN in inhibiting pSMAD1/5/8 was then compared to that of known BMP4 inhibitor LDN. As expected, a sustained basal application of BMP4 resulted in sustained pSMAD1/5/8 response, while a single short pulse of BMP4 generated a response that lasted 3 hrs (Figure 3.1A-B). Most strikingly, addition of NOGGIN in the apical compartment completely shut down ongoing BMP4 signaling within 2 hrs. Thus, NOGGIN trafficking from apical to basal occurs within a 2-hr window. pSMAD1/5/8 inhibition by apical NOGGIN occurred slower compared to inhibition by the small compound inhibitor LDN, and yet faster than when BMP4 was removed after a pulse (Figure 3.1C-D). Moreover, NOGGIN's inhibitory effect was maintained for up to 3 hrs after NOGGIN washout (Figure 3.1E). This result is consistent with previous report that NOGGIN binds strongly to heparan sulfate proteoglycans on the cell surface (Paine-Saunders et al., 2002).

To independently control for physiological morphogen levels and kinetics, we tested the efficacy of NOGGIN inhibition in a context of BMP4 expressing cells. BMP4-producing cells, diluted in

a background of WT-RUES2, were induced to secret the ligand. The epithelium was then challenged with various concentrations of recombinant NOGGIN, applied apically or basally. While basally-applied NOGGIN was most effective at inhibiting BMP4 signaling, apically-applied NOGGIN was also capable of switching off sustained BMP4 signaling in a dose-dependent manner (Figure 3.2A-B). Analysis by Western blot confirms that apical NOGGIN rapidly quenches the response to a preceding pulse of BMP4 (Figure 3.2C).

Overall, these experiments demonstrate that apically-applied NOGGIN functionally and efficiently inhibits basal BMP4, and with similar kinetics as basal BMP4 washout. Moreover, retention of the inhibitory effect after NOGGIN washout suggests mechanisms of internalization and trafficking of NOGGIN from the apical to basal compartment where BMP4 is present.

Figure 3.1: Apically-Delivered Recombinant NOGGIN Inhibited Basally-Applied Recombinant BMP4

(A) 1-hr pulse application of recombinant BMP4 (10 ng ml^{-1}) elicited a pulse of pSMAD1/5/8 response that lasted 3 hours. (B) Sustained application of recombinant BMP4 (10 ng ml^{-1}) elicited a sustained pSMAD1/5/8 response. (C) This pSMAD1/5/8 response was rapidly inhibited by LDN (a BMP inhibitor that blocks the transcriptional activity of BMPR1 receptors ALK2 and ALK3) (0.1 μM). (D) This pSMAD1/5/8 response was also inhibited by apically-applied recombinant hNOGGIN (250 ng ml^{-1}) (right). Horizontal axes indicate elapsed time following BMP4 application. (E) NOGGIN inhibitory effect on pSMAD1/5/8 was maintained for up to 3 hours after NOGGIN washout. Pre-treatment of hESCs with apical NOGGIN for (250 ng ml^{-1}; 2 hr) was followed by different time intervals before basal BMP4 (10 ng ml^{-1}; 1 hr) was added. The interval between each addition of BMP4 increased by 1 hr with each iteration.

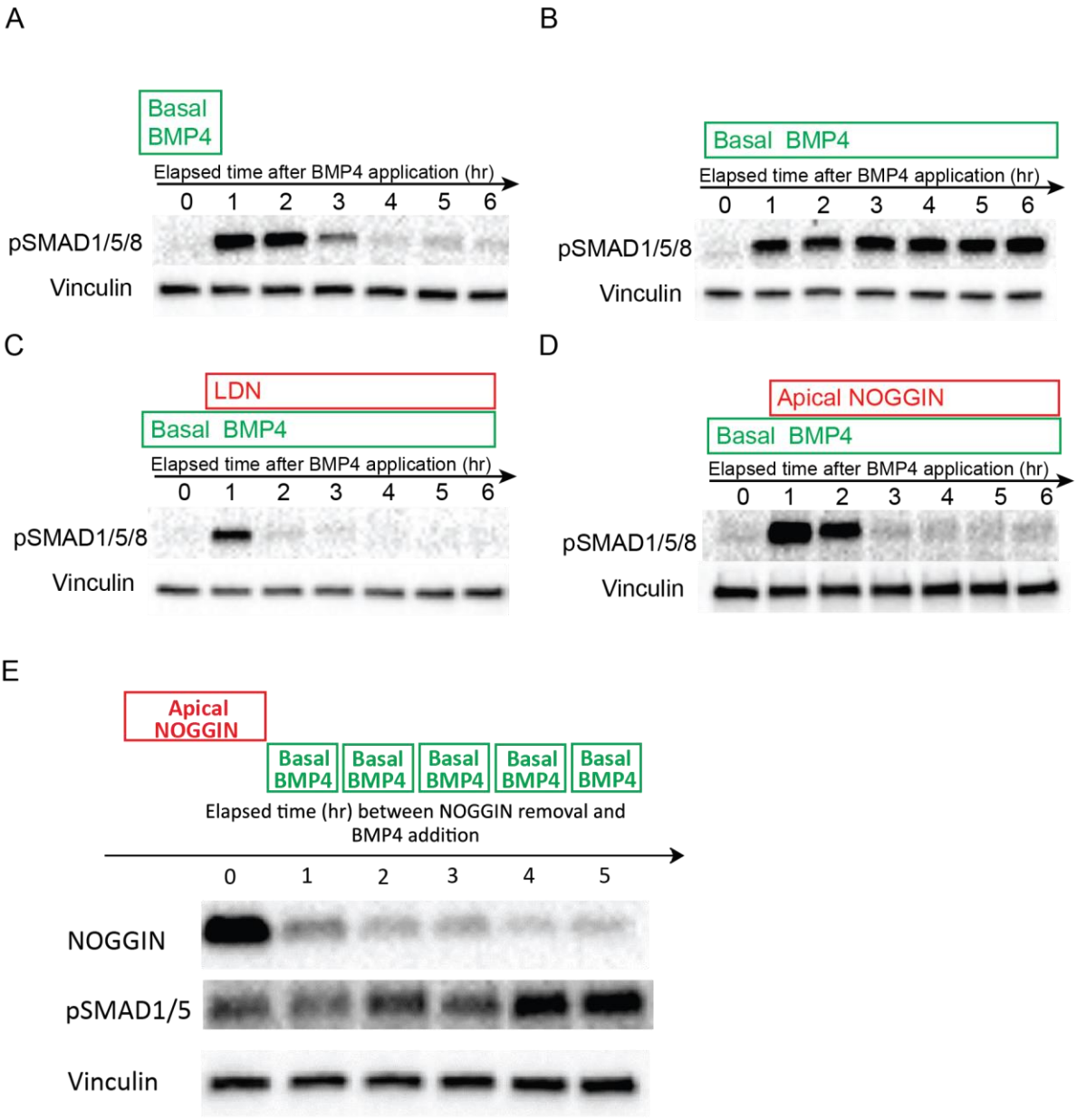
A
Basal
BMP4
Elapsed time after BMP4 application (hr)
0 1 2 3 4 5 6
pSMAD1/5/8
Vinculin
B
Basal BMP4
Elapsed time after BMP4 application (hr)
0 1 2 3 4 5 6
pSMAD1/5/8
Vinculin
C
LDN
Basal BMP4
Elapsed time after BMP4 application (hr)
0 1 2 3 4 5 6
pSMAD1/5/8
Vinculin
D
Apical NOGGIN
Basal BMP4
Elapsed time after BMP4 application (hr)
0 1 2 3 4 5 6
pSMAD1/5/8
Vinculin
E
Apical
NOGGIN
Basal
BMP4
Basal
BMP4
Basal
BMP4
Basal
BMP4
Basal
BMP4
Elapsed time (hr) between NOGGIN removal and
BMP4 addition
0 1 2 3 4 5
NOGGIN
pSMAD1/5
Vinculin

Figure 3.2: Secreted NOGGIN Inhibited BMP4 Signaling In The Epithelium

(A) Apically-applied recombinant hNOGGIN inhibited BMP4 signaling within the epithelium. TRE::xBMP4-myc hESCs; CAG::H2B-mCitrine were mixed with WT hESCs (ratio 1:200) and induced to produce BMP4 for 22 hr. Different concentrations of recombinant hNOGGIN was added to the layer apically or basally for 2 hr. 250 ng ml^{-1} NOGGIN efficiently inhibited autonomous pSMAD1/5/8 in BMP4-secreting cells. Scale bar = 100 μm. (B) Quantification of inhibitory efficacies of apically- and basally-applied recombinant hNOGGIN. Exponential curves were fitted to the datapoints. The exponential function is described by the constant "cst" which is the prefactor of the exponent function and the spreading length (in μm) which characterizes the function's rate of decay. Error bars = SEM. (C) pSMAD1/5/8 induced by basally-applied recombinant BMP4 was inhibited by apically- and basally-applied recombinant NOGGIN. WT hESCs were induced by a 1.5-hr pulse of BMP4 (10 ng ml^{-1}). Subsequently, BMP4 was washed out and simultaneously NOGGIN (250 ng ml^{-1}) was applied apically or basally for 2 hr. Cell lysates were collected to analyze with Western blot. (The first experiment is a control with no added NOGGIN).

A

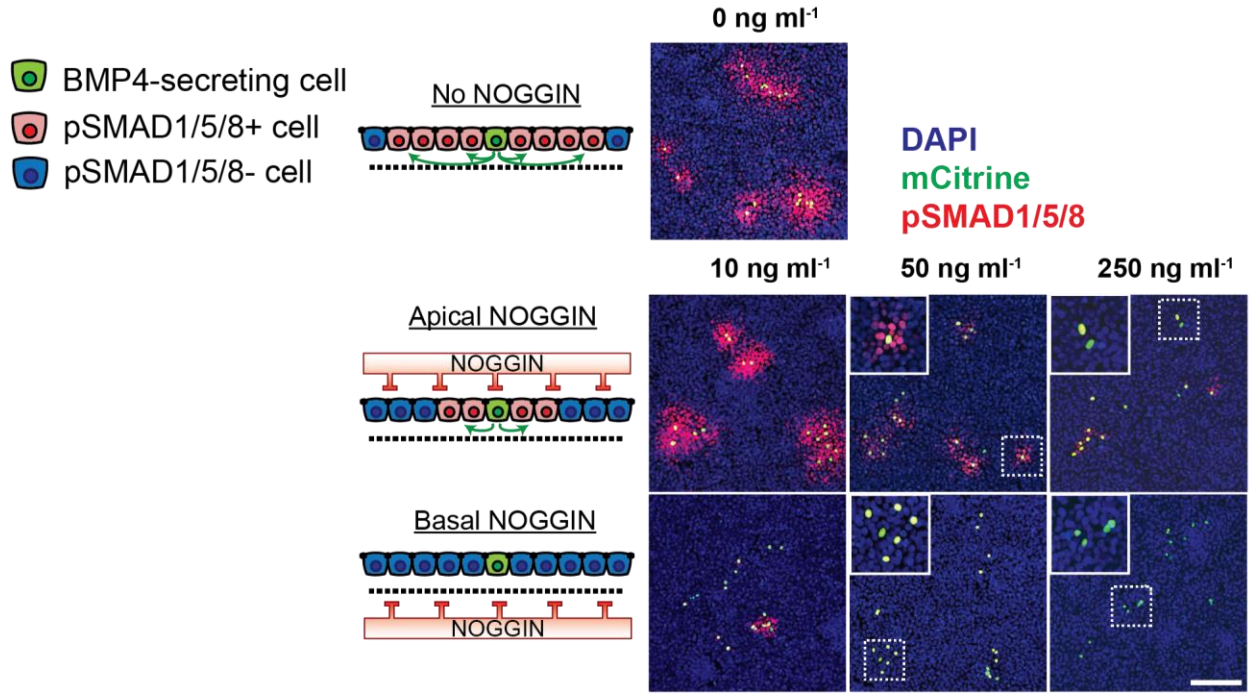
BMP4-secreting cell
pSMAD1/5/8+ cell
pSMAD1/5/8- cell
No NOGGIN
Apical NOGGIN
NOGGIN
Basal NOGGIN
NOGGIN
0 ng ml-1
10 ng ml-1
50 ng ml-1
250 ng ml-1
DAPI
mCitrine
pSMAD1/5/8

B

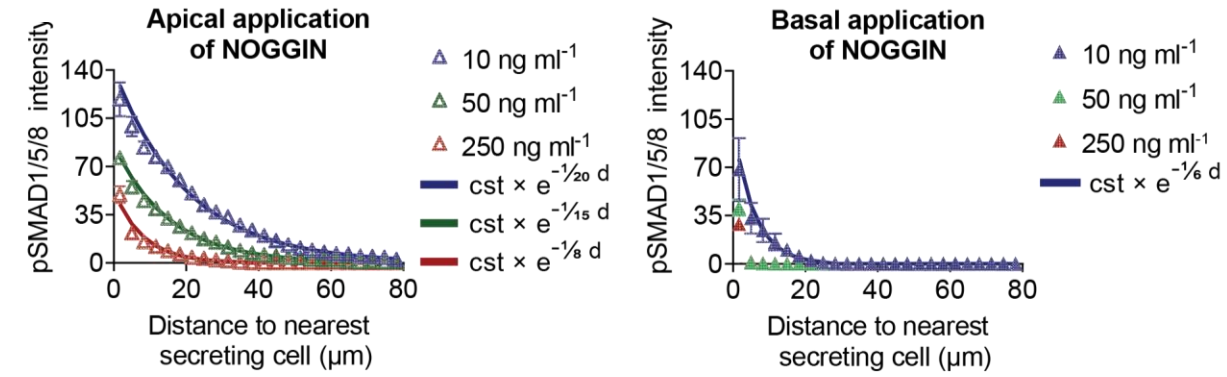
Apical application of NOGGIN
pSMAD1/5/8 intensity
140
105
70
35
0
0
20
40
60
80
Distance to nearest secreting cell (μm)
10 ng ml-1
50 ng ml-1
250 ng ml-1
cst × e-1/20 d
cst × e-1/15 d
cst × e-1/8 d
Basal application of NOGGIN
pSMAD1/5/8 intensity
Distance to nearest secreting cell (μm)
10 ng ml-1
50 ng ml-1
250 ng ml-1
cst × e-1/6 d

C

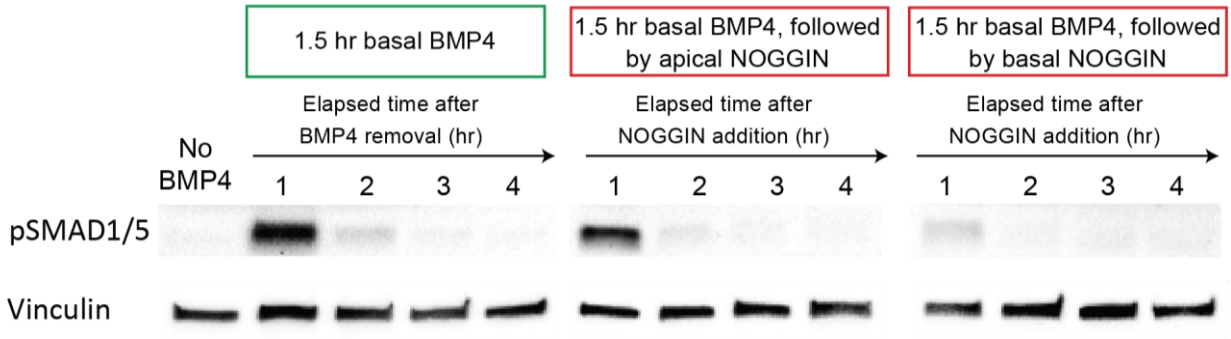
1.5 hr basal BMP4
1.5 hr basal BMP4, followed by apical NOGGIN
1.5 hr basal BMP4, followed by basal NOGGIN
Elapsed time after BMP4 removal (hr)
Elapsed time after NOGGIN addition (hr)
Elapsed time after NOGGIN addition (hr)
No BMP4
1
2
3
4
pSMAD1/5
Vinculin

3.2 NOGGIN Diffuses Across the Apical Compartment

We hypothesized that diffusion in the extracellular medium at the apical side was a major mechanism for NOGGIN's long-range propagation in the epithelium. To test this, we customized a glass-bottomed microfluidic culture platform, which supported controlled perfusion flow rates, and applied apical laminar flow (Material and Methods, Figure 3.3). This microfluidic system supported the epithelialization of hESCs while maintaining their pluripotency at both low and high flow rates (Figure 3.4). We also confirmed that both glass and filter substrates led to similar BMP4 signaling range and spreading dynamics (Figure 3.5).

We utilized this microfluidic device to validate our hypothesis by demonstrating that by briefly switching a flow of 10 µl/hr to a high flow rate of 1000 µl/hr, we can wash away secreted NOGGIN at the apical side and lessen or eliminate its inhibition. Since we have demonstrated earlier that BMP4 was basally secreted, application of an apical flow should not perturb its local spreading. As a control, we diluted BMP4 secreting cells into the WT-RUES2 epithelium at a ratio of 1:200, which allowed us to quantify the spread of pSMAD1/5/8 activity around isolated BMP4 sources (Figure 3.6A-B). After 6 hrs of doxycycline induction, no difference in BMP4 signaling ranges between low and high flow regimes was detected, except for an increase in the amplitude of pSMAD1/5/8 intensity, in the high flow condition, consistent with a washout of endogenous inhibitors induced by BMP4 stimulation (Etoc et al., 2016). This minimal effect of flow on BMP4 lateral spreading is consistent with BMP4's basal secretion and its uptake in nearby cells.

Increasing the ratio of BMP4-secreting cells in WT-RUES2 to 1:10 led to uniform expression of pSMAD1/5/8 in both low and high flow conditions (Figure 3.6C). However, when a small number of NOGGIN-secreting cells (1:500) were added, this pSMAD1/5/8 expression was inhibited at low flow rate (Fig 4D). In contrast, high apical flow showed active BMP4 signaling only in cells a distance away from NOGGIN-secreting cells (Figure 3.7). Thus, high apical flow reduced NOGGIN inhibition spread consistent with its apical secretion and activity when apically supplied. The persistence of BMP4 inhibition specifically around the NOGGIN-secreting cells in the high flow condition argues that the flow was neither generically activating BMP4 signaling by another route such as shear stress, nor washing out some unknown inhibitor. Moreover, the shear rate on the cells at the highest flow is 0.03 dynes/cm^2 which is 30 times less than the lowest value that elicits a response in endothelial cells (Ballermann et al., 1998). The simplest explanation of our data is thus that the flow washed away NOGGIN and precluded its transport to the cells furthest from the NOGGIN secreting cells. Overall, these experiments concur that NOGGIN traveled in the apical extracellular space while BMP4 used the basolateral space.

Figure 3.3: Schematics of the Microfluidic Device

A PDMS layer (red), cast from a custom 3D-printed mold, was sandwiched between two glass slides to form a tightly-sealed chamber. Chamber dimensions were 55 mm x 2 mm x 0.5 mm. The top slide had drilled inlet and outlet holes. The culture chamber and tubing were securely fastened by a custom clamping device. (A) Top view. (B) Side view. (C) The calculated Reynold's numbers for the two flow conditions showed that the flow inside the chamber was laminar.

A

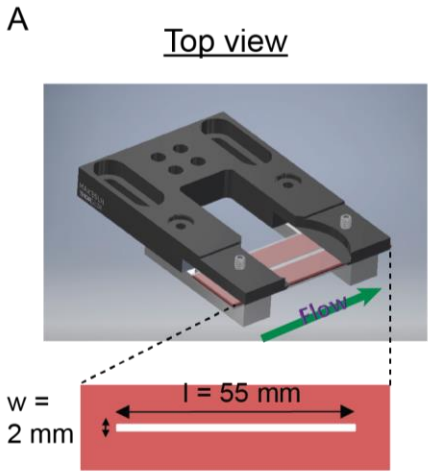

B

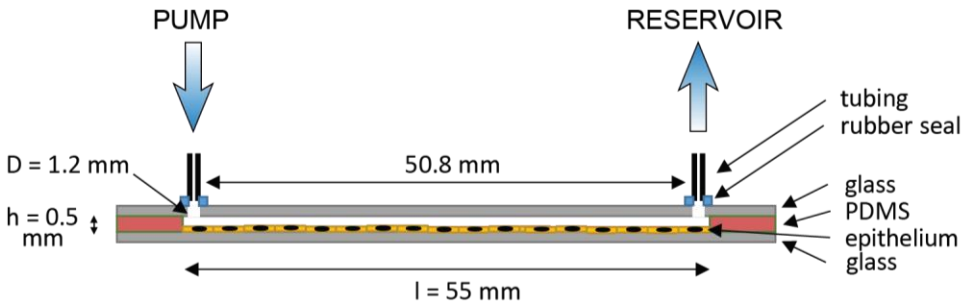

C

$$\boldsymbol{Re} = \frac{Q \cdot D_H}{\nu \cdot A}$$

$$Q_{\text{low flow}} = 10\ \mu\text{l h}^{-1} = 0.00278\ \text{mm}^3\,\text{s}^{-1}$$
$$Q_{\text{high flow}} = 1000\ \mu\text{l h}^{-1} = 0.278\ \text{mm}^3\,\text{s}^{-1}$$

$$D_H = \frac{4 \cdot w \cdot h}{2(w+h)} = \frac{4 \cdot 2\ \text{mm} \cdot 0.5\ \text{mm}}{2(2\ \text{mm} + 0.5\ \text{mm})} = 0.8\ \text{mm}$$

$$\nu_{\text{water, 37oC}} = 0.6959\ \text{mm}^2\,\text{s}^{-1}$$
$$A = w \cdot h = 2\ \text{mm} \cdot 0.5\ \text{mm} = 1\ \text{mm}^2$$

$$\boldsymbol{Re}_{\text{low flow}} = \frac{Q \cdot D_H}{\nu \cdot A} = \frac{0.00278\ \text{mm}^3\,\text{s}^{-1} \cdot 0.8\ \text{mm}}{0.6959\ \text{mm}^2\,\text{s}^{-1} \cdot 1\ \text{mm}^2} = 0.00320$$
$$\boldsymbol{Re}_{\text{high flow}} = \frac{Q \cdot D_H}{\nu \cdot A} = \frac{0.278\ \text{mm}^3\,\text{s}^{-1} \cdot 0.8\ \text{mm}}{0.6959\ \text{mm}^2\,\text{s}^{-1} \cdot 1\ \text{mm}^2} = 0.320$$

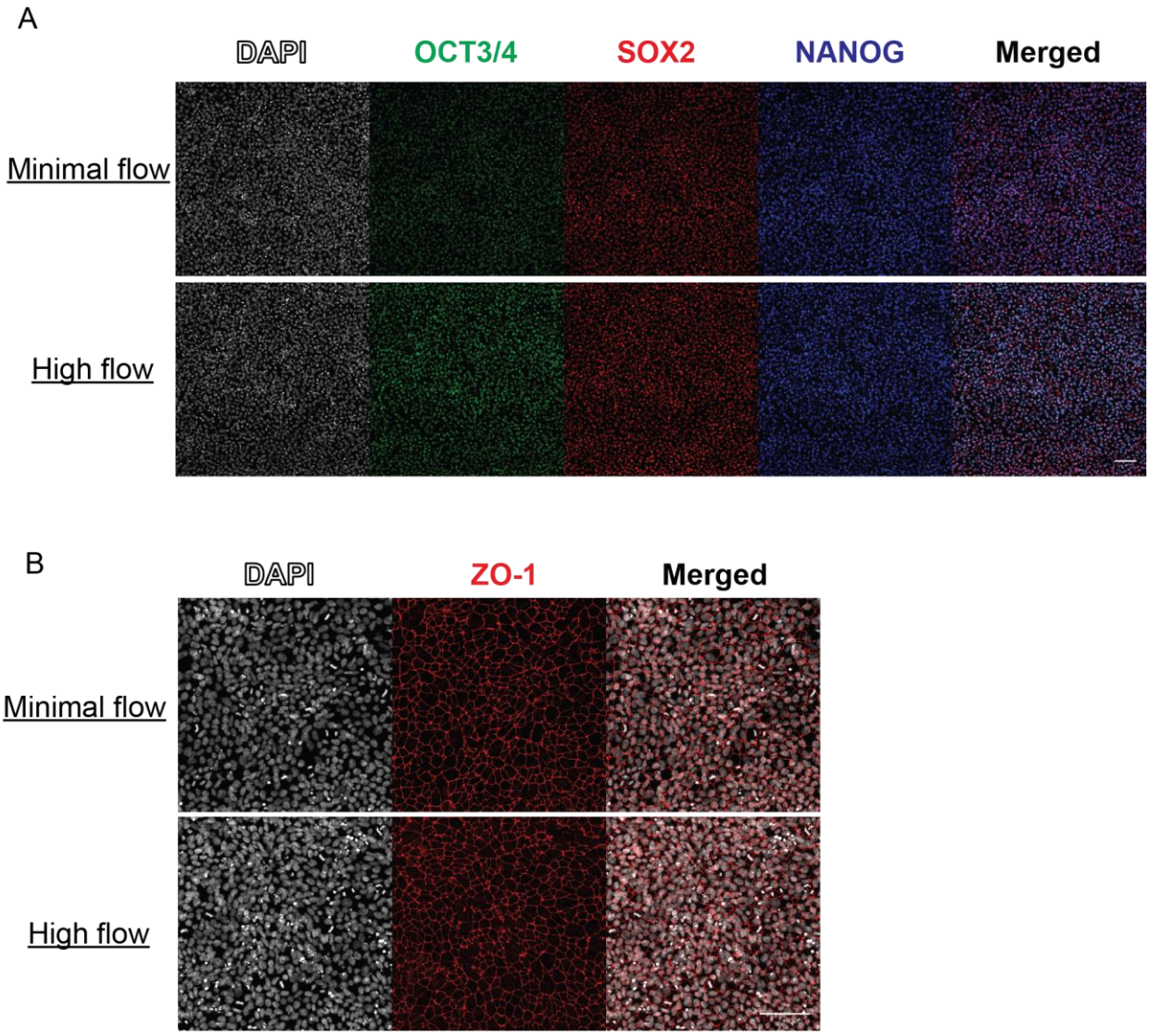

Figure 3.4: Validation of the Cell Culture Condition Within the Microfluidic Device

(A) hESCs maintained pluripotency under minimal flow in microfluidic culture. After hESCs were cultured on glass-bottomed microfluidic chamber under minimal flow (10 µl hr^{-1}) overnight, the flow rate was increased to 1000 µl hr^{-1} (High flow) for 9 hr. Cells in the microfluidic chamber were stained for pluripotency markers OCT3/4, SOX2, and NANOG. (B) Cells were also stained for tight junction markers ZO-1.

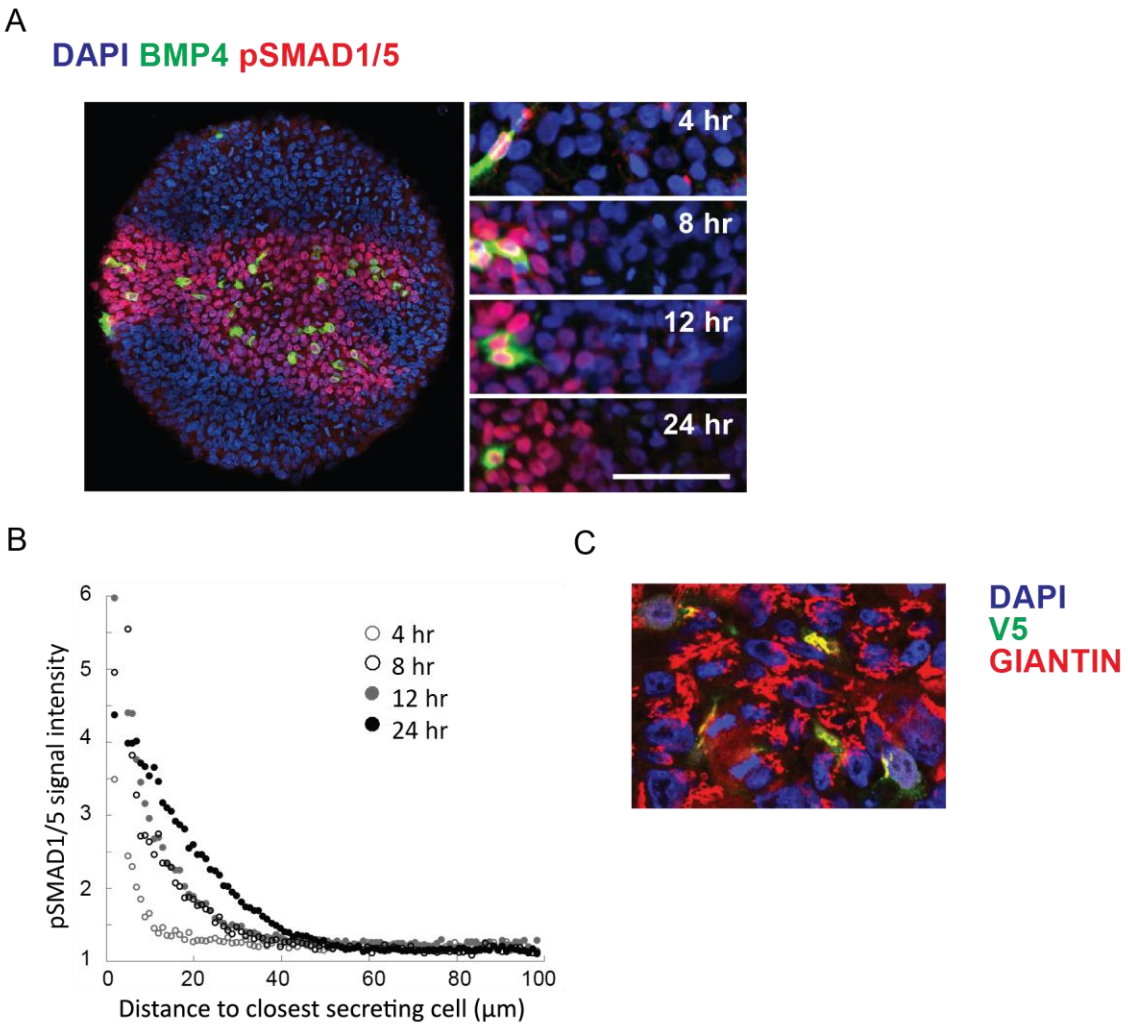

Figure 3.5: BMP4 Signaling Propagated on Glass Substrate

(A) TRE::xBMP4-myc cells were co-cultured with WT hESCs (ratio 1:200) on glass micropatterned chip. The cells were induced to produce BMP4 for the specified durations. pSMAD1/5/8 immunolabeling defined the range of BMP4 signaling. Scale bars = 100 µm. (B) Quantification of BMP4 signaling propagation as a function of time on glass substrates. The rate of spreading was comparable to cells on filters in Fig 1E. (C) Intense V5 labeling overlapping with Golgi marker GIANTIN (Linstedt and Hauri, 1993) indicated TRE::hNOGGIN-V5 cells.

Figure 3.6: Apical Flow Did Not Affect BMP4 Signal Propagation

(A) A mixture of TRE::BMP4-myc; CAG::H2B-mCitrine and WT hESCs (ratio 1:500) was cultured overnight in microfluidic chambers. For all experiments in this figure, cells were induced to produce BMP4 under minimal (10 μl hr^{-1}) or high apical flow (1000 μl hr^{-1}) conditions for 6 hrs, before being stained for pSMAD1/5/8. (B) Quantification of the effect of apical flow on BMP4 signal propagation. Exponential curves were fitted to the datapoints. The exponential function is described by the constant "cst" which is the prefactor of the exponent function and the spreading length (in μm) which characterizes the function's rate of decay. Error bars = SEM. (C) Epithelia with a 1:10 ratio of BMP4 secreting to naive cells exhibited homogenous pSMAD1/5/8 activation under both minimal and high flow conditions. Error bars = SEM. Scale bars = 100 μm.

A

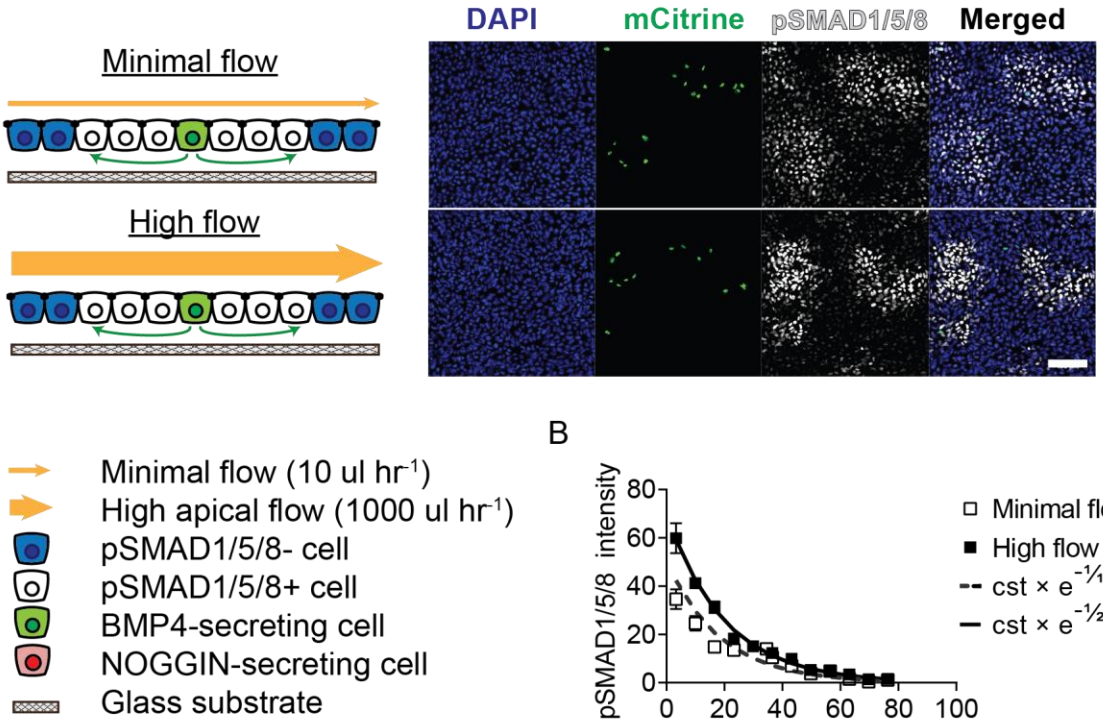
DAPI
mCitrine
pSMAD1/5/8
Merged
Minimal flow
High flow
Minimal flow (10 ul hr-1)
High apical flow (1000 ul hr-1)
pSMAD1/5/8- cell
pSMAD1/5/8+ cell
BMP4-secreting cell
NOGGIN-secreting cell
Glass substrate

B

pSMAD1/5/8 intensity
80
60
40
20
0
0
20
40
60
80
100
Distance to nearest secreting cell (μm)
Minimal flow
High flow
cst × e-1/19 d
cst × e-1/20 d

C

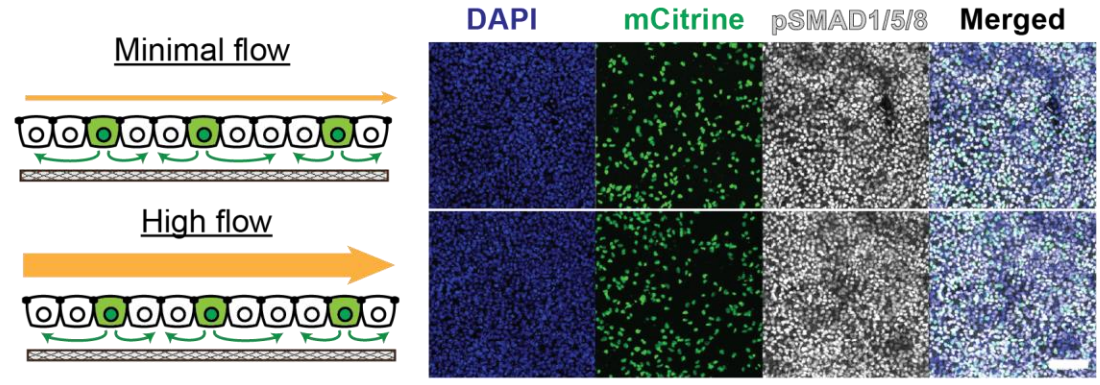
DAPI
mCitrine
pSMAD1/5/8
Merged
Minimal flow
High flow

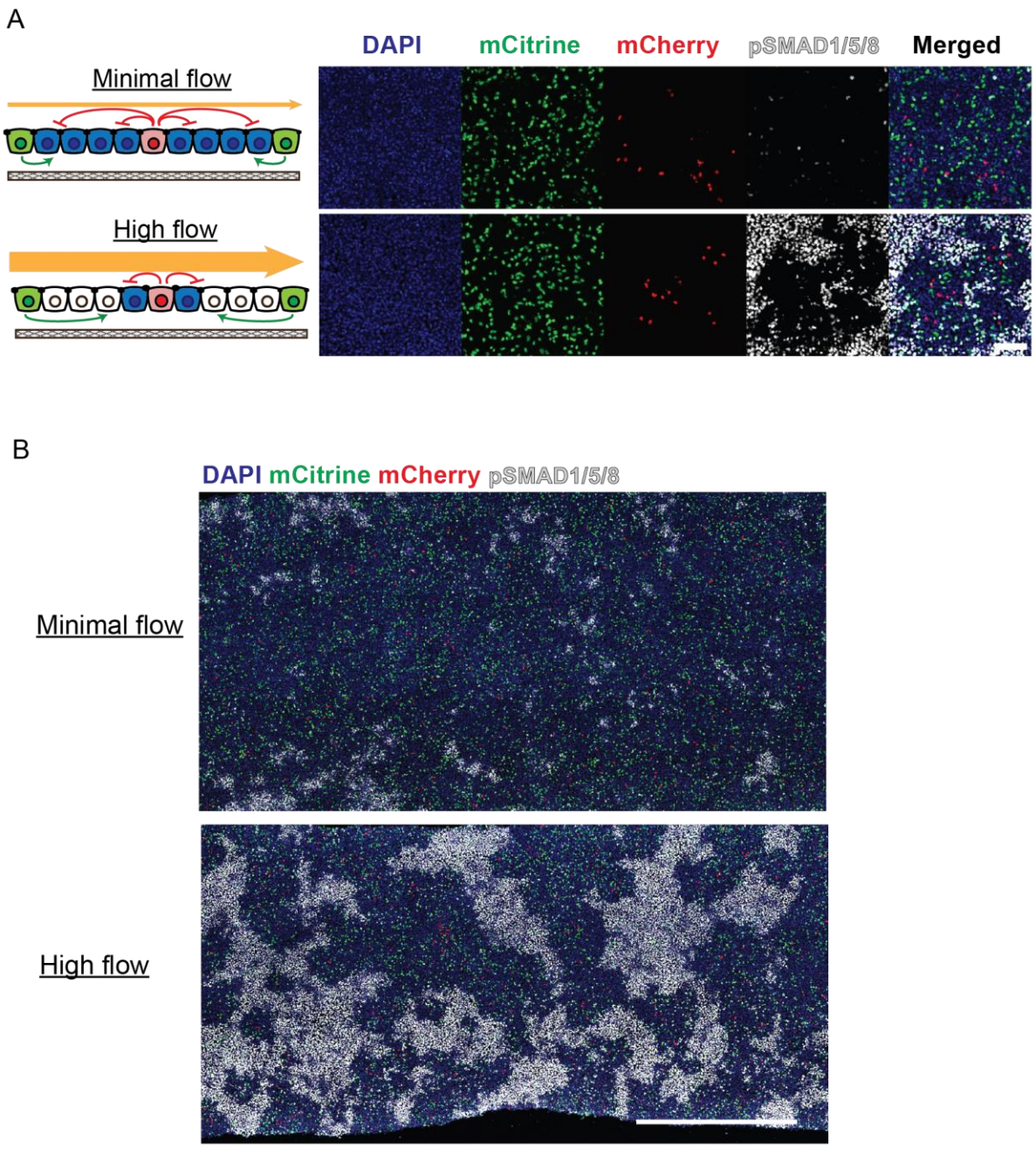

Figure 3.7: Apical Flow Perturbed NOGGIN Inhibition in the Epithelium

(A) High apical flow perturbed NOGGIN inhibition. A mixture of TRE::V5-NOGGIN; CAG::H2B-mCherry, TRE::BMP4-myc; CAG::H2B-mCtrine, and WT hESCs (ratio 1:50:500) was cultured in microfluidic chambers. High apical flow perturbed NOGGIN's long-range inhibitory effects. Error bars = SEM. Scale bars = 100 μm. (B) The epithelium within the microfluidic chamber corresponding to the data shown in Figure 4D. A wider view of the epithelium showed the differences in pSMAD1/5/8 response as related to different patterns of distribution of and degrees of proximity to the TRE::xBMP4-myc; CAG::H2B-mCitrine and TRE::hNOGGIN-V5; CAG::H2B-mCherry. Scale bar = 1000 μm.

CHAPTER 4. NOGGIN ENDOCYTOTIC ROUTE

4.1 NOGGIN's Subcellular Localization

To further examine how apically-spreading NOGGIN protein trafficked intracellularly to inhibit BMP4, we mixed a small number of NOGGIN-secreting with WT-RUES2 (1:100) and assessed the subcellular localization of NOGGIN throughout the layer by staining the V5 tag after 8 hrs of induction followed by 1 hr of basal BMP4 application (Figure 4.1A-B). As expected for secreting cells, high concentration of NOGGIN was found in the golgi (Supp Fig 5E). pSMAD1/5/8 expression delineated the range of NOGGIN activity in surround cells (Fig 5A-B). Unexpectedly, however, in receiving cells, NOGGIN was mostly found at the basolateral domain. Quantification of NOGGIN localization in the Z plane indicated that NOGGIN consistently localized below tight junctions as demarcated by ZO-1 labeling (Figure 4.1C). This NOGGIN lateral accumulation tightly overlapped with the expression patterns of BMPR1a and BMPR2 (Figure 4.2A-B). In addition to labeling the baso-lateral domain, NOGGIN immunostaining also appeared as discrete puncta of various sizes, dispersed in the cytoplasm, indicative of endocytic vesicles in the apical pole of the cells, both at and below the level of tight junction marker ZO-1 (Figure 4.2C). Taken together, our results suggest that following apical secretion from the source, NOGGIN enters receiving cells on the apical side, trafficks through endocytotic vesicular compartments, and ultimately reaches the basolateral side near BMP receptors.

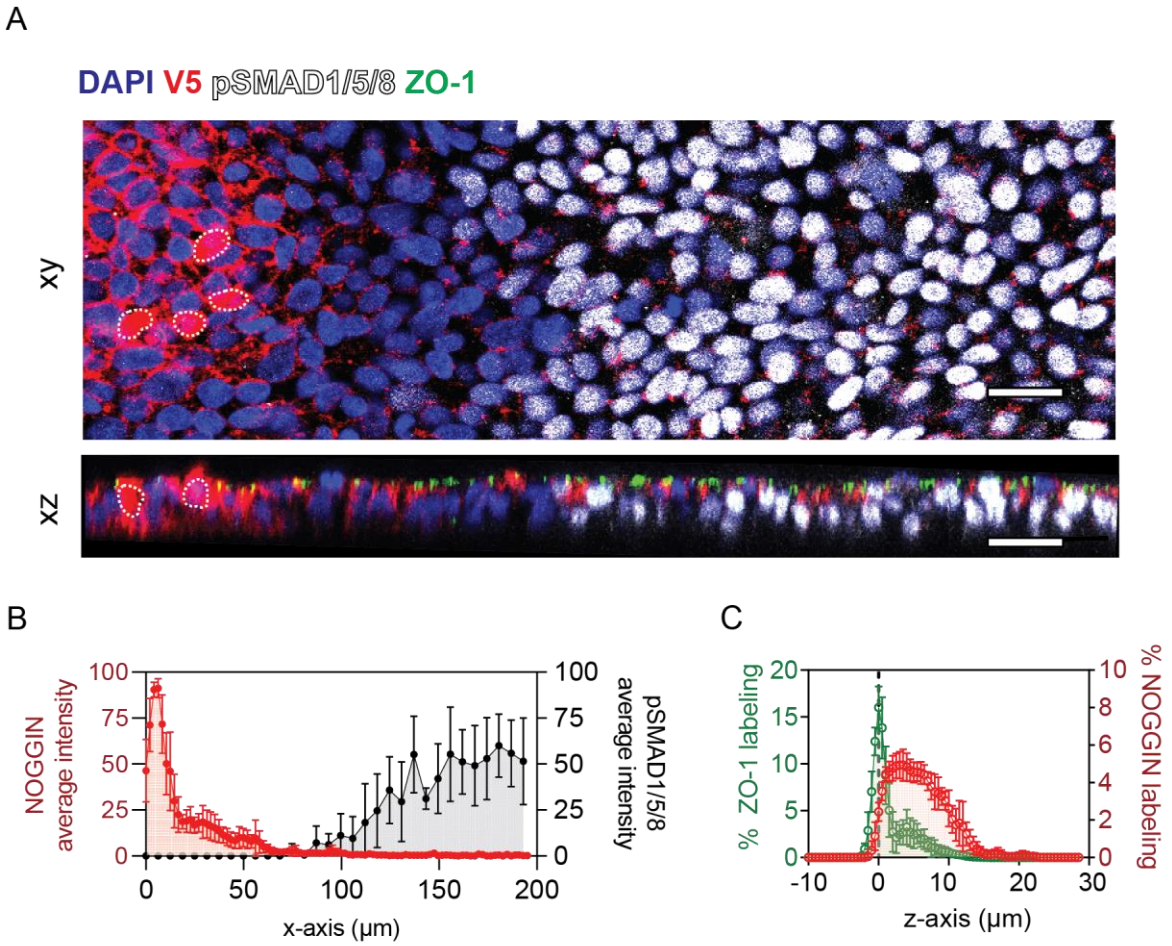

Figure 4.1: NOGGIN Spread to Neighboring Cells away from Secreting Cells and Was Detected Laterally Beneath Tight Junctions

(A) A small number of TRE::V5-NOGGIN cells were co-cultured with WT hESCs on filter. Cells were induced to produce NOGGIN for 8 hrs before BMP4 (10 ng ml^{-1}) was applied basally for 1 hr. NOGGIN immunolabeling was done with α-V5 antibodies. White dashed outlines indicate NOGGIN-secreting cells. Top (xy): confocal image of the epithelium through a single z-plane. Bottom (xz): sagittal (z-plane) view of the same epithelium. Scale bars = 25 μm. (B) Quantification of NOGGIN and pSMAD1/5/8 average pixel intensity profiles relative to each other along the x-axis. (The peak of NOGGIN intensity correlates with the location of a NOGGIN-secreting cell.) As NOGGIN intensity dropped off, pSMAD1/5/8 intensity increased. Error bars = SD. (C) Quantification of NOGGIN distribution along the z-axis with respect to ZO-1. NOGGIN localized at and below the level of tight junctions. Error bars = SD.

Figure 4.2: NOGGIN Co-Localized with BMPR and Was Detected as Puncta in Receiving Cells

(A) Sagittal (z-plane) view showing NOGGIN co-localizing with BMPR1a and BMPR2. TRE::V5-NOGGIN cells were co-cultured with TRE::BMPR1A-Myc or TRE::BMPR2-HA hESCs on filter (ratio 1:100). Cells were induced to express NOGGIN and BMPR1A/BMPR2 for 24 hrs. BMPR1A and BMPR2 labeling was detected by α-Myc antibodies and α-HA antibodies, respectively. Subsequently, NOGGIN-BMPR co-localization was analyzed in cells at least 5-cell-diameter away from NOGGIN-producing cells. (B) Quantification of the overlap of BMPR1a (left axis, purple) and BMPR2 (right axis, green) with NOGGIN. NOGGIN expression profile was used as a reference to determine the relative z-position. Error bars = SD. (C) Sagittal (z-plane) view showing NOGGIN localization in the epithelium. TRE::V5-NOGGIN cells were co-cultured with WT hESCs (ratio 1:200). Cells were induced to express NOGGIN for 24 hrs. Subsequently, NOGGIN localization was analyzed in cells 5-cell-distance away from NOGGIN-producing cells. Zoom-out panels show transverse views at the corresponding z-position. NOGGIN appeared as puncta (white arrows) at and below tight junction levels. Scale bars = 25 μm.

A

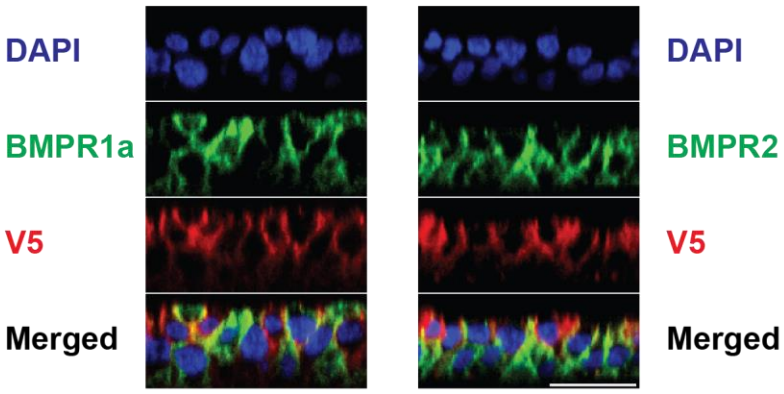
DAPI
BMPR1a
V5
Merged
DAPI
BMPR2
V5
Merged

B

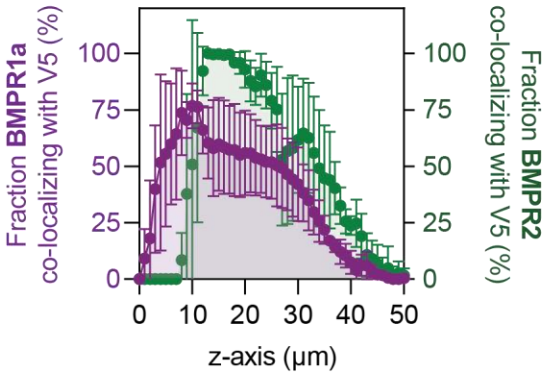
Fraction BMPR1a co-localizing with V5 (%)
Fraction BMPR2 co-localizing with V5 (%)
100
75
50
25
0
0 10 20 30 40 50
z-axis (μm)

C

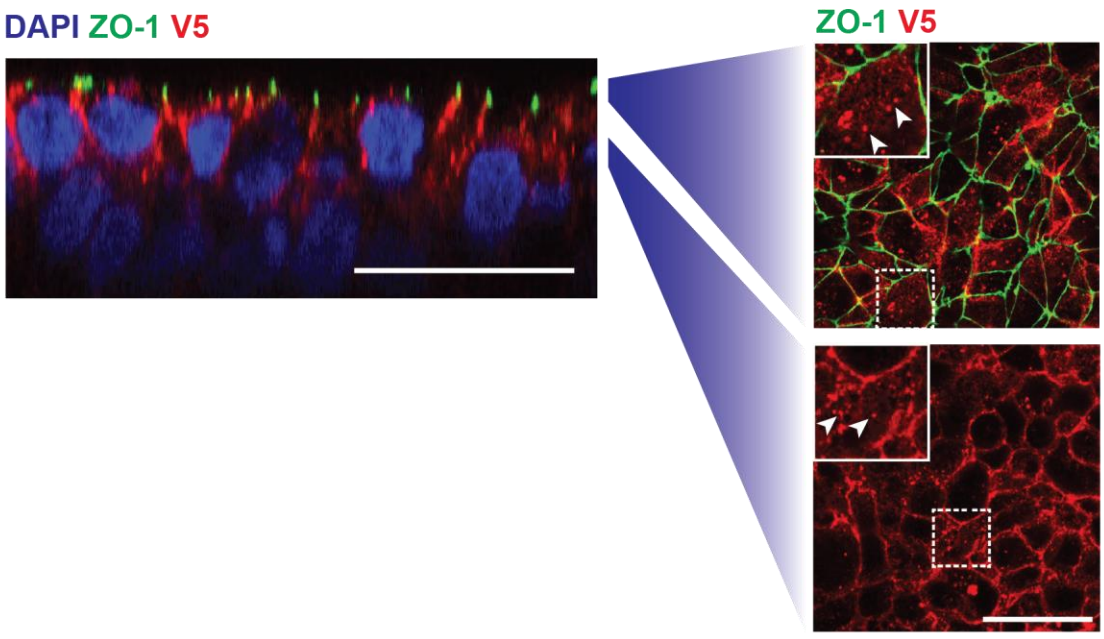
DAPI ZO-1 V5
ZO-1 V5

4.2 NOGGIN Trans-Epithelial Transport

We suspected that trafficking of NOGGIN was a prerequisite for its effect on pSMAD1/5/8 levels. Taking advantage of the physical properties of the plasma membrane, lowering the temperature of the cell culture is a commonly used method for nonspecific inhibition of endocytosis (Brunner et al., 2020). WT-RUES2 were first basally stimulated with BMP4, then NOGGIN was added apically or basally either at 37°C or at 4°C. At 4°C, the inhibitory effect NOGGIN has on pSMAD1/5/8 was eliminated, regardless of whether NOGGIN was added apically or basally (Figure 4.3). This result suggests that the trafficking of NOGGIN is crucial for its modulatory effect on BMP4 signaling.

We then hypothesized that NOGGIN was endocytosed specifically via clathrin-dependent endocytosis, similar to BMP2 and BMPR (Hartung et al., 2006, Paarmann et al., 2016). In order to probe NOGGIN endocytosis, we took advantage of the small molecule Dyngo4a which inhibits dynamin – an essential regulator for the internalization of endocytotic vesicles via clathrin-mediated endocytosis and micropinocytosis (McCluskey et al., 2013). When recombinant NOGGIN was presented to the apical or basal compartment, the protein was internalized as demonstrated by Western Blot on the cell lysates. Only apical internalization was effectively blocked by Dyngo4a concurrent treatment, demonstrating the specific requirement for dynamin in apical NOGGIN uptake (Figure 4.4A-B). On the other hand, Dyngo4a pre-treatment did not affect BMP4 signaling (Figure 4.4C).

Various other pharmacological inhibitors of endocytosis were tested for their efficacy in inhibiting NOGGIN internalization (Table 4.1). Of all inhibitors tested, Dyngo4a remained the most efficient

at suppressing NOGGIN apical internalization (Figure 4.4D-E). Our result suggests that NOGGIN apical internalization was actin-dependent and could be mediated via different endocytotic mechanisms such as clathrin-dependent endocytosis, caveolae-dependent endocytosis, and micropinocytosis. It is worth noting that although pharmacological inhibitors are convenient to use, their specificity and cell-type-dependency remain an issue (Ivanov, 2008, Vercauteren et al., 2010, Dutta and Donaldson, 2012).

We next tested whether NOGGIN underwent apical-to-basal transcytosis. To this end, we collected V5-tagged-NOGGIN-conditioned media from the apical culture media of NOGGIN-secreting cells. This conditioned media was applied to the apical compartment atop polarized hESC epithelium for up to 48 hrs. Consistent with transcytosis, V5-tagged-NOGGIN was recovered in the opposite side of the filter, in the basal compartment starting at 36 hrs after application (Figure 4.5A). Following the experiment, immunofluorescence and permeability assays were performed on the same hESC samples to confirm epithelial barrier integrity (Figure 4.5B-D). This demonstration of NOGGIN transcytosis explains the detection of NOGGIN in the basal media at 24 hrs in the NOGGIN secretion experiment (Figure 2.12A). The difference in timeline for NOGGIN basal detection in these two experiments can be explained by the difference between continuous NOGGIN production in the secretion experiment and gradual NOGGIN degradation within the conditioned media in the transcytosis experiment. Together, these results again support the hypothesis that NOGGIN undergoes apical-to-basal transcytosis.

Next, to dissect the specific endocytotic pathways associated with NOGGIN transport, we carried out a series of co-localization analyses between NOGGIN and various endosomal markers. The

presence of NOGGIN in specific endosomal compartments: pinocytotic vesicles, apical sorting endosomes (ASE), early endosomes (EE), apical recycling endosomes (ARE), common recycling endosomes (CRE), and basal sorting endosomes (BSE) was measured by quantitative immunofluorescence co-localization (Sheff et al., 1999, Perez Bay et al., 2016, Lapierre et al., 2012, Li et al., 2015, Cresawn et al., 2007, Simonsen et al., 1998, Brown et al., 2000, Knight et al., 1995, Odorizzi et al., 1996). NOGGIN-producing cells diluted in a WT hESC epithelium (1:100) were induced to secrete NOGGIN for 24 hrs. Paired immunostaining of V5 and multiple endosomal markers was then performed in receiving cells, followed by co-localization analysis. Confocal microscopy was able to resolve domain-selective labeling of the markers for pinocytotic vesicles, ASE, and ARE: pinocytotic vesicles and ASE were found exclusively in the apical region while the majority of ARE was found in the supranuclear region (Figure 4.6A). The distribution of the total overlap between NOGGIN and each endosomal marker in all z-positions was computed (Figure 4.6B-C). NOGGIN's z-profiles (Figure 4.8A) and each corresponding endosomes' z-profiles were plotted in the z-plane relative to the tight junction marker ZO-1 (Figure 4.8B) (for summary of endosomal markers, see Fig 7; for full protocol description, see Methods). Co-localization profiles (Figure 4.8C) indicate that most of the co-localization between NOGGIN-V5 and endosomal markers occurred at the level at or below tight junctions.

The fraction of NOGGIN-V5 that co-localized with each endosomal marker at different z-positions was computed. The overlap data (left axis, black) was graphed against the fluorescence profile of the respective endosome (right axis, green) (Figure 4.7A). V5 labeling was found to localize with markers for pinocytotic vesicles (labeled by Dextran-10'), ASE (labeled by WGA-10'), EE (labeled by early endosome antigen 1 EEA1), CRE (labeled by Transferrin-45'), and BSE (labeled

by Transferrin-5'). Co-localization was not observed between V5 and ARE (labeled by Rab11a). To verify that the co-localization fraction represented valid, meaningful localization, the fraction of endosomal markers that co-localized with NOGGIN was graphed against the fluorescence profile of the respective endosome (Figure 4.7B). Thus these results suggest that upon endocytosis by pinocytotic vesicles, NOGGIN travels through EE and ASE before arriving at the CRE. From the CRE, NOGGIN is directed to the BSE and finally targeted for exocytosis to the inter-cellular space where BMP receptors are localized at the basolateral membrane (Figure 4.9).

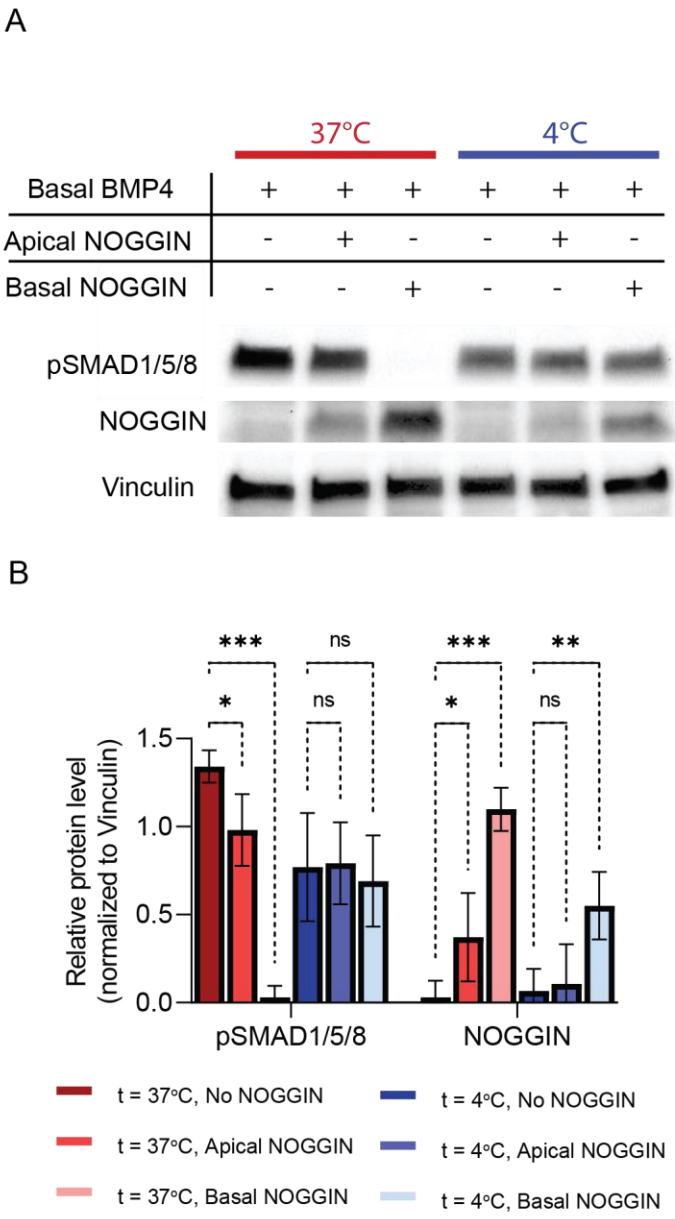

Figure 4.3: NOGGIN Inhibitory Effects on Psmad1/5/8 Was Eliminated at Low Temperature

(A) WT-RUES2 were stimulated with basal recombinant BMP4 (50 ng ml^{-1}). After 1.5 hr, NOGGIN (250 ng ml^{-1}) was added to the culture either apically or basally, and the culture was kept at 37ºC or moved to 4ºC. After 2 hrs, cell lysates were collected for Western blot analysis. (B) Quantification of the effect of cold temperature on NOGGIN internalization and pSMAD1/5/8 inhibition. Error bars = SD. Dunnett's multiple comparison statistical tests were performed with n = 6 (ns = not significant; * $p \leq 0.05$; ** $p \leq 0.01$; *** $p \leq 0.001$).

Figure 4.4: NOGGIN Apical Internalization Was Dynamin-Dependent

(A) NOGGIN was apically internalized via dynamin-dependent endocytosis. Recombinant NOGGIN (250 ng ml^{-1}) was added apically to WT hESCs with or without dynamin inhibitor Dyngo4a (100 mM). After 2 hrs, cell lysates were collected for Western blot analysis. 2-hr concurrent treatment of Dyngo4a blocked NOGGIN internalization. (B) Quantification of the effect of Dyngo4a in inhibiting NOGGIN internalization. Error bars = SD. Tukey's multiple comparison statistical test was performed with n = 3 (ns = not significant; * $p \leq 0.05$; ** $p \leq 0.01$; *** $p \leq 0.001$). (C) Dynamin-dependent endocytosis of BMP4 was not required for BMP4 signaling WT hESCs were stimulated with BMP4 (50 ng ml^{-1}; 30 min) with or without 30-min pre-treatment of Dyngo4a (100 mM) The drug did not affect the response to basal BMP4. Cell lysates were collected for Western blot analysis. (D) NOGGIN internalization was inhibited by different endocytosis inhibitors. WT hESCs were cultured on transwell filters. Recombinant NOGGIN (250 ng ml^{-1}) was added to the apical compartment. Each inhibitor was also added to the apical compartment. A detailed description of the concentration used for each inhibitors and the effects of each inhibitor can be found in Supplementary Table 1. After 2 hrs, the cell lysates were collected for Western blotting. (E) Quantification of the effects of different endocytosis inhibitors on NOGGIN internalization. Error bars = SD. Dunnett's multiple comparison statistical tests were performed with n = 3 (ns = not significant; * $p \leq 0.05$; ** $p \leq 0.01$; *** $p \leq 0.001$).

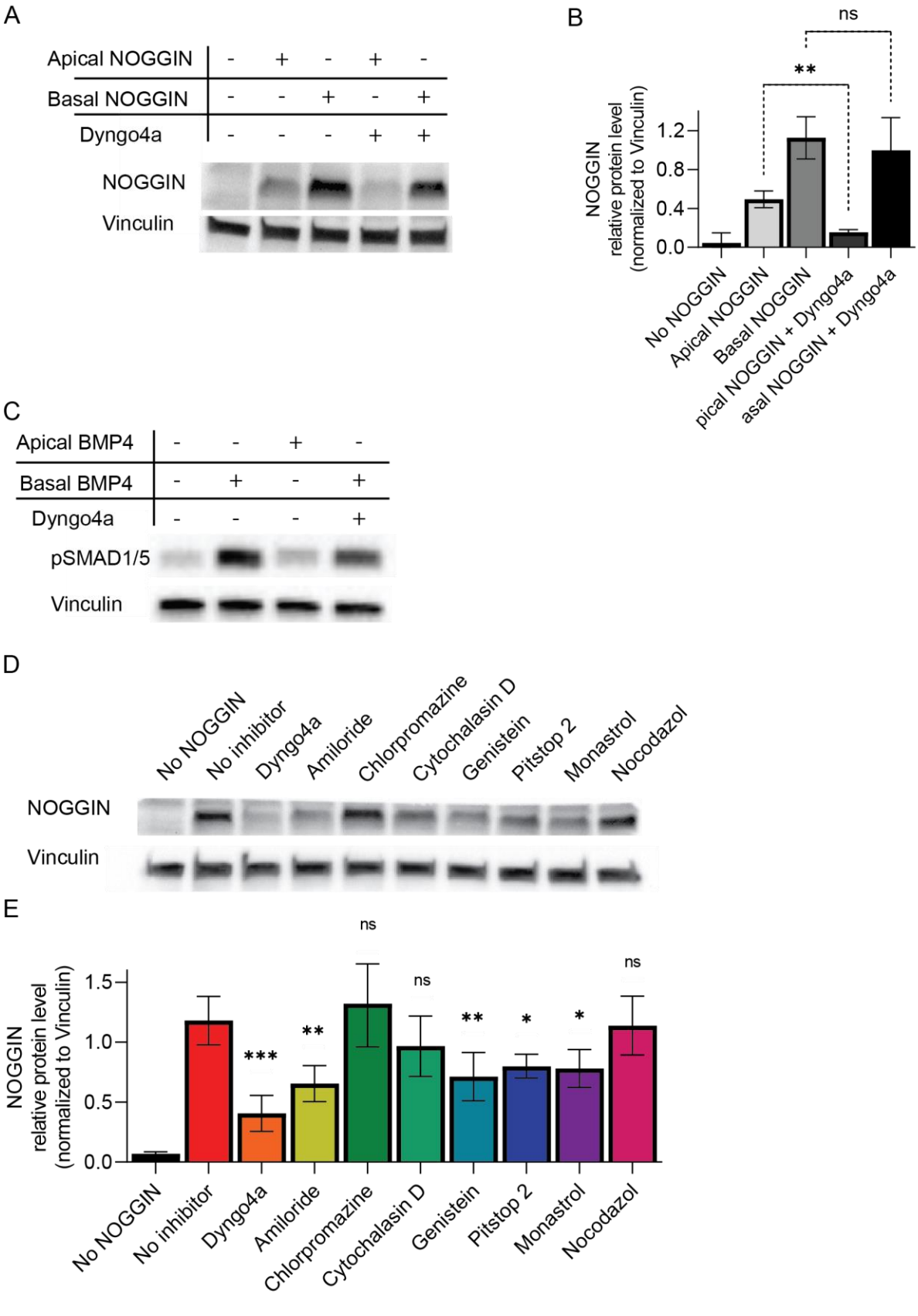
A
Apical NOGGIN - + - + -
Basal NOGGIN - - + - +
Dyngo4a - - - + +
NOGGIN
Vinculin
B
ns
**
NOGGIN relative protein level (normalized to Vinculin)
1.2
0.8
0.4
0.0
No NOGGIN
Apical NOGGIN
Basal NOGGIN
pical NOGGIN + Dyngo4a
asal NOGGIN + Dyngo4a
C
Apical BMP4 - - + -
Basal BMP4 - + - +
Dyngo4a - - - +
pSMAD1/5
Vinculin
D
No NOGGIN
No inhibitor
Dyngo4a
Amiloride
Chlorpromazine
Cytochalasin D
Genistein
Pitstop 2
Monastrol
Nocodazol
NOGGIN
Vinculin
E
ns
ns
ns
***
**
**
*
*
NOGGIN relative protein level (normalized to Vinculin)
1.5
1.0
0.5
0.0
No NOGGIN
No inhibitor
Dyngo4a
Amiloride
Chlorpromazine
Cytochalasin D
Genistein
Pitstop 2
Monastrol
Nocodazol

Table 4.1: List of Pharmacological Inhibitors Used and Their Reported Effects on Endocytosis

Inhibitor	Final Concentration	Effect(s)	Internalization pathway(s) affected	References
Dyngo4a	100 uM	• dynamin inhibition	• Clathrin-dependent endocytosis	(Park et al., 2013) (McCluskey et al., 2013)
Amiloride	100 uM	• sodium-protein exchanger inhibition actin disruption	• Macropinocytosis	(Delvaux et al., 1990, Lagana et al., 2000, Koivusalo et al., 2010, Dutta and Donaldson, 2012)
Chlorpromazine	*100 uM*	• *clathrin mis-assembly*	• Clathrin-dependent endocytosis	*(Wang et al., 1993)*
Cytochalasin D	*10 uM*	• *actin depolymerization*	• *Clathrin-dependent endocytosis* • *Macropinocytosis*	*(Schliwa, 1982, Sampath and Pollard, 1991, Jackman et al., 1994, Fujimoto et al., 2000)*
Genistein	100 uM	• tyrosine kinase inhibition • actin disruption • dynamin inhibition	• Caveolae-dependent endocytosis	(Akiyama et al., 1987, Aoki et al., 1999, Nabi and Le, 2003)
Pitstop 2	33 uM	• clathrin inhibition	• Clathrin-dependent endocytosis • Clathrin-independent endocytosis	(von Kleist et al., 2011, Dutta et al., 2012, Willox et al., 2014)
Monastrol	100 uM	• kinesin inhibition calcium-channel inhibition	• Clathrin-dependent endocytosis	(Mayer et al., 1999, Harasztosi et al., 2018, Witte et al., 2020, Abassi et al., 2009, Huang et al., 2017, Yao et al., 2017)
Nocodazol	*16.6 uM*	• *microtubule disruption*	• *Clathrin-dependent endocytosis*	*(Hoebeke et al., 1976, Hamm-Alvarez et al., 1996, Vasquez et al., 1997, Subtil and Dautry-Varsat, 1997)*

Figure 4.5: NOGGIN Underwent Apical-To-Basal Transcytosis

(A) NOGGIN-V5-conditioned E8 media was applied to the apical compartment for the specified durations. Media from the apical and basal compartments were analyzed with Western blot. The presence of NOGGIN in the basal compartment was detected after 36 hrs. (B) Cells maintained normal ZO-1 expression following transcytosis experiment. Following transcytosis experiment in Figure 6E, the same epithelia were evaluated for expression pattern of tight junction marker ZO-1. All epithelia examined showed an intact mesh of ZO-1. Scale bar = 100 μm. (C) Epithelia were impermeable to 40-kDA dextran after the transcytosis experiment. Following transcytosis experiment in Figure 6E, the same epithelia was evaluated for epithelial permeability at the corresponding times. 40-kDA dextran-TxRed (25 mg/ml) was added to the apical chamber, for 1 hour (37ºC, 5% CO2), with or without a pre-treatment of chelating agent EDTA (50 mM, 30 min). Fluorescence intensity in the basolateral compartment was measured by a fluoro-meter (NanoDrop 2000), set at an absorbance of 589 nm. Epithelial permeability was assessed by measuring the TxRed-labeled dextran flux from the apical to the basolateral chambers. (D) Epithelium integrity was maintained during 48 hrs filter culture. We compared the permeability of epithelia seeded with 200,000 hESCs (standard culture condition used throughout this study) and epithelia seeded with 50,000 hESCs (low cell density condition). While the epithelia prepared with standard protocol demonstrated impermeability, the epithelia seeded with less cells demonstrated leakiness: 40-kDA Dextran-FITC added to the top media was found in the basal media in the latter condition but not the first.

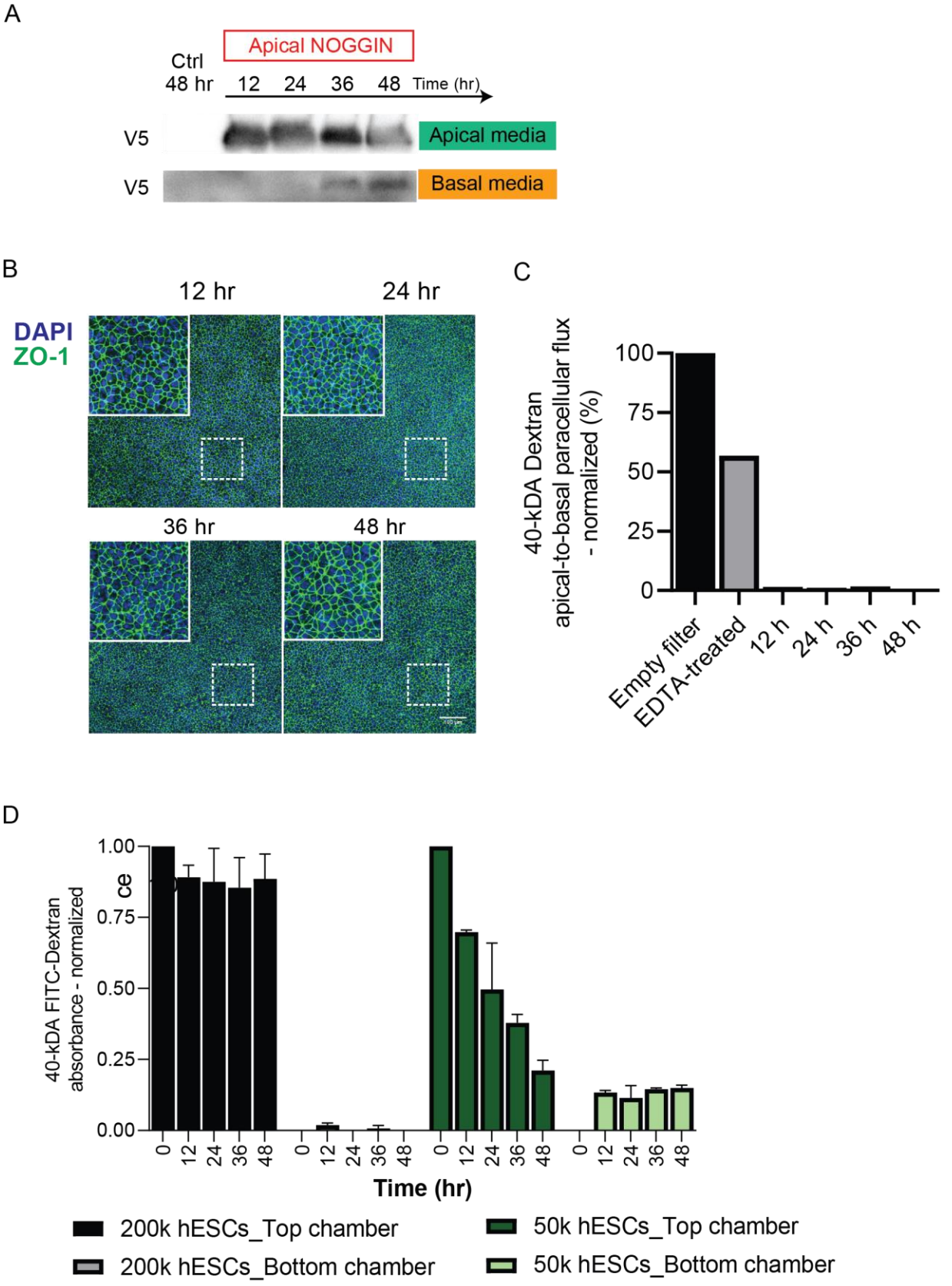
A
Apical NOGGIN
Ctrl
48 hr
12
24
36
48
Time (hr)
V5
Apical media
V5
Basal media
B
12 hr
24 hr
DAPI
ZO-1
36 hr
48 hr
C
40-kDA Dextran
apical-to-basal paracellular flux
- normalized (%)
100
75
50
25
0
Empty filter
EDTA-treated
12 h
24 h
36 h
48 h
D
40-kDA FITC-Dextran
absorbance - normalized
1.00
0.75
0.50
0.25
0.00
0
12
24
36
48
Time (hr)
200k hESCs_Top chamber
200k hESCs_Bottom chamber
50k hESCs_Top chamber
50k hESCs_Bottom chamber

Figure 4.6: NOGGIN Was Transported Through Endosomal Compartments

(A) NOGGIN colocalized with various endosomal vesicles. 10-kDA Dextran (10-min apical incubation) labeled pinocytotic vesicles. WGA (wheat germ agglutinin) (10-min apical incubation) labeled ASE (Apical Sorting Endosomes). EEA1 antibodies labeled EE (Early Endosomes). Rab11A antibodies labeled ARE (Apical Recycling Endosomes). Transferrin (45-min basal incubation) (Tf 45') labeled CRE (Common Recycling Endosomes). Transferrin (5 min basal incubation) (Tf 5') labeled BSE (Basal Sorting Endosomes). Left: Schema. Right: Data showing two confocal sections in the apical (top) and supranuclear (bottom) regions. Scale bars = 25 μm. (B) Quantification of the total fraction of NOGGIN co-localizing with each endosomal marker. (C) Quantification of the total fraction of each endosomal marker co-localizing with NOGGIN. For both (G-H), box and whisker plots display minimum, first quartile, median, third quartile, and maximum.

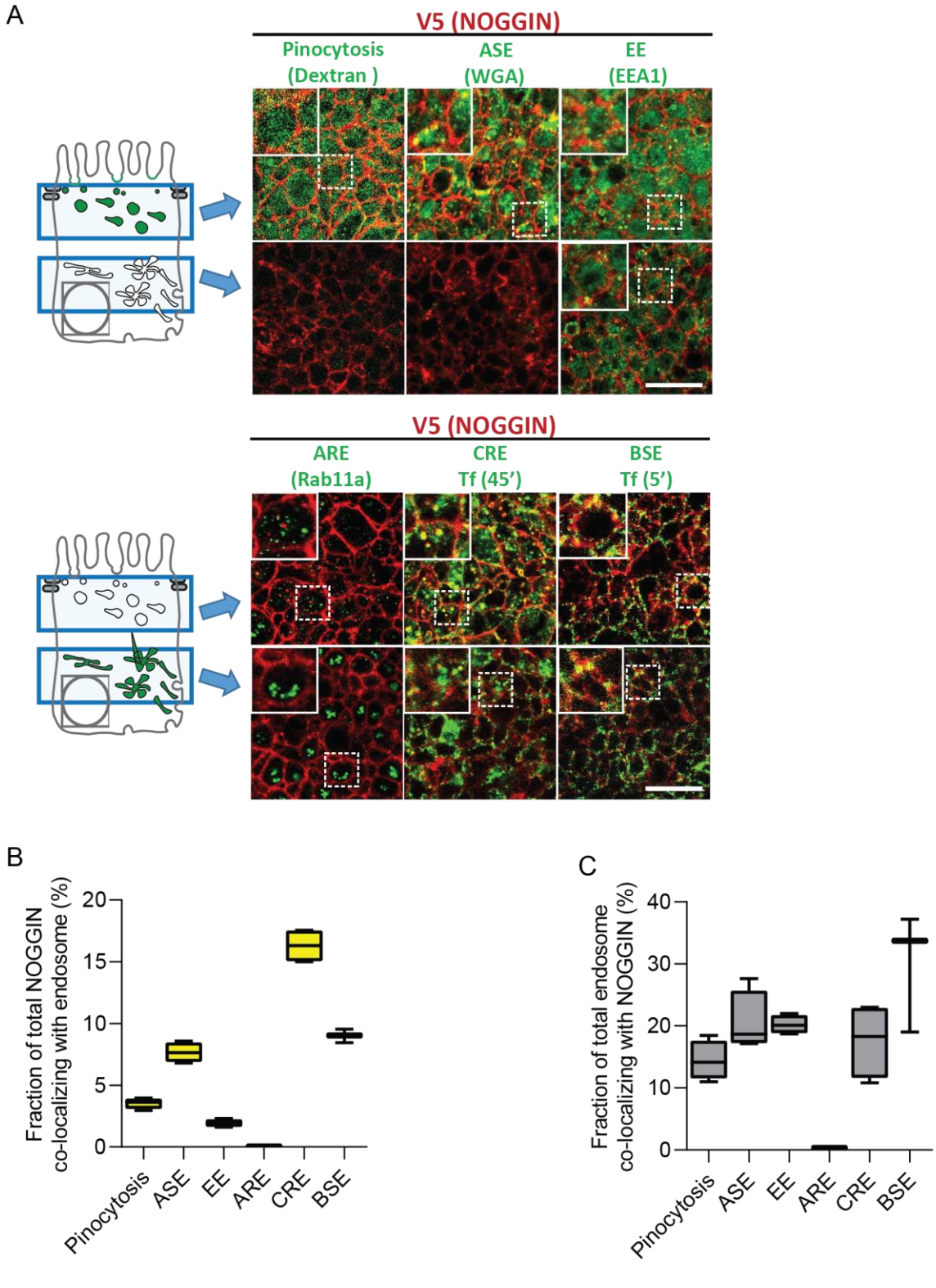
A
V5 (NOGGIN)
Pinocytosis
(Dextran)
ASE
(WGA)
EE
(EEA1)
V5 (NOGGIN)
ARE
(Rab11a)
CRE
Tf (45')
BSE
Tf (5')
B
Fraction of total NOGGIN
co-localizing with endosome (%)
20
15
10
5
0
Pinocytosis
ASE
EE
ARE
CRE
BSE
C
Fraction of total endosome
co-localizing with NOGGIN (%)
40
30
20
10
0
Pinocytosis
ASE
EE
ARE
CRE
BSE

Figure 4.7: NOGGIN Co-localized with Different Endosomal Markers Throughout the Z-Axis

(A) Fraction of NOGGIN co-localizing with endocytotic vesicles (left axis, black) at each z-position with respect to the profile of the respective marker (right axis, green) at the corresponding z-position. Datapoints were taken 0.5 μm apart. Fluorescence labeling was binarized. (B) Fraction of endosome marker co-localizing with NOGGIN (black) with respect to the distribution of each marker (blue, shaded) in throughout the z-axis. (This is the reciprocal of the quantification in Fig 6I). Fluorescence labeling was binarized. All samples were aligned in Z based on ZO-1 labeling (indicated by red dashed line). In all analysis, fluorescence labeling was binarized. were taken 0.5 μm apart. All samples were aligned in the z-axis based on ZO-1 labeling (indicated by red dashed line). Error bars = SD.

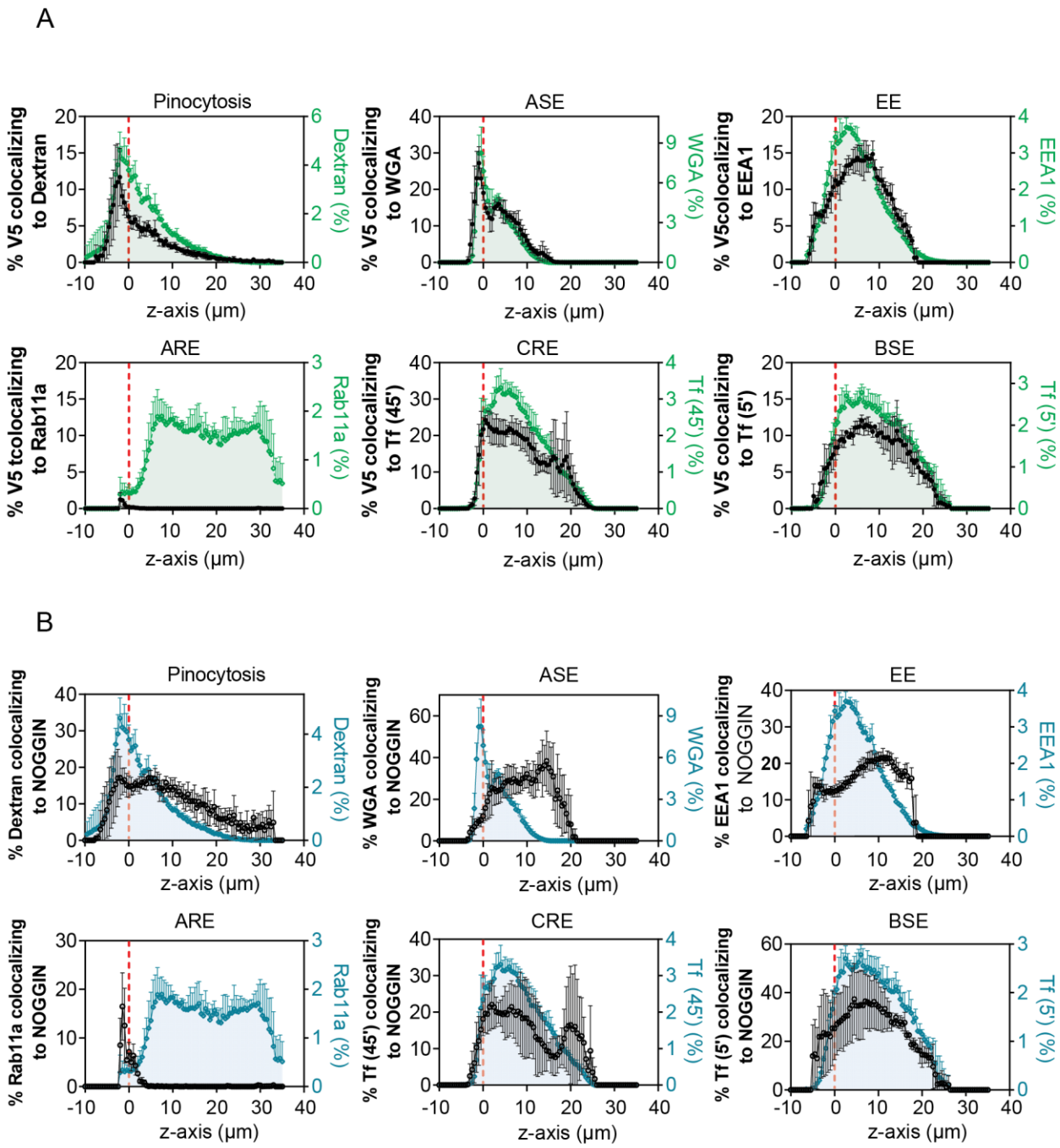
A
Pinocytosis
% V5 colocalizing to Dextran
Dextran (%)
ASE
% V5 colocalizing to WGA
WGA (%)
EE
% V5colocalizing to EEA1
EEA1 (%)
ARE
% V5 tcolocalizing to Rab11a
Rab11a (%)
CRE
% V5 colocalizing to Tf (45')
Tf (45') (%)
BSE
% V5 colocalizing to Tf (5')
Tf (5') (%)
z-axis (µm)
B
Pinocytosis
% Dextran colocalizing to NOGGIN
Dextran (%)
ASE
% WGA colocalizing to NOGGIN
WGA (%)
EE
% EEA1 colocalizing to NOGGIN
EEA1 (%)
ARE
% Rab11a colocalizing to NOGGIN
Rab11a (%)
CRE
% Tf (45') colocalizing to NOGGIN
Tf (45') (%)
BSE
% Tf (5') colocalizing to NOGGIN
Tf (5') (%)
z-axis (µm)

Figure 4.8: Distribution of ZO-1, NOGGIN, and NOGGIN-Endosome Overlap as a Function in the Z-Axis

(A) Profile of NOGGIN distribution along the Z-axis for each data set corresponding to a different endosomal marker. (The area under the curve indicates total NOGGIN labeling (100%)). (B) Profile of ZO-1 distribution along the Z-axis for each data set corresponding to a different endosomal marker. For each field of view, the peak of the curve was set as the 0-point of Z. The distribution of all other markers were aligned to this point of reference. (The area under the curve indicates total ZO-1 labeling (100%)). (C) Distribution of all NOGGIN-endosome co-labeled regions along the Z-axis. (The area under the curve indicates all total overlap area (100%)). All samples were aligned in the z-axis based on ZO-1 labeling (indicated by red dashed line). Error bars = SD.

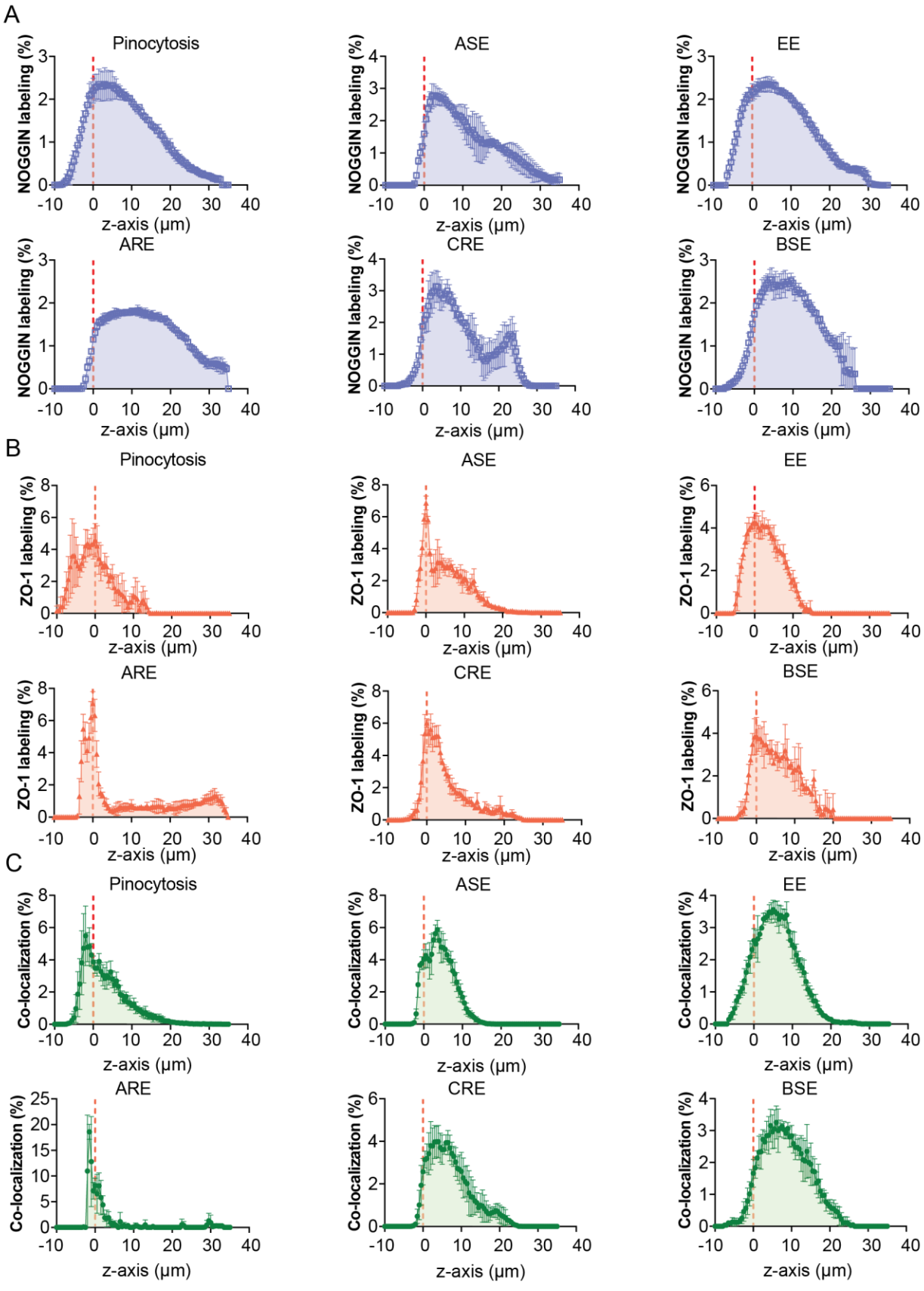
A
Pinocytosis
ASE
EE
ARE
CRE
BSE
NOGGIN labeling (%)
z-axis (μm)
B
Pinocytosis
ASE
EE
ARE
CRE
BSE
ZO-1 labeling (%)
z-axis (μm)
C
Pinocytosis
ASE
EE
ARE
CRE
BSE
Co-localization (%)
z-axis (μm)

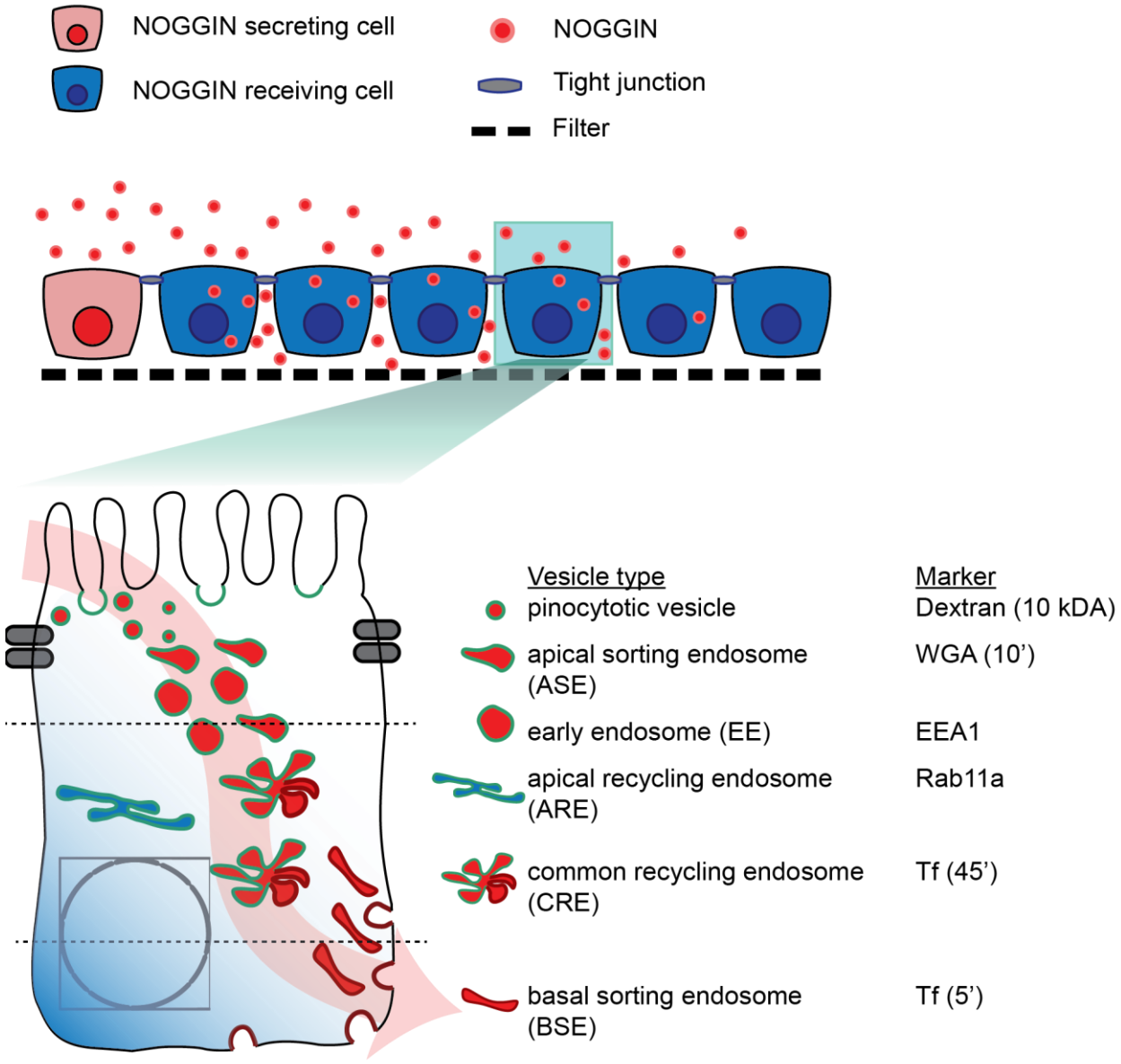

Figure 4.9: Schematics of Transcytosis Route Through Which NOGGIN (Red) Is Trafficked From the Apical to the Basolateral Extracellular Domain

(Top) Schematics of hESC epithelium on filter
(Bottom) Schematics of NOGGIN transcytosis route. Note that NOGGIN (red) travels through pinocytotic vesicles, ASE, EE, CRE, and BSE. ARE is shown in blue as it is not engaged in the trafficking of NOGGIN.

CHAPTER 5. CONCLUSIONS AND FUTURE DIRECTIONS

5.1 Challenging the Classical Reaction-Diffusion Model in Morphogenesis

The surprising observation that in a model human epiblast, a pair of secreted morphogen and inhibitor that directly bind each other are in fact initially secreted into opposite extracellular spaces forces a reconsideration of our current understanding of the molecular mechanisms underlying embryonic pattern formation (Figure 5.1). That BMP4 is secreted baso-laterally is consistent with the localization of the BMP receptors (Etoc et al., 2016, Zhang et al., 2019). NOGGIN apical secretion into an opposite compartment separate from BMP4, which was not anticipated by current models, might represent a necessary mechanism as it would prevent immediate binding and inactivation of both factors and thus enable their patterning roles over large distances. Elucidation of NOGGIN localization and mechanism of transport sheds light on intracellular BMP gradient formation and signaling, which are an important facet of gastrulation and embryonic patterning.

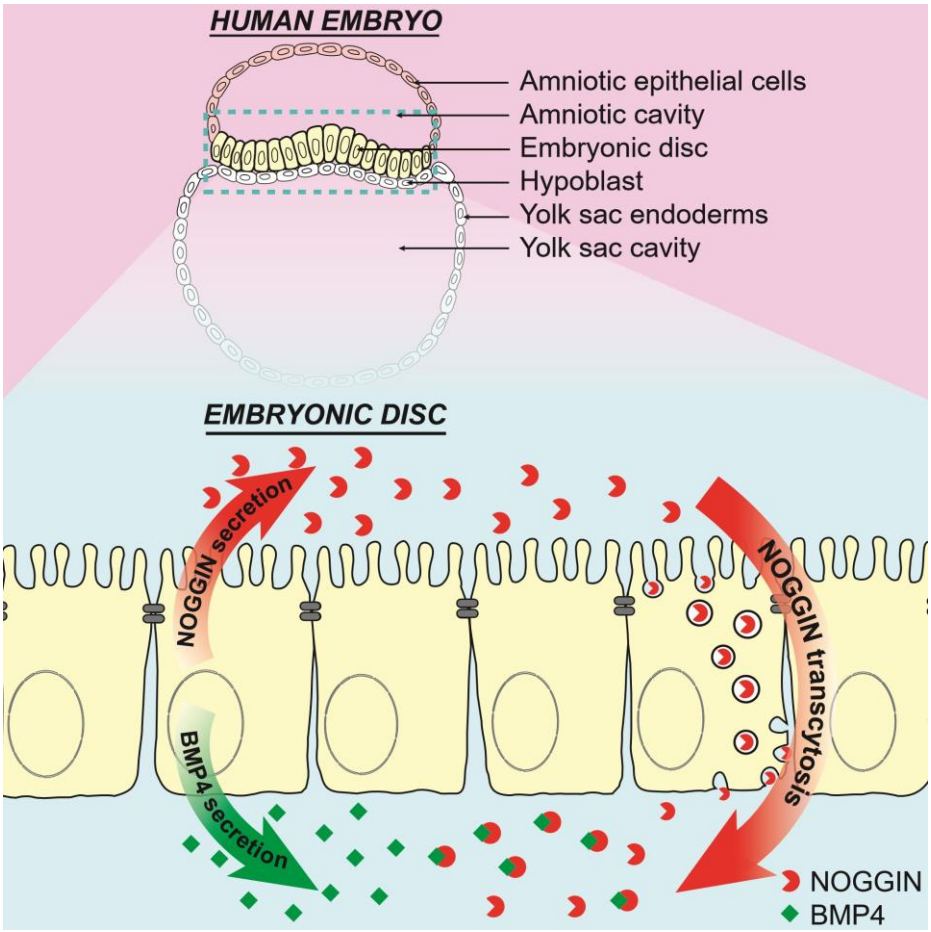

Figure 5.1: Schematics of NOGGIN-BMP Duality

NOGGIN is selectively secreted from the apical side of the human embryonic disc while BMP4 is secreted from the basal side. NOGGIN is then internalized from the apical side by transcytosis to the basal/baso-lateral membrane close to the BMP receptors.

The spread of BMP4 and NOGGIN activity from a localized source was consistent with Turing's reaction-diffusion model, which postulates that the inhibitor must travel faster than ligand. The spread of NOGGIN was long-ranged, and almost 8 times greater than the lateral spread of BMP4 which remained restricted to only 2-3 adjacent cell neighbors. The differential diffusion rates may be regulated by the extracellular matrix as NOGGIN and BMP4 bind components of the extracellular matrix with different affinities (Rider and Mulloy, 2017, Paine-Saunders et al., 2002, Ohkawara et al., 2002). Additionally, the biophysical and geometrical properties of the apical and basal extracellular compartments differ. Therefore, the possibility that secreted molecules generally diffuse further at the apical side than at the basal side cannot be excluded. This situation has been shown to be the case in the luminal cavity of the implanting mammalian embryo, where the amniotic cavity on the apical side of the epithelia allows for the rapid transport of secreted factors, potentially to concentrate and homogenize inhibition through all cells lining the lumen (Simunovic et al., 2019, Zhang et al., 2019).

One caveat of our experimental design is that in the absence of detection methods to visualize endogenous signals, we had to rely on over-expression systems which produce protein levels higher than those found *in vivo*. However, time- and concentration-response curves show smooth variations, and our results for exogenously applied BMP4 or NOGGIN are consistent with those from the DOX induced cell lines. Thus, cells at a distance from the source do experience a graded concentration profile. These cells at the boundary near those that do and do not respond to pSMAD1/5/8 encounter relevant concentrations of morphogen/inhibitor. Therefore, given the limitation of current technologies, we believe the cellular responses occurring at the boundary are indicative of what happens *in vivo.* Another notable point of discussion is that although the

endocytotic vesicles described in this study transport the bulk of NOGGIN transcytosis, not 100% of NOGGIN is accounted for. Therefore, there may be other unidentified endocytotic vesicles involved in NOGGIN's apical-to-basal transcytosis.

5.2 The Importance of Oppositely-Polarized Morphogen and Its Inhibitor

The polarized secretion of NOGGIN and BMP4 exemplifies how an epithelium can create a sharp boundary within an embryo. Cells on the apical side would have BMP inhibited while those on the basal side would experience BMP signaling. This phenomena was recently proposed in connection with WNT signaling in the developing epidermis where a single-layer multipotent epithelial progenitor defines the boundary between WNT activity on its basal side and WNT repression on its apical side (Matos et al., 2020). Moreover, it becomes increasingly clear that during gastrulation, while important signals are supplied by the visceral endoderm or hypoblast, signal reception is controlled by epithelial cell polarity (Zhang et al., 2019, Etoc et al., 2016). How epithelial cell types integrate morphogen signals will have to be incorporated in models of epiblast symmetry breaking to understand communication between embryonic and extra-embryonic populations.

5.3 Further Investigation into the BMP4-NOGGIN Duality

The baso-lateral targeting of NOGGIN makes sense as it might be more efficient for an inhibitor to shield a small pool of very localized receptors than a diluted batch of ligand distributed through the more extended extra-cellular space. However, while we have shown that NOGGIN can undergo transcytosis and neutralize basally-introduced BMP4, the location where NOGGIN first interacts with BMP4 remains ambiguous. It remains unclear whether NOGGIN directly enters the

same pool within endosomal compartments as BMP4, or whether BMP4 is constitutively degraded after endocytosis (Hartung et al., 2006; Paarmann et al., 2016). Therefore, this work does not eliminate the possibility that BMP4 and NOGGIN meet inside transport vesicles.

Further experiments can be performed to determine the exact cellular location where NOGGIN binds BMP4. Potential approaches include: (1) visualizing NOGGIN-BMP4 complexes via proximity ligation assays in combination with immunofluorescence labeling of cellular structures; (2) separately tagging the two proteins and using super-resolution microscopy; and (3) dual labeling with electron microscopy. These methods will allow us to visualize at high resolution the dynamics of NOGGIN intracellular transport in receiving cells. Such experiments will determine the mechanism of NOGGIN internalization at the apical surface, its proximity with BMP receptors BMPRI/BMPRII, and the meeting place. Some preliminary data of immune-gold labeling of NOGGIN is shown in Figure 5.2.

Another area of future investigation is the impact of this ligand-inhibitor polarization on patterning. This work does not experimentally address how the proposed novel secretion and transcytosis mechanisms translates into a direct impact on cell fate induction. Such follow-up work will shed light on the link between the novel mechanism of signaling proposed by this study and the ultimate impact of such a mechanism. It will also be interesting to incorporate the impact of NOGGIN transcytosis into the quantitative model by (Etoc et al., 2016), which integrates edge sensing and inhibitors, to predict human fate positioning in human gastruloids. Incorporating NOGGIN transcytosis as an additional variable will either modulate or further reinforce the current model.

Lastly, it would be compelling to address the *in vivo* relevance and the evolutionarily conservation of this novel mechanism of morphogen signaling. Notably, the chick embryo and the human embryo share the flat embryonic disc morphology. Thus, the chick embryos aptly model the polarized epithelial disc that is central to the findings of this study. Secretion for the ligand/inhibitor pair can be probed in this system to determine whether the polarized secretion can be observed *in vivo*. In addition, descriptive and functional grafting studies in early chick embryos can be performed: agarose beads coated with either BMP4 or NOGGIN will be presented either on the apical or basal side of the chick epiblast, and polarized cell response will be measured by pSMAD1 and cell fate staining (Figure 5.3). If successful, results from this aim would provide crucial *in vivo* relevance support for the of the *in vitro* data. Some preliminary data of BMP4 and NOGGIN bead grafts on HH stage 4 chick embryos is shown in Figure 5.4.

Figure 5.2: <u>Preliminary Data</u> Showing NOGGIN Being Endocytosed from the Apical Surface and Trafficked to the Intercellular Space

TRE::NOGGIN-V5 RUES2 cells were diluted in RUES2 (1:100) Cell were cultured on transwell filters under standard pluripotency conditions. Cell were induced with Dox for 24 hrs to produce NOGGIN-V5. The filters were processed for electron microscopy. Nanogold particle labeling with silver enhancement was performed. Then, ultrathin sections (100nm) were negative-stained with uranyl acetate (UA). UA stain is grey. NOGGIN-V5 stain is black.
(A) The apical surface (top) of the hESC epithelium is decorated with microvilli.
(B) Abundant NOGGIN is observed at the apical surface.
(C) NOGGIN endocytotic events captured

A

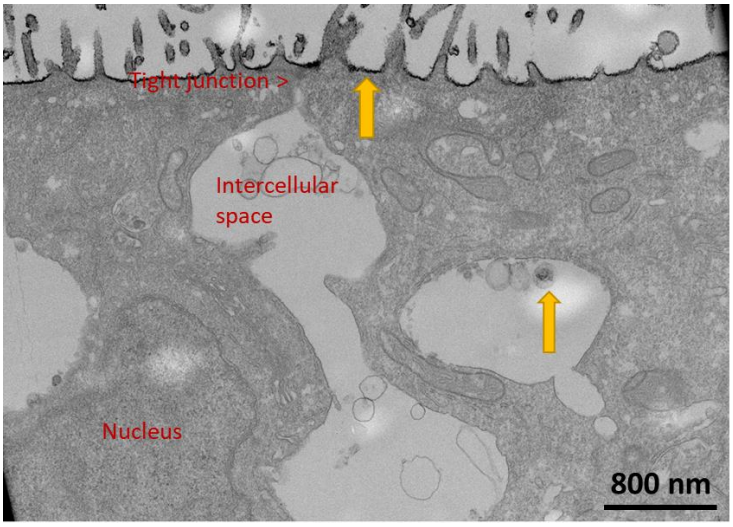
Tight junction >
Intercellular space
Nucleus
800 nm

B

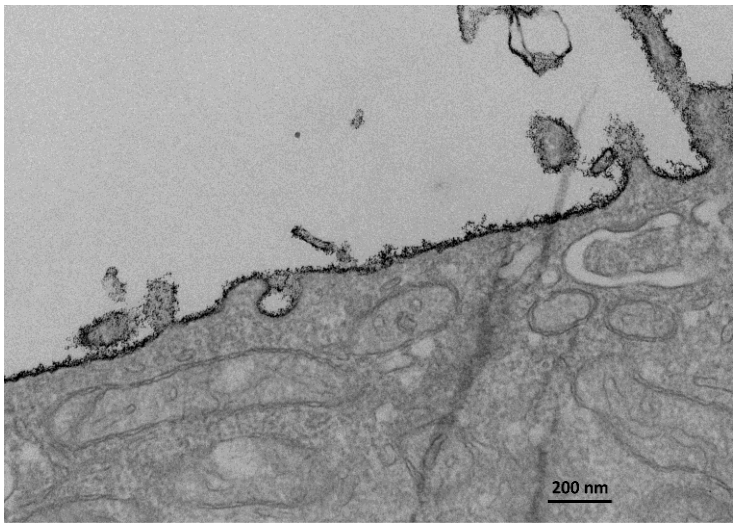
200 nm

C

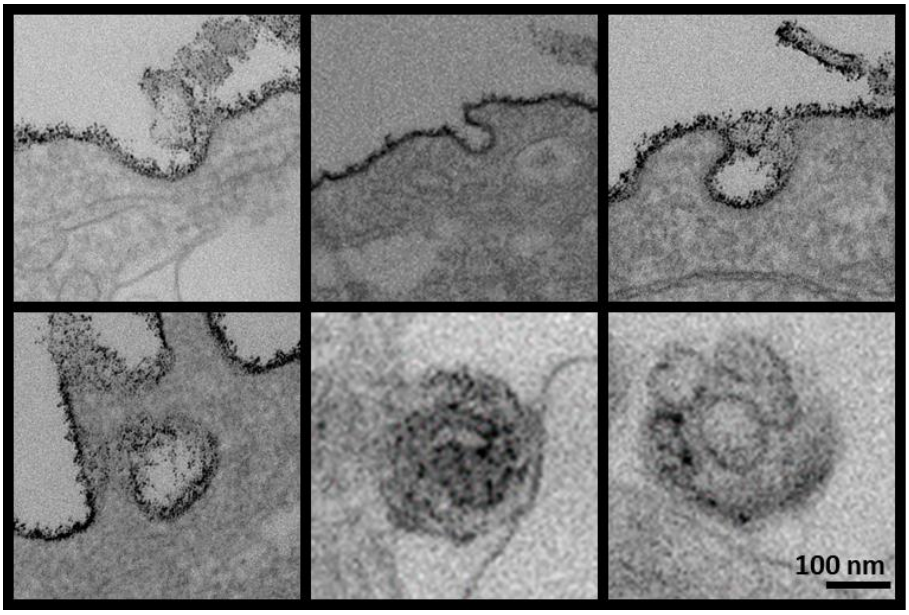
100 nm

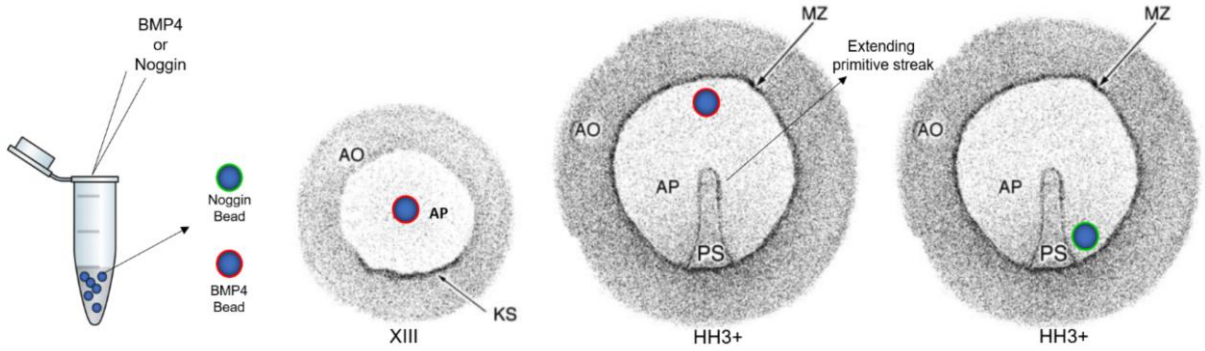

Figure 5.3: Schematics of BMP4 and NOGGIN-Soaked Bead Graft on Chick Embryos

Chick embryos are incubated to reach HH stage 3-4.

BMP4 coated beads will be implanted in the central zone of area pellucida and in the anterior region of the embryo. NOGGIN coated beads will be placed in the posterior region, lateral to the extending primitive streak.

AO = area opaca,
AP = area pellucida, MZ = marginal zone, KS = Koller's sickle, PS = primitive streak.

Graphics modified from (Bodenstein and Stern, 2005).

Figure 5.4: Preliminary Data Showing the pSMAD1/5/8 Activation in Response to Apically/Basally-placed BMP4/NOGGIN Beads

We have tried to apply BMP4 and NOGGIN on the dorsal and ventral sides of the chick embryos using beads and conditioned media. The beads were destructive to the delicate epithelial structure of the early chick embryos. Thus, we tried the application of BMP4-myc- and NOGGIN-V5-conditioned media to either the Dorsal or Ventral side of the HH3-stage chick embryo, which corresponds to the Apical and Basal side of the epithelial disc.

Unfortunately, the experiments didn't give conclusive results despite various troubleshooting of culture system, concentration, and temporal conditions. We ran into reproducibility issues, which inhibited analysis.

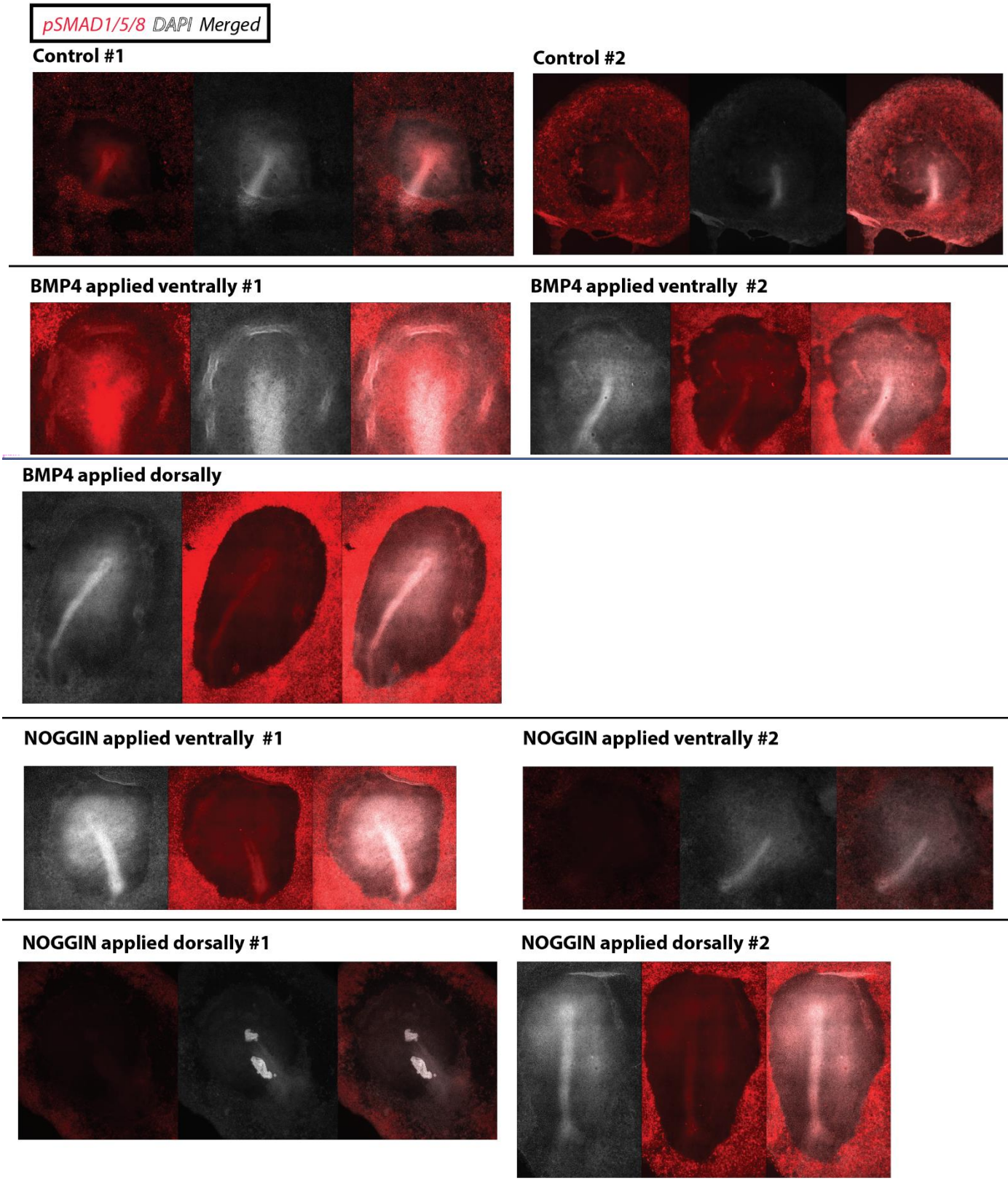
pSMAD1/5/8 DAPI Merged
Control #1
Control #2
BMP4 applied ventrally #1
BMP4 applied ventrally #2
BMP4 applied dorsally
NOGGIN applied ventrally #1
NOGGIN applied ventrally #2
NOGGIN applied dorsally #1
NOGGIN applied dorsally #2

5.4 Polarized Epithelia Restrict Morphogen Patterning in Unexpected Ways

Epithelial polarity also operates to control vesicular trafficking machineries and regulates vectorial transport (Rodriguez-Boulan et al., 2005, Rodriguez-Boulan and Macara, 2014). We have traced the path of NOGGIN from the early sorting endosomes on the apical side, to the basal sorting endosomes, and finally to the baso-lateral location next to the BMP receptors.

We showed previously that ACTIVIN/NODAL receptors are also baso-laterally localized in human gastruloids grown in confined geometry as well as when cultured on filters (Etoc et al., 2016). It is therefore tempting to speculate that a similar scenario between ligands and inhibitors might be at play. Indeed, ACTIVIN/NODAL inhibitors such as LEFTY1/2 and CERBERUS have also been shown to be induced directly by activation of the SMAD2/3 pathway (Yoney et al., 2018). Interestingly, we did not observe an apical-basal asymmetry in the reception of recombinant WNT3A protein in our RUES2 colonies (Martyn et al., 2019). While this suggests that these types of segregated secretion of ligands/inhibitors might be unique to the TGFβ signaling pathway, we note that in the Drosophila wing, transcytosis of Wnt from the apical to basal compartment and its inhibition by Notum are essential for patterning (Yamazaki et al., 2016). Thus, as in the case of human-specific induction of NOGGIN by BMP4, these might represent species-specific attributes. Probing signaling dynamics in other polarized epithelia holds the promise of unveiling more surprises.

Stem cell-based, self-organizing models of human development provide a robust tool to discover early aspect of human embryogenesis which otherwise would be impossible to scrutinize (Tyser, 2020). Among many other contributions, these tools allowed for the discovery of polarized signal

reception in hESC colonies and its *in vivo* relevance for BMP4 signaling in the amniotic cavity of the mouse embryo (Etoc et al., 2016, Zhang et al., 2019). This scenario can be reiterated overtime during multiple stages of embryonic development. For example, the early neural tube consists of a polarized epithelium that both sends and receives multiple signals. In mouse, NOGGIN and SHH secreted from the floor plate and notochord impinge on the cells of the ventral neural tube, while BMP4 secreted from the roof plate and ectoderm impinges on the cells of the dorsal neural tube (Brent and Tabin, 2002, McMahon et al., 1998, Ybot-Gonzalez et al., 2007). Thus, polarized secretion and reception may play a role in dorsal/central specifications and subsequently influence surrounding tissues such as neural crests and somites. Therefore, epithelial polarity represents part of the toolkit used by embryos for robust developmental patterning through secreted molecules.

APPENDIX. An Artist's Illustration of NOGGIN Transcytosis

An anthropomorphic depiction of NOGGIN (red) on an adventure to find BMP4 (green). NOGGIN's journey across the cellular landscape was facilitated by various transportation modes (endosomal vesicles).

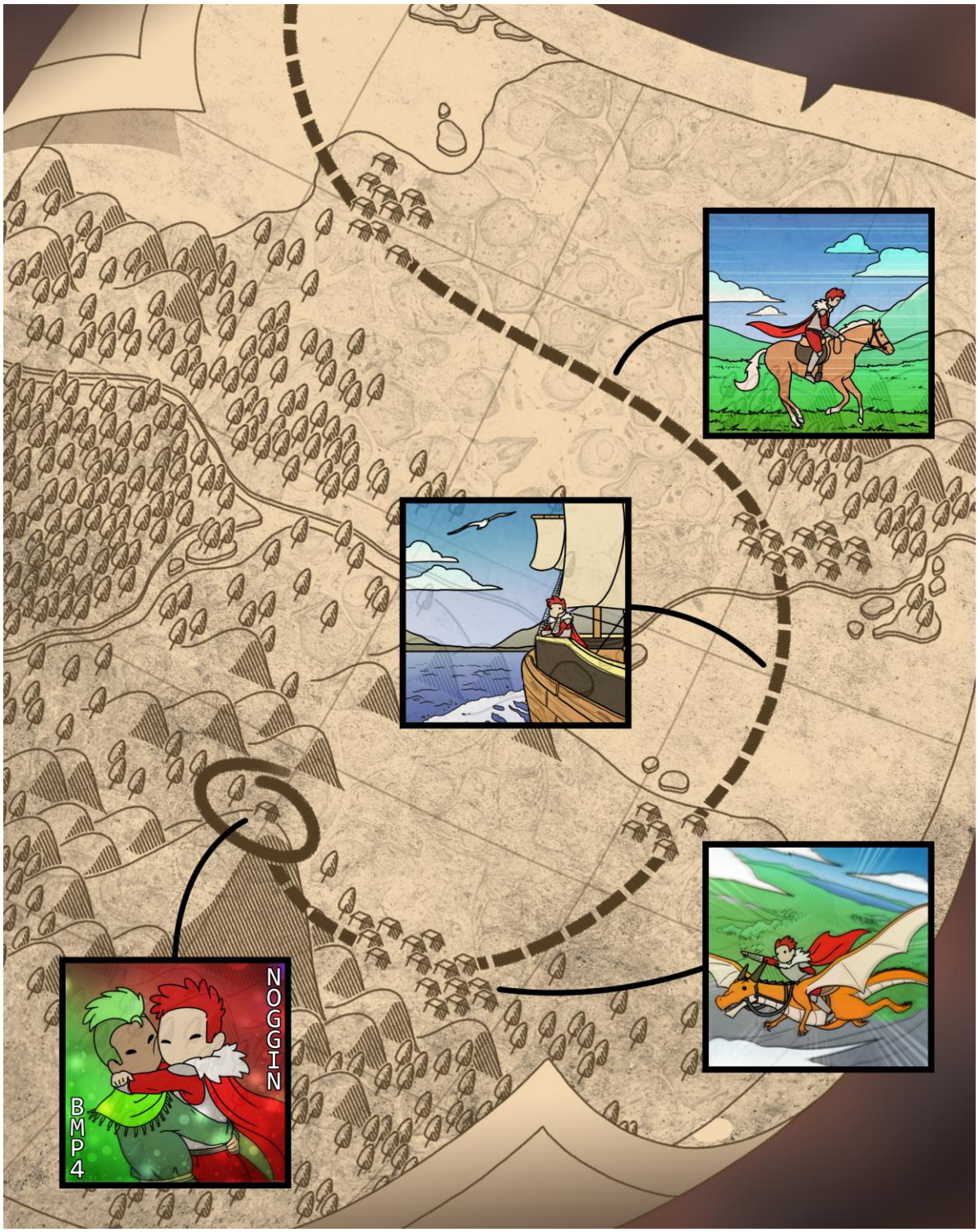

MATERIALS AND METHODS

Table 6.1: Key reagents and resources

REAGENT or RESOURCE	SOURCE	IDENTIFIER
Antibodies		
anti-EEA1 (rabbit pAb)	Abcam Cat. #: ab2900	RRID: AB_2262056
anti-Nanog (goat pAb)	R and D Systems Cat. #: AF1997	RRID: AB_355097
anti-NOGGIN (rabbit pAb)	Abcam Cat. #: ab16054	RRID: AB_470248
anti-Oct3/4 (mouse mAb)	BD Biosciences Cat. #: 611203	RRID: AB_398737
anti-pSMAD1/5/8 (rabbit mAb)	Cell Signaling Cat. #: 9516S	RRID: AB_491015
Anti-Rab11A (rabbit mAb)	Invitrogen Cat. #: 700184	RRID: AB_2532295
anti-Sox2 (rabbit mAb)	Cell Signaling Cat. #: 3579	RRID: AB_2195767
anti-V5 (mouse mAb)	Thermo Fisher Cat. #: R960-25	RRID: AB_2556564
anti-Vinculin (mouse mAb)	Millipore Cat. #: 05-386	RRID: AB_11212640
anti-ZO1 (rabbit pAb)	Invitrogen Cat. #: 61-7300	RRID: AB_2533938
anti-GIANTIN (rabbit pAb)	BioLegend Cat. #: 924301	RRID: AB_2801254
Chemicals, peptides, and recombinant proteins		

Dyngo-4a	Abcam Cat. #: ab120192	CAS: 1256493-34-1
Amiloride hydrochloride	Sigma-Aldrich Cat. #: A7410	CAS: 2016-88-8
Chlorpromazine hydrochloride	Sigma-Aldrich Cat. #: C8138	CAS: 69-09-0
Cytochalasin D	Sigma-Aldrich Cat. #: C8273	CAS: 22144-77-0
Genistein	Sigma-Aldrich Cat. #: G6649	CAS: 446-72-0
Monastrol	Tocris Cat. #: 1305	CAS: 254753-54-3
Pitstop 2	Sigma-Aldrich Cat. #: SML1169	CAS: 1332879-52-3
Nocodazol	Sigma-Aldrich Cat. #: SML1665	CAS: 31430-18-9
Experimental models: cell lines		
Human: RUES2 hESC line (NIH approval number NIH hESC-09-0013; RRID:CVCL_B810)	The Rockefeller University Human Pluripotent Stem Cell Core	RRID:CVCL_B810
Oligonucleotides		
BMP4-KO CRISPR guide RNA 1_F caccgCTAGTTTGATACCTGAGACG	This paper	N/A
BMP4-KO CRISPR guide RNA 1_R aaacCGTCTCAGGTATCAAACTAGC	This paper	N/A
BMP4-KO CRISPR guide RNA 2_F caccgCGCCGAGATTCAGGGCCACG	This paper	N/A
BMP4-KO CRISPR guide RNA 2_R aaacCGTGGCCCTGAATCTCGGCGC	This paper	N/A

qPCR primer GAPDH_F GTGGACCTGACCTGCCGT	This paper	N/A
qPCR primer GAPDH_R GGAGGAGTGGGTGTCGCT	This paper	N/A
qPCR primer BMP4_F CTGGTCTTGAGTATCCTGAGCG	This paper	N/A
qPCR primer BMP4_R TCACCTCGTTCTCAGGGATGCT	This paper	N/A
qPCR primer NOGGIN_F GAAGCTGCGGAGGAAGTTAC	This paper	N/A
qPCR primer NOGGIN_R TACAGCACGGGGCAGAAT	This paper	N/A

EXPERIMENTAL MODEL AND SUBJECT DETAILS

Routine hESC line maintenance

Experiments were performed with RUES2 hESC line (NIH hESC-09-0013; RRID:CVCL_B810). Cells were tested for mycoplasma infection before beginning experiments and then again at 2-month intervals. Cell lines were routinely maintained on tissue culture dishes coated with Matrigel (BD Biosciences, 1:40 dilution). Dishes were coated in Matrigel overnight at 4 °C and then incubated at 37 °C for 1 h immediately before the cells were seeded on the surface. All hESC lines were grown in HUESM medium (DMEM supplemented with 20% knockout serum replacement, 1×B27 supplement without vitamin A, 0.1 mM non-essential amino acids, 2 mM GlutaMax and 0.1 mM 2-mercaptoethanol) that was conditioned by mouse embryonic fibroblasts (MEF-CM) and supplemented with 20 ng/ml bFGF. The medium was changed daily. Cells were passaged as aggregates using ReLeSR (Stem Cell Technologies), or as single cells using Accutase (Stem Cell Technologies).

Cell line generation

Human Noggin cDNA was amplified by PCR from a cDNA clone obtained from Thermo Scientific (MHS6278-202841236). V5 tag was inserted at the N-terminal end for NOGGIN, upstream of the start codon by insertion into the PCR primers. Construct for the expression of Myc-tagged xBMP4 was generated previously (Degnin et al., 2004, Cui et al., 2001). The inserts were then separately cloned into a bi-cistronic vector expressing constitutively a puromycine resistance. The gene to be expressed was placed downstream of the Tet responsive element (Fig. 1B and Fig 2A). The CRISPR/Cas9 system was used to generate a BMP4-Knockout RUES2 hESC line by targeting exon 3 of the BMP4 gene (ENGS 125378) (Supp. Fig. 1B).

Nucleofection was carried out using the Cell Line Nucelofector Kit L (Lonza, Walkersville, MD) and the B-016 setting of a Nucleofector II instrument. Nucleofected cells were plated into MEF-CM supplemented with 10 μM Rock-inhibitor. Antibiotic selection was started at day 4 and continued for 7 days. Cells that survived selection were passaged as single cells using Accutase, plated in MEF-CM supplemented with 10 μM Rock-inhibitor, and allowed to grow into colonies. Colonies arising from a single cell were handpicked, expanded, and screened for correct targeting by PCR amplification of the genomic region and Sanger sequencing. Correctly targeted clones were subsequently transfected with ePiggyBac plasmids containing a nuclear marker (H2B-mCitrine or H2B-mCherry cassettes) (Lacoste et al., 2009). Individual clones were again isolated and controlled for normal karyotype (G-banding) and pluripotency maintenance. Once the clones had been successfully established, they were assayed functionally: brightness for the morphological reporter, pSMAD1/5 activation for the BMP4-expressing line, BMP4 inhibition for the NOGGIN-expressing line, and BMP4 mRNA expression for the BMP4-KO lines.

All cell lines were sequenced and karyotyped (GTL banding; Cell Line Genetics) as part of routine culture quality control.

2D model epiblast

Except the microfluidic experiment, all experiments were done with hESCs grown on transwell filters. Transwell polycarbonate membrane (Corning, 3413) inserts, 6.5 mm in diameter, were coated for 2 h at 37 °C with 100 µl of 10 mg ml^{-1} laminin 521 (BioLamina) diluted in PBS+/+. The membrane was rinsed with PBS+/+. The cells were dissociated as single cells with Accutase and then resuspended in MEF-CM + 20 ng ml^{-1} bFGF + 10 µM RI. The same medium containing 200,000 cells in 100 µl was added on top of the membrane and 600 µl of the same medium (without cells) was added to the bottom of each filter insert. This volume condition kept the culture system in hydrostatic equilibrium. The RI was washed out 2 h later (from both filter compartments).

18-20 h after seeding, MEF-CM + 20 ng ml^{-1} bFGF + 0.2 µg ml^{-1} doxycyline was added to the top and bottom chambers if induction of expression vectors was required. 0.2 µg ml^{-1} doxycyline was determined to be the saturating dose for the overexpression of TRE::NOGGIN-V5 hESCs (Figure 2.7).

If media were to be collected for western blotting, E8 medium (STEMCEL Technology) + 0.2 µg ml^{-1} doxycyline was used instead because serum produced by MEF-CM causes large non-specific bands that confound analysis.

METHOD DETAILS

qPCR

WT RUES2 hESCs were cultured on Transwell filters. 18-20 h after seeding, doxycycline (0, 0.01 μg ml^{-1}, 0.05 μg ml^{-1}, 0.2 μg ml^{-1}, and 1 μg ml^{-1}) or recombinant BMP4 (0 ng ml^{-1}, 10 ng ml^{-1} and 50 ng ml^{-1}) was added to the transwell for 2 h, 6 h, or 12 h. Cells were lyzed in Trizol (Thermo Fisher Scientific) and their total RNA was isolated using RNeasy mini kit (QIAGEN). cDNA was synthesized using the Maxima H Minus First Strand cDNA Synthesis Kit (Life Technologies). qRT-PCR for selected genes were performed using PowerUp SYBR Green Master Mix (Life Technologies) in a QuantStudio 6 Pro PCR Systems (Applied Biosystems).

Immunostaining

At specified time points, filters were fixed with 4% PFA (Electron Microscopy) for 20 min, washed twice with PBS, permeablized with 0.5% Triton X-100 in PBS (PBST) for 15 min, and then blocked with 3% normal donkey serum in 0.1% PBST for 1 h. Cultures were incubated overnight with primary antibodies in this blocking buffer at 4°C, washed three times with 0.1% PBST for 30 min each, and then incubated with secondary antibodies (diluted 1:500) (Life Technologies: donkey anti-rabbit, donkey anti-mouse or donkey anti-goat antibodies conjugated with Alexa Fluor 488, 555 or 647) and DAPI (1 ug ml^{-1}) in blocking solution for 1 h before being washed three times with 0.1% PBST for 30 min each. Transwell filters were removed from the inserts and mounted with excess ProLong Gold antifade mountant (Invitrogen) onto glass coverslips. Coverslips were sealed with nail polish before antifade mountant dries to preserve cellular structures in the z-plane.

Endosome labeling

Culture of cells on filters were prepared as described above. Cells were stimulated with 0.2 μg ml^{-1} doxycycline for 24 hrs prior to endosome labeling.

Endosome labeling protocols for ASE, BSE, and CRE were adapted from (Perez Bay et al., 2016). In short, the ASE is labeled by 5-minute apical incubation with WGA-FITC (Sigma-Aldrich, L4895), the BSE by 5-minute basal incubation with transferrin-CF488, and the CRE by 45-minute basal incubation with transferrin-CF488 (Biotium, #00081). Macro- and micro-pinocytosis vesicles were labeled by 10-minute apical incubation with 10kDA Dextran-FITC (Li et al., 2015). The ARE and EE were labeled via immunofluorescence by Rab11A and EEA1, respectively. Following labeling of endosomal compartments, cells were processed for immunolabeling as described above.

Imaging

All confocal images were acquired on Inverted Zeiss LSM 780 laser scanning confocal microscope (Zeiss) with a 20x/0.8 numerical aperture (NA) or 60X/1.4 NA oil-immersion objective lens. The confocal pinhole was set to 1 Airy unit. For z-stacks, the z-spacing was 0.5 μm.

Western blotting

Cell lysate collection: After being briefly washed with cold PBS+/+, cells were directly lysed on filters with RIPA lysis and extraction buffer (Thermo Scientific) supplemented with 1X proteinase inhibitor as per manufacturer's recommendation for monolayer-cultured mammalian cells.

Medium collection: Media from the apical and basolateral chambers were collected directly from transwell filters. Due to the differential volumes used in culture, the apical medium was diluted 6x

to normalize to the basal medium. Samples were supplemented with 1X proteinase inhibitor (Thermo Scientific) before being centrifuged at ~14,000 x g for 15 minutes to remove cell debris. For all western blotting experiments, collected samples were denatured and reduced in NuPAGE LDS buffer (Invitrogen) and NuPAGE reducing reagent (Invitrogen) at 70°C for 10 minutes. SDS-PAGE in 4-15% Mini-PROTEAN TGX precast gels (BIO-RAD) under reducing conditions was performed. Protein transfer was performed with Trans-Blot® Turbo™ Mini PVDF (BIO-RAD) according to manufacturer's instructions.

Following transfer, membranes were blocked with 5% non-fat dried milk in 1X Tris-Buffered Saline with 0.1% Tween® 20 Detergent (TBST) for 1 h. Membranes were incubated overnight with primary antibodies in 3% BSA in TBST at 4°C. After 3 15-minute washes with TBST, membranes were incubated with secondary antibodies (AffiniPure Fab Fragment Donkey Anti-Rabbit or Donkey Anti-Mouse IgG; Jackson ImmunoResearch Lab) in 3% BSA in TBST for 1 h. After 3 15-minute washes with TBST, detection was performed with Pierce™ ECL Western Blotting Substrate (Thermo Scientific) or SuperSignal West Femto Maximum Sensitivity Substrate (Thermo Scientific), following manufacturer's instructions.

Transcytosis inhibition

WT RUES2 hESCs were cultured on Transwell filters as described above. 250 ng ml^{-1} recombinant human NOGGIN (R&D Systems; 6057) was added to the apical compartment. For nonspecific inhibition of endocytosis, the filters were moved to 4°C for 2 hours. For pharmacological inhibition of endocytosis, inhibitors were individually added to the apical compartment for 2 hours; the final concentrations of each inhibitor are listed in Supplementary

Table 1. After 2 hours, the cell lysates were collected and processed for Western blotting as described previously.

Microfluidic device fabrication

75 x 25 mm glass slides (VWR) were sonicated in acetone and isopronanol for 20 min each and rinsed with deionized water.

The custom microfluidic device consisted of a polymethylsiloxane (PDMS) structure layer having a flow channel sandwiched between two glass slides. The PDMS structure layer was made by mixing PDMS curing agent and base polymer (Sylgard 184; Dow Corning) at a ratio of 1:10 before casting PDMS prepolymer onto a 3D-printed mold and baking at 40°C for 12 h. On one side, the PDMS layer was permanently attached via plasma bonding to a glass slide which had custom-drilled inlet and outlet holes (1.2-mm diameter). On the other side, the PDMS layer was reversibly attached via surface adhesion to another glass slide which would provide the surface for cells to be cultured. This reversible attachment allowed for easy disassembly of the flow chamber system and removal of the glass slide containing the cell epithelium, thus simplifying subsequent immunostaining steps.

The completed flow cell was inserted into a custom metal clamping frame where inlet and outlet tubing was screwed on for a tight seal (Supplementary Fig. 1). Before usage, the microfluidic device was sterilized under UV light for 30 min.

Microfluidic flow assay

Microfluidic chambers were coated for 2 hrs at 37 °C with 100 µl of 10 mg ml^{-1} laminin 521 (BioLamina) diluted in PBS+/+. The cells were dissociated as single cells with Accutase and then resuspended in MEF-CM + 20 ng ml^{-1} bFGF + 10 µM RI + 100 U ml^{-1} penicillin–streptomycin. The same medium containing 4 × 10^{6} cells ml^{-1} was slowly flowed in to the chamber at a rate of 100 µl minute^{-1} until the chamber surface was covered evenly and entirely by cells. 2 h later, the RI and excess cells were flowed out at a rate of 3 ml h^{-1}; then, the flow rate was set to 10 µl h^{-1}. 30-36 h after seeding, if induction of expression vectors was required, MEF-CM + 20 ng ml^{-1} bFGF + 0.2 µg ml^{-1} doxycyline was quickly flowed in at a rate of 3 ml h^{-1} for 30 minutes. The flow rate was then set to 10 µl h^{-1} or 1000 µl h^{-1} for minimal flow or high flow conditions, respectively.

After 6 hrs, 4% PFA (Electron Microscopy) was quickly flowed into the chamber and the epithelium was fixed for 20 minutes. The microfluidic chamber was then disassembled, and the epithelium on glass slide immunostained as described above.

Transcytosis

Collecting NOGGIN-conditioned medium: RUES2-ePB-TRE::V5-NOGGIN cells were cultured on Geltrex-coated dishes (Thermo Fisher; A1413302) at a density of 2.5 × 10^{5} cells cm^{-2}. The cells were stimulated with 0.2 µg ml^{-1} doxycyline for in 2 ml E8 36 h. NOGGIN-conditioned E8 medium was then centrifuged to remove cell debris, and supplemented with 1X Knockout-SR, 1X MEM NEAA, 1X GlutaMAX, 1X Insulin/Transferrin/Selenium, 1X Pyruvate, 1X B27 without vitamin A, 1X 2-Mercaptoethanol, and 20 ng ml^{-1} bFGF .

NOGGIN-conditioned medium was added to either the apical or basal compartment of transwell filter cassette before being collected after 36 h for western blotting as described above.

Epithelium membrane integrity was assessed via fluorescent-conjugated 40-kDA Dextran-TxRed/40-kDA Dextran-FITC permeability assay and immuno visualization of an apical meshwork of ZO-1.

QUANTIFICATION AND STATISTICAL ANALYSIS

Image Analysis

Image processing and analysis for endosome co-localization were carried out with the ImageJ software. Following background subtraction, the image was converted to binary, then median filtering was applied. NOGGIN/endosome overlap was obtained via the Image Calculator plugin with the operator "min." A Z-axis profile was generated for each channel.

$$\%\ \text{NOGGIN co-localizing to an endosome} = \frac{\text{overlap}}{\text{total V5 labeling}}\ 100\%$$

$$\%\ \text{endosome co-localizing to V5} = \frac{\text{overlap}}{\text{total endosome labeling}}\ 100\%$$

These operations were applied for all the confocal sections of a confocal stack in each 50 μm x 50 μm region of interest. 4 regions of interest were analyzed per group.

pSMAD1/5 signal propagation analysis: A median filter with a box size of ~2/3 of a nuclear radius was applied to all images to eliminate extreme values while preserving edges. The nuclei of BMP secreting cells were defined by thresholding the strong nuclear marker, which is easily done since their average density is 1:200. The nuclear masks were all verified visually. A distance function was computed for each pixel giving its location to the nearest pixel in a BMP secreting cell. The pSMAD1 signal was averaged in distance bins ~ nuclear radius, with an additional constraint that

pixels within the bin distance from the image boundaries were excluded. The first bin included all pixels within the nuclei of the secreting cells (distance 0), which were generally higher than the surroundings. A background level of pSMAD1 was defined by the lowest 10% of pixels that are simultaneously fall within the highest 75% of the DAPI intensity range. (The nuclei occupy at least 50% of the image area.) The background pSMAD1 level was computed and subtracted separately for each image, but were generally consistent across all images to about 10-20%.

Statistical Methods

All values are reported as the mean where the error bars represent SD or SEM, as described in the figure's legend. For all experiments $^{*}p<0.05$, $^{**}p<0.01$, $^{***}p<0.001$. Statistical quantification was performed on the statistical graphing software GraphPad Prism v9.0.

REFERENCES

(WHO), W. H. O. 2010. Birth Defects. Sixty-third World Health Assembly. *Report by the Secretariat.*

ABASSI, Y. A., XI, B., ZHANG, W., YE, P., KIRSTEIN, S. L., GAYLORD, M. R., FEINSTEIN, S. C., WANG, X. & XU, X. 2009. Kinetic cell-based morphological screening: prediction of mechanism of compound action and off-target effects. *Chem Biol,* 16**,** 712-23.

AFFOLTER, M. & BASLER, K. 2007. The Decapentaplegic morphogen gradient: from pattern formation to growth regulation. *Nat Rev Genet,* 8**,** 663-74.

AKIYAMA, T., ISHIDA, J., NAKAGAWA, S., OGAWARA, H., WATANABE, S., ITOH, N., SHIBUYA, M. & FUKAMI, Y. 1987. Genistein, a specific inhibitor of tyrosine-specific protein kinases. *J Biol Chem,* 262**,** 5592-5.

AKIYAMA, T., KAMIMURA, K., FIRKUS, C., TAKEO, S., SHIMMI, O. & NAKATO, H. 2008. Dally regulates Dpp morphogen gradient formation by stabilizing Dpp on the cell surface. *Dev Biol,* 313**,** 408-19.

AOKI, T., NOMURA, R. & FUJIMOTO, T. 1999. Tyrosine phosphorylation of caveolin-1 in the endothelium. *Exp Cell Res,* 253**,** 629-36.

AONO, A., HAZAMA, M., NOTOYA, K., TAKETOMI, S., YAMASAKI, H., TSUKUDA, R., SASAKI, S. & FUJISAWA, Y. 1995. Potent ectopic bone-inducing activity of bone morphogenetic protein-4/7 heterodimer. *Biochem Biophys Res Commun,* 210**,** 670-7.

ARNOLD, S. J. & ROBERTSON, E. J. 2009. Making a commitment: cell lineage allocation and axis patterning in the early mouse embryo. *Nat Rev Mol Cell Biol,* 10**,** 91-103.

ASPENBERG, P., JEPPSSON, C. & ECONOMIDES, A. N. 2001. The bone morphogenetic proteins antagonist Noggin inhibits membranous ossification. *J Bone Miner Res,* 16**,** 497-500.

BALLERMANN, B. J., DARDIK, A., ENG, E. & LIU, A. 1998. Shear stress and the endothelium. *Kidney Int Suppl,* 67**,** S100-8.

BECCARI, L., MORIS, N., GIRGIN, M., TURNER, D. A., BAILLIE-JOHNSON, P., COSSY, A. C., LUTOLF, M. P., DUBOULE, D. & ARIAS, A. M. 2018. Multi-axial self-organization properties of mouse embryonic stem cells into gastruloids. *Nature,* 562**,** 272-276.

BEGEMANN, G., SCHILLING, T. F., RAUCH, G. J., GEISLER, R. & INGHAM, P. W. 2001. The zebrafish neckless mutation reveals a requirement for raldh2 in mesodermal signals that pattern the hindbrain. *Development,* 128**,** 3081-94.

BELENKAYA, T. Y., HAN, C., YAN, D., OPOKA, R. J., KHODOUN, M., LIU, H. & LIN, X. 2004. Drosophila Dpp morphogen movement is independent of dynamin-mediated endocytosis but regulated by the glypican members of heparan sulfate proteoglycans. *Cell,* 119**,** 231-44.

BEN-HAIM, N., LU, C., GUZMAN-AYALA, M., PESCATORE, L., MESNARD, D., BISCHOFBERGER, M., NAEF, F., ROBERTSON, E. J. & CONSTAM, D. B. 2006. The nodal precursor acting via activin receptors induces mesoderm by maintaining a source of its convertases and BMP4. *Dev Cell,* 11**,** 313-23.

BODENSTEIN, L. & STERN, C. D. 2005. Formation of the chick primitive streak as studied in computer simulations. *J Theor Biol,* 233**,** 253-69.

BOLLENBACH, T., KRUSE, K., PANTAZIS, P., GONZALEZ-GAITAN, M. & JULICHER, F. 2007. Morphogen transport in epithelia. *Phys Rev E Stat Nonlin Soft Matter Phys,* 75**,** 011901.

BRAGDON, B., MOSEYCHUK, O., SALDANHA, S., KING, D., JULIAN, J. & NOHE, A. 2011. Bone morphogenetic proteins: a critical review. *Cell Signal,* 23**,** 609-20.

BRENT, A. E. & TABIN, C. J. 2002. Developmental regulation of somite derivatives: muscle, cartilage and tendon. *Curr Opin Genet Dev,* 12**,** 548-57.

BRISCOE, J., CHEN, Y., JESSELL, T. M. & STRUHL, G. 2001. A hedgehog-insensitive form of patched provides evidence for direct long-range morphogen activity of sonic hedgehog in the neural tube. *Mol Cell,* 7**,** 1279-91.

BRISCOE, J. & SMALL, S. 2015. Morphogen rules: design principles of gradient-mediated embryo patterning. *Development,* 142**,** 3996-4009.

BRISCOE, J. & THEROND, P. P. 2013. The mechanisms of Hedgehog signalling and its roles in development and disease. *Nat Rev Mol Cell Biol,* 14**,** 416-29.

BROWN, P. S., WANG, E., AROETI, B., CHAPIN, S. J., MOSTOV, K. E. & DUNN, K. W. 2000. Definition of distinct compartments in polarized Madin-Darby canine kidney (MDCK) cells for membrane-volume sorting, polarized sorting and apical recycling. *Traffic,* 1**,** 124-40.

BRUNET, L. J., MCMAHON, J. A., MCMAHON, A. P. & HARLAND, R. M. 1998. Noggin, cartilage morphogenesis, and joint formation in the mammalian skeleton. *Science,* 280**,** 1455-7.

BRUNNER, P., HASTAR, N., KAEHLER, C., BURDZINSKI, W., JATZLAU, J. & KNAUS, P. 2020. AMOT130 drives BMP-SMAD signaling at the apical membrane in polarized cells. *Mol Biol Cell,* 31**,** 118-130.

CANALIS, E., ECONOMIDES, A. N. & GAZZERRO, E. 2003. Bone morphogenetic proteins, their antagonists, and the skeleton. *Endocr Rev,* 24**,** 218-35.

CENTERS FOR DISEASE, C. & PREVENTION 2008. Update on overall prevalence of major birth defects--Atlanta, Georgia, 1978-2005. *MMWR Morb Mortal Wkly Rep,* 57**,** 1-5.

CHAPMAN, S. C., SCHUBERT, F. R., SCHOENWOLF, G. C. & LUMSDEN, A. 2002. Analysis of spatial and temporal gene expression patterns in blastula and gastrula stage chick embryos. *Dev Biol,* 245**,** 187-99.

CHEN, Y. & SCHIER, A. F. 2001. The zebrafish Nodal signal Squint functions as a morphogen. *Nature,* 411**,** 607-10.

CHRISTIANSON A, H. C., MODELL B. 2006. The Hidden Toll of Dying and Disabled Children. March of Dimes Birth Defects Foundation.

CORNER, G. W. 1954. *George Linius Streeter - A Biographical Memoir*, National Academy of Sciences.

COUNCIL, N. R. C., H.E.S.C.R.A. 2010. Final Report of the National Academies' Human Embryonic Stem Cell Research Advisory Committee and 2010 Amendments to the National Academies' Guidelines for Human Embryonic Stem Cell Research. *National Academies Press.*

CRESAWN, K. O., POTTER, B. A., OZTAN, A., GUERRIERO, C. J., IHRKE, G., GOLDENRING, J. R., APODACA, G. & WEISZ, O. A. 2007. Differential involvement of endocytic compartments in the biosynthetic traffic of apical proteins. *EMBO J,* 26**,** 3737-48.

CRICK, F. 1970. Diffusion in Embryogenesis. *Nature,* 225**,** 420-&.

CUI, Y., HACKENMILLER, R., BERG, L., JEAN, F., NAKAYAMA, T., THOMAS, G. & CHRISTIAN, J. L. 2001. The activity and signaling range of mature BMP-4 is regulated by sequential cleavage at two sites within the prodomain of the precursor. *Genes Dev,* 15**,** 2797-802.

DALE, L., HOWES, G., PRICE, B. M. & SMITH, J. C. 1992. Bone morphogenetic protein 4: a ventralizing factor in early Xenopus development. *Development,* 115**,** 573-85.

DALEY, G. Q., HYUN, I., APPERLEY, J. F., BARKER, R. A., BENVENISTY, N., BREDENOORD, A. L., BREUER, C. K., CAULFIELD, T., CEDARS, M. I., FREY-VASCONCELLS, J., HESLOP, H. E., JIN, Y., LEE, R. T., MCCABE, C., MUNSIE, M., MURRY, C. E., PIANTADOSI, S., RAO, M., ROOKE, H. M., SIPP, D., STUDER, L., SUGARMAN, J., TAKAHASHI, M., ZIMMERMAN, M. & KIMMELMAN, J. 2016. Setting Global Standards for Stem Cell Research and Clinical Translation: The 2016 ISSCR Guidelines. *Stem Cell Reports,* 6**,** 787-797.

DAVIDSON, K. C., MASON, E. A. & PERA, M. F. 2015. The pluripotent state in mouse and human. *Development,* 142**,** 3090-9.

DEGLINCERTI, A., CROFT, G. F., PIETILA, L. N., ZERNICKA-GOETZ, M., SIGGIA, E. D. & BRIVANLOU, A. H. 2016a. Self-organization of the in vitro attached human embryo. *Nature,* 533**,** 251-4.

DEGLINCERTI, A., ETOC, F., GUERRA, M. C., MARTYN, I., METZGER, J., RUZO, A., SIMUNOVIC, M., YONEY, A., BRIVANLOU, A. H., SIGGIA, E. & WARMFLASH, A. 2016b. Self-organization of human embryonic stem cells on micropatterns. *Nat Protoc,* 11**,** 2223-2232.

DEGNIN, C., JEAN, F., THOMAS, G. & CHRISTIAN, J. L. 2004. Cleavages within the prodomain direct intracellular trafficking and degradation of mature bone morphogenetic protein-4. *Mol Biol Cell,* 15**,** 5012-20.

DEJIMA, K., KANAI, M. I., AKIYAMA, T., LEVINGS, D. C. & NAKATO, H. 2011. Novel contact-dependent bone morphogenetic protein (BMP) signaling mediated by heparan sulfate proteoglycans. *J Biol Chem,* 286**,** 17103-11.

DELVAUX, M., BASTIE, M. J., CHENTOUFI, J., CRAGOE, E. J., JR., VAYSSE, N. & RIBET, A. 1990. Amiloride and analogues inhibit Na(+)-H+ exchange and cell proliferation in AR42J pancreatic cell line. *Am J Physiol,* 259**,** G842-9.

DEMONTIS, F. & DAHMANN, C. 2007. Apical and lateral cell protrusions interconnect epithelial cells in live Drosophila wing imaginal discs. *Dev Dyn,* 236**,** 3408-18.

DUTTA, D. & DONALDSON, J. G. 2012. Search for inhibitors of endocytosis: Intended specificity and unintended consequences. *Cell Logist,* 2**,** 203-208.

DUTTA, D., WILLIAMSON, C. D., COLE, N. B. & DONALDSON, J. G. 2012. Pitstop 2 is a potent inhibitor of clathrin-independent endocytosis. *PLoS One,* 7**,** e45799.

ENTCHEV, E. V., SCHWABEDISSEN, A. & GONZALEZ-GAITAN, M. 2000. Gradient formation of the TGF-beta homolog Dpp. *Cell,* 103**,** 981-91.

ETOC, F., METZGER, J., RUZO, A., KIRST, C., YONEY, A., OZAIR, M. Z., BRIVANLOU, A. H. & SIGGIA, E. D. 2016. A Balance between Secreted Inhibitors and Edge Sensing Controls Gastruloid Self-Organization. *Dev Cell,* 39**,** 302-315.

FABREGAT, A., SIDIROPOULOS, K., VITERI, G., MARIN-GARCIA, P., PING, P., STEIN, L., D'EUSTACHIO, P. & HERMJAKOB, H. 2018. Reactome diagram viewer: data structures and strategies to boost performance. *Bioinformatics,* 34**,** 1208-1214.

FENG, X. H. & DERYNCK, R. 2005. Specificity and versatility in tgf-beta signaling through Smads. *Annu Rev Cell Dev Biol,* 21**,** 659-93.

FUJIMOTO, L. M., ROTH, R., HEUSER, J. E. & SCHMID, S. L. 2000. Actin assembly plays a variable, but not obligatory role in receptor-mediated endocytosis in mammalian cells. *Traffic,* 1**,** 161-71.

FUJISE, M., TAKEO, S., KAMIMURA, K., MATSUO, T., AIGAKI, T., IZUMI, S. & NAKATO, H. 2003. Dally regulates Dpp morphogen gradient formation in the Drosophila wing. *Development,* 130**,** 1515-22.

GALLET, A., STACCINI-LAVENANT, L. & THEROND, P. P. 2008. Cellular trafficking of the glypican Dally-like is required for full-strength Hedgehog signaling and wingless transcytosis. *Dev Cell,* 14**,** 712-25.

GIERER, A. & MEINHARDT, H. 1972. A theory of biological pattern formation. *Kybernetik,* 12**,** 30-9.

GILMOUR, D., REMBOLD, M. & LEPTIN, M. 2017. From morphogen to morphogenesis and back. *Nature,* 541**,** 311-320.

GRAFF, J. M. 1997. Embryonic patterning: to BMP or not to BMP, that is the question. *Cell,* 89**,** 171-4.

GRANDEL, H., LUN, K., RAUCH, G. J., RHINN, M., PIOTROWSKI, T., HOUART, C., SORDINO, P., KUCHLER, A. M., SCHULTE-MERKER, S., GEISLER, R., HOLDER, N., WILSON, S. W. & BRAND, M. 2002. Retinoic acid signalling in the zebrafish embryo is necessary during pre-segmentation stages to pattern the anterior-posterior axis of the CNS and to induce a pectoral fin bud. *Development,* 129**,** 2851-65.

GRAY, A. M. & MASON, A. J. 1990. Requirement for activin A and transforming growth factor--beta 1 pro-regions in homodimer assembly. *Science,* 247**,** 1328-30.

GREEN, J. B. & SHARPE, J. 2015. Positional information and reaction-diffusion: two big ideas in developmental biology combine. *Development,* 142**,** 1203-11.

GROPPE, J., GREENWALD, J., WIATER, E., RODRIGUEZ-LEON, J., ECONOMIDES, A. N., KWIATKOWSKI, W., AFFOLTER, M., VALE, W. W., IZPISUA BELMONTE, J. C. & CHOE, S. 2002. Structural basis of BMP signalling inhibition by the cystine knot protein Noggin. *Nature,* 420**,** 636-42.

GUO, J. & WU, G. 2012. The signaling and functions of heterodimeric bone morphogenetic proteins. *Cytokine Growth Factor Rev,* 23**,** 61-7.

GURDON, J. B. & BOURILLOT, P. Y. 2001. Morphogen gradient interpretation. *Nature,* 413**,** 797-803.

HAMM-ALVAREZ, S. F., SONEE, M., LORAN-GOSS, K. & SHEN, W. C. 1996. Paclitaxel and nocodazole differentially alter endocytosis in cultured cells. *Pharm Res,* 13**,** 1647-56.

HAN, C., BELENKAYA, T. Y., KHODOUN, M., TAUCHI, M., LIN, X. & LIN, X. 2004. Distinct and collaborative roles of Drosophila EXT family proteins in morphogen signalling and gradient formation. *Development,* 131**,** 1563-75.

HARASZTOSI, C., KLENSKE, E., BADUM, S., HARASZTOSI, E. & GUMMER, A. W. 2018. Double fluorescent labelling of a bipolar epithelial cell in vitro: The outer hair cell. *J Neurosci Methods,* 293**,** 310-320.

HARMANSA, S., ALBORELLI, I., BIELI, D., CAUSSINUS, E. & AFFOLTER, M. 2017. A nanobody-based toolset to investigate the role of protein localization and dispersal in Drosophila. *Elife,* 6.

HARRISON, S. E., SOZEN, B., CHRISTODOULOU, N., KYPRIANOU, C. & ZERNICKA-GOETZ, M. 2017. Assembly of embryonic and extraembryonic stem cells to mimic embryogenesis in vitro. *Science,* 356.

HARTUNG, A., BITTON-WORMS, K., RECHTMAN, M. M., WENZEL, V., BOERGERMANN, J. H., HASSEL, S., HENIS, Y. I. & KNAUS, P. 2006. Different routes of bone morphogenic protein (BMP) receptor endocytosis influence BMP signaling. *Mol Cell Biol,* 26**,** 7791-805.

HAZAMA, M., AONO, A., UENO, N. & FUJISAWA, Y. 1995. Efficient expression of a heterodimer of bone morphogenetic protein subunits using a baculovirus expression system. *Biochem Biophys Res Commun,* 209**,** 859-66.

HIDALGO, D. A. H., Z.; ROMANOVA-MICHAELIDES, M.; GONZÁLEZ-GAITÁN, M.; JÜLICHER F. 2019. Dynamic modes of morphogen transport. *arXiv,* 1909.13280.

HIKASA, H. & SOKOL, S. Y. 2013. Wnt signaling in vertebrate axis specification. *Cold Spring Harb Perspect Biol,* 5**,** a007955.

HOEBEKE, J., VAN NIJEN, G. & DE BRABANDER, M. 1976. Interaction of oncodazole (R 17934), a new antitumoral drug, with rat brain tubulin. *Biochem Biophys Res Commun,* 69**,** 319-24.

HSIUNG, F., RAMIREZ-WEBER, F. A., IWAKI, D. D. & KORNBERG, T. B. 2005. Dependence of Drosophila wing imaginal disc cytonemes on Decapentaplegic. *Nature,* 437**,** 560-3.

HUANG, J. J., WANG, Y. J., ZHANG, M., ZHANG, P., LIANG, H., BAI, H. J., YU, X. J. & YANG, H. T. 2017. Functional expression of the Ca(2+) signaling machinery in human embryonic stem cells. *Acta Pharmacol Sin,* 38**,** 1663-1672.

HUANGFU, D. & ANDERSON, K. V. 2006. Signaling from Smo to Ci/Gli: conservation and divergence of Hedgehog pathways from Drosophila to vertebrates. *Development,* 133**,** 3-14.

HYUN, I., WILKERSON, A. & JOHNSTON, J. 2016. Embryology policy: Revisit the 14-day rule. *Nature,* 533**,** 169-71.

ISRAEL, D. I., NOVE, J., KERNS, K. M., KAUFMAN, R. J., ROSEN, V., COX, K. A. & WOZNEY, J. M. 1996. Heterodimeric bone morphogenetic proteins show enhanced activity in vitro and in vivo. *Growth Factors,* 13**,** 291-300.

IVANOV, A. I. 2008. Pharmacological inhibition of endocytic pathways: is it specific enough to be useful? *Methods Mol Biol,* 440**,** 15-33.

JACKMAN, M. R., SHURETY, W., ELLIS, J. A. & LUZIO, J. P. 1994. Inhibition of apical but not basolateral endocytosis of ricin and folate in Caco-2 cells by cytochalasin D. *J Cell Sci,* 107 (Pt 9)**,** 2547-56.

JONES, C. M., DALE, L., HOGAN, B. L., WRIGHT, C. V. & SMITH, J. C. 1996. Bone morphogenetic protein-4 (BMP-4) acts during gastrula stages to cause ventralization of Xenopus embryos. *Development,* 122**,** 1545-54.

JONES, C. M., LYONS, K. M., LAPAN, P. M., WRIGHT, C. V. & HOGAN, B. L. 1992. DVR-4 (bone morphogenetic protein-4) as a posterior-ventralizing factor in Xenopus mesoderm induction. *Development,* 115**,** 639-47.

KNIGHT, A., HUGHSON, E., HOPKINS, C. R. & CUTLER, D. F. 1995. Membrane protein trafficking through the common apical endosome compartment of polarized Caco-2 cells. *Mol Biol Cell,* 6**,** 597-610.

KOIVUSALO, M., WELCH, C., HAYASHI, H., SCOTT, C. C., KIM, M., ALEXANDER, T., TOURET, N., HAHN, K. M. & GRINSTEIN, S. 2010. Amiloride inhibits macropinocytosis by lowering submembranous pH and preventing Rac1 and Cdc42 signaling. *J Cell Biol,* 188**,** 547-63.

KONDO, S. & MIURA, T. 2010. Reaction-diffusion model as a framework for understanding biological pattern formation. *Science,* 329**,** 1616-20.

KONG, J. H., SIEBOLD, C. & ROHATGI, R. 2019. Biochemical mechanisms of vertebrate hedgehog signaling. *Development,* 146.

KORNBERG, T. B. 2017. Distributing signaling proteins in space and time: the province of cytonemes. *Curr Opin Genet Dev,* 45**,** 22-27.

KOZMIKOVA, I. & KOZMIK, Z. 2020. Wnt/beta-catenin signaling is an evolutionarily conserved determinant of chordate dorsal organizer. *Elife,* 9.

KRUSE, K., PANTAZIS, P., BOLLENBACH, T., JULICHER, F. & GONZALEZ-GAITAN, M. 2004. Dpp gradient formation by dynamin-dependent endocytosis: receptor trafficking and the diffusion model. *Development,* 131**,** 4843-56.

LAGANA, A., VADNAIS, J., LE, P. U., NGUYEN, T. N., LAPRADE, R., NABI, I. R. & NOEL, J. 2000. Regulation of the formation of tumor cell pseudopodia by the Na(+)/H(+) exchanger NHE1. *J Cell Sci,* 113 (Pt 20)**,** 3649-62.

LANDER, A. D., NIE, Q. & WAN, F. Y. 2002. Do morphogen gradients arise by diffusion? *Dev Cell,* 2**,** 785-96.

LAPIERRE, L. A., DUCHARME, N. A., DRAKE, K. R., GOLDENRING, J. R. & KENWORTHY, A. K. 2012. Coordinated regulation of caveolin-1 and Rab11a in apical recycling compartments of polarized epithelial cells. *Exp Cell Res,* 318**,** 103-13.

LAWRENCE, P. A. 1988. Background to bicoid. *Cell,* 54**,** 1-2.

LECUIT, T., BROOK, W. J., NG, M., CALLEJA, M., SUN, H. & COHEN, S. M. 1996. Two distinct mechanisms for long-range patterning by Decapentaplegic in the Drosophila wing. *Nature,* 381**,** 387-93.

LEE, R. T., ZHAO, Z. & INGHAM, P. W. 2016. Hedgehog signalling. *Development,* 143**,** 367-72.

LI, L., WAN, T., WAN, M., LIU, B., CHENG, R. & ZHANG, R. 2015. The effect of the size of fluorescent dextran on its endocytic pathway. *Cell Biol Int,* 39**,** 531-9.

LINSTEDT, A. D. & HAURI, H. P. 1993. Giantin, a novel conserved Golgi membrane protein containing a cytoplasmic domain of at least 350 kDa. *Mol Biol Cell,* 4**,** 679-93.

LITTLE, S. C. & MULLINS, M. C. 2009. Bone morphogenetic protein heterodimers assemble heteromeric type I receptor complexes to pattern the dorsoventral axis. *Nat Cell Biol,* 11**,** 637-43.

LIU, A. 2019. Proteostasis in the Hedgehog signaling pathway. *Semin Cell Dev Biol,* 93**,** 153-163.

MARTYN, I., BRIVANLOU, A. H. & SIGGIA, E. D. 2019. A wave of WNT signaling balanced by secreted inhibitors controls primitive streak formation in micropattern colonies of human embryonic stem cells. *Development,* 146.

MASSAGUE, J., SEOANE, J. & WOTTON, D. 2005. Smad transcription factors. *Genes Dev,* 19**,** 2783-810.

MATOS, I., ASARE, A., LEVORSE, J., OUSPENSKAIA, T., DE LA CRUZ-RACELIS, J., SCHUHMACHER, L. N. & FUCHS, E. 2020. Progenitors oppositely polarize WNT activators and inhibitors to orchestrate tissue development. *Elife,* 9.

MAYER, T. U., KAPOOR, T. M., HAGGARTY, S. J., KING, R. W., SCHREIBER, S. L. & MITCHISON, T. J. 1999. Small molecule inhibitor of mitotic spindle bipolarity identified in a phenotype-based screen. *Science,* 286**,** 971-4.

MCCLUSKEY, A., DANIEL, J. A., HADZIC, G., CHAU, N., CLAYTON, E. L., MARIANA, A., WHITING, A., GORGANI, N. N., LLOYD, J., QUAN, A., MOSHKANBARYANS, L., KRISHNAN, S., PERERA, S., CHIRCOP, M., VON KLEIST, L., MCGEACHIE, A. B., HOWES, M. T., PARTON, R. G., CAMPBELL, M., SAKOFF, J. A., WANG, X.,

SUN, J. Y., ROBERTSON, M. J., DEANE, F. M., NGUYEN, T. H., MEUNIER, F. A., COUSIN, M. A. & ROBINSON, P. J. 2013. Building a better dynasore: the dyngo compounds potently inhibit dynamin and endocytosis. *Traffic,* 14**,** 1272-89.

MCGOUGH, I. J., VECCHIA, L., BISHOP, B., MALINAUSKAS, T., BECKETT, K., JOSHI, D., O'REILLY, N., SIEBOLD, C., JONES, E. Y. & VINCENT, J. P. 2020. Glypicans shield the Wnt lipid moiety to enable signalling at a distance. *Nature,* 585**,** 85-90.

MCMAHON, J. A., TAKADA, S., ZIMMERMAN, L. B., FAN, C. M., HARLAND, R. M. & MCMAHON, A. P. 1998. Noggin-mediated antagonism of BMP signaling is required for growth and patterning of the neural tube and somite. *Genes Dev,* 12**,** 1438-52.

MISHINA, Y., SUZUKI, A., UENO, N. & BEHRINGER, R. R. 1995. Bmpr encodes a type I bone morphogenetic protein receptor that is essential for gastrulation during mouse embryogenesis. *Genes Dev,* 9**,** 3027-37.

MITRANI, E., ZIV, T., THOMSEN, G., SHIMONI, Y., MELTON, D. A. & BRIL, A. 1990. Activin can induce the formation of axial structures and is expressed in the hypoblast of the chick. *Cell,* 63**,** 495-501.

MORGAN, T. H. 1901. Regeneration in the egg, embryo, and adult. *American Naturalist,* 35**,** 949-973.

MORIKAWA, M., DERYNCK, R. & MIYAZONO, K. 2016. TGF-beta and the TGF-beta Family: Context-Dependent Roles in Cell and Tissue Physiology. *Cold Spring Harb Perspect Biol,* 8.

MOUSTAKAS, A. & HELDIN, C. H. 2009. The regulation of TGFbeta signal transduction. *Development,* 136**,** 3699-714.

MULLER, P., ROGERS, K. W., YU, S. R., BRAND, M. & SCHIER, A. F. 2013. Morphogen transport. *Development,* 140**,** 1621-38.

MULLOR, J. L., CALLEJA, M., CAPDEVILA, J. & GUERRERO, I. 1997. Hedgehog activity, independent of decapentaplegic, participates in wing disc patterning. *Development,* 124**,** 1227-37.

NABI, I. R. & LE, P. U. 2003. Caveolae/raft-dependent endocytosis. *J Cell Biol,* 161**,** 673-7.

NALLET-STAUB, F., YIN, X., GILBERT, C., MARSAUD, V., BEN MIMOUN, S., JAVELAUD, D., LEOF, E. B. & MAUVIEL, A. 2015. Cell density sensing alters TGF-beta signaling in a cell-type-specific manner, independent from Hippo pathway activation. *Dev Cell,* 32**,** 640-51.

NELLEN, D., BURKE, R., STRUHL, G. & BASLER, K. 1996. Direct and long-range action of a DPP morphogen gradient. *Cell,* 85**,** 357-68.

NEUMANN, C. J. & COHEN, S. M. 1997. Long-range action of Wingless organizes the dorsal-ventral axis of the Drosophila wing. *Development,* 124**,** 871-80.

NISHIMATSU, S. & THOMSEN, G. H. 1998. Ventral mesoderm induction and patterning by bone morphogenetic protein heterodimers in Xenopus embryos. *Mech Dev,* 74**,** 75-88.

O'RAHILLY, R. & MULLER, F. 2010. Developmental stages in human embryos: revised and new measurements. *Cells Tissues Organs,* 192**,** 73-84.

ODORIZZI, G., PEARSE, A., DOMINGO, D., TROWBRIDGE, I. S. & HOPKINS, C. R. 1996. Apical and basolateral endosomes of MDCK cells are interconnected and contain a polarized sorting mechanism. *J Cell Biol,* 135**,** 139-52.

OHKAWARA, B., IEMURA, S., TEN DIJKE, P. & UENO, N. 2002. Action range of BMP is defined by its N-terminal basic amino acid core. *Curr Biol,* 12**,** 205-9.

PAARMANN, P., DORPHOLZ, G., FIEBIG, J., AMSALEM, A. R., EHRLICH, M., HENIS, Y. I., MULLER, T. & KNAUS, P. 2016. Dynamin-dependent endocytosis of Bone Morphogenetic Protein2 (BMP2) and its receptors is dispensable for the initiation of Smad signaling. *Int J Biochem Cell Biol,* 76**,** 51-63.

PAINE-SAUNDERS, S., VIVIANO, B. L., ECONOMIDES, A. N. & SAUNDERS, S. 2002. Heparan sulfate proteoglycans retain Noggin at the cell surface: a potential mechanism for shaping bone morphogenetic protein gradients. *J Biol Chem,* 277**,** 2089-96.

PARK, R. J., SHEN, H., LIU, L., LIU, X., FERGUSON, S. M. & DE CAMILLI, P. 2013. Dynamin triple knockout cells reveal off target effects of commonly used dynamin inhibitors. *J Cell Sci,* 126**,** 5305-12.

PENNIMPEDE, T., CAMERON, D. A., MACLEAN, G. A., LI, H., ABU-ABED, S. & PETKOVICH, M. 2010. The role of CYP26 enzymes in defining appropriate retinoic acid exposure during embryogenesis. *Birth Defects Res A Clin Mol Teratol,* 88**,** 883-94.

PEREZ BAY, A. E., SCHREINER, R., BENEDICTO, I., PAZ MARZOLO, M., BANFELDER, J., WEINSTEIN, A. M. & RODRIGUEZ-BOULAN, E. J. 2016. The fast-recycling receptor Megalin defines the apical recycling pathway of epithelial cells. *Nat Commun,* 7**,** 11550.

PETROPOULOS, S., PANULA, S. P., SCHELL, J. P. & LANNER, F. 2016. Single-cell RNA sequencing: revealing human pre-implantation development, pluripotency and germline development. *J Intern Med,* 280**,** 252-64.

QUININAO, C., PROCHIANTZ, A. & TOUBOUL, J. 2015. Local homeoprotein diffusion can stabilize boundaries generated by graded positional cues. *Development,* 142**,** 1860-8.

RAMIREZ-WEBER, F. A. & KORNBERG, T. B. 1999. Cytonemes: cellular processes that project to the principal signaling center in Drosophila imaginal discs. *Cell,* 97**,** 599-607.

RE'EM-KALMA, Y., LAMB, T. & FRANK, D. 1995. Competition between noggin and bone morphogenetic protein 4 activities may regulate dorsalization during Xenopus development. *Proc Natl Acad Sci U S A,* 92**,** 12141-5.

RHINN, M. & DOLLE, P. 2012. Retinoic acid signalling during development. *Development,* 139**,** 843-58.

RIDER, C. C. & MULLOY, B. 2017. Heparin, Heparan Sulphate and the TGF-beta Cytokine Superfamily. *Molecules,* 22.

RIVRON, N., PERA, M., ROSSANT, J., MARTINEZ ARIAS, A., ZERNICKA-GOETZ, M., FU, J., VAN DEN BRINK, S., BREDENOORD, A., DONDORP, W., DE WERT, G., HYUN, I., MUNSIE, M. & ISASI, R. 2018a. Debate ethics of embryo models from stem cells. *Nature,* 564**,** 183-185.

RIVRON, N. C., FRIAS-ALDEGUER, J., VRIJ, E. J., BOISSET, J. C., KORVING, J., VIVIE, J., TRUCKENMULLER, R. K., VAN OUDENAARDEN, A., VAN BLITTERSWIJK, C. A. & GEIJSEN, N. 2018b. Blastocyst-like structures generated solely from stem cells. *Nature,* 557**,** 106-111.

RODRIGUEZ-BOULAN, E., KREITZER, G. & MUSCH, A. 2005. Organization of vesicular trafficking in epithelia. *Nat Rev Mol Cell Biol,* 6**,** 233-47.

RODRIGUEZ-BOULAN, E. & MACARA, I. G. 2014. Organization and execution of the epithelial polarity programme. *Nat Rev Mol Cell Biol,* 15**,** 225-42.

RODRIGUEZ, T. A., SRINIVAS, S., CLEMENTS, M. P., SMITH, J. C. & BEDDINGTON, R. S. 2005. Induction and migration of the anterior visceral endoderm is regulated by the extra-embryonic ectoderm. *Development,* 132**,** 2513-20.

ROGERS, K. W. & SCHIER, A. F. 2011. Morphogen Gradients: From Generation to Interpretation. *Annual Review of Cell and Developmental Biology, Vol 27,* 27**,** 377-407.

ROSSANT, J. 2015. Mouse and human blastocyst-derived stem cells: vive les differences. *Development,* 142**,** 9-12.

ROY, S., HSIUNG, F. & KORNBERG, T. B. 2011. Specificity of Drosophila cytonemes for distinct signaling pathways. *Science,* 332**,** 354-8.

RULANDS, S., KLUNDER, B. & FREY, E. 2013. Stability of localized wave fronts in bistable systems. *Phys Rev Lett,* 110**,** 038102.

SAMPATH, P. & POLLARD, T. D. 1991. Effects of cytochalasin, phalloidin, and pH on the elongation of actin filaments. *Biochemistry,* 30**,** 1973-80.

SAWALA, A., SUTCLIFFE, C. & ASHE, H. L. 2012. Multistep molecular mechanism for bone morphogenetic protein extracellular transport in the Drosophila embryo. *Proc Natl Acad Sci U S A,* 109**,** 11222-7.

SCHLIWA, M. 1982. Action of cytochalasin D on cytoskeletal networks. *J Cell Biol,* 92**,** 79-91.

SCHMID, B., FURTHAUER, M., CONNORS, S. A., TROUT, J., THISSE, B., THISSE, C. & MULLINS, M. C. 2000. Equivalent genetic roles for bmp7/snailhouse and bmp2b/swirl in dorsoventral pattern formation. *Development,* 127**,** 957-67.

SCHMIERER, B. & HILL, C. S. 2007. TGFbeta-SMAD signal transduction: molecular specificity and functional flexibility. *Nat Rev Mol Cell Biol,* 8**,** 970-82.

SHAHBAZI, M. N. 2020. Mechanisms of human embryo development: from cell fate to tissue shape and back. *Development,* 147.

SHAHBAZI, M. N., JEDRUSIK, A., VUORISTO, S., RECHER, G., HUPALOWSKA, A., BOLTON, V., FOGARTY, N. N. M., CAMPBELL, A., DEVITO, L., ILIC, D., KHALAF, Y., NIAKAN, K. K., FISHEL, S. & ZERNICKA-GOETZ, M. 2016. Self-organization of the human embryo in the absence of maternal tissues. *Nat Cell Biol,* 18**,** 700-708.

SHAHBAZI, M. N. & ZERNICKA-GOETZ, M. 2018. Deconstructing and reconstructing the mouse and human early embryo. *Nat Cell Biol,* 20**,** 878-887.

SHAO, Y., TANIGUCHI, K., TOWNSHEND, R. F., MIKI, T., GUMUCIO, D. L. & FU, J. 2017. A pluripotent stem cell-based model for post-implantation human amniotic sac development. *Nat Commun,* 8**,** 208.

SHEFF, D. R., DARO, E. A., HULL, M. & MELLMAN, I. 1999. The receptor recycling pathway contains two distinct populations of early endosomes with different sorting functions. *J Cell Biol,* 145**,** 123-39.

SIMONSEN, A., LIPPE, R., CHRISTOFORIDIS, S., GAULLIER, J. M., BRECH, A., CALLAGHAN, J., TOH, B. H., MURPHY, C., ZERIAL, M. & STENMARK, H. 1998. EEA1 links PI(3)K function to Rab5 regulation of endosome fusion. *Nature,* 394**,** 494-8.

SIMUNOVIC, M., METZGER, J. J., ETOC, F., YONEY, A., RUZO, A., MARTYN, I., CROFT, G., YOU, D. S., BRIVANLOU, A. H. & SIGGIA, E. D. 2019. A 3D model of a human epiblast reveals BMP4-driven symmetry breaking. *Nat Cell Biol,* 21**,** 900-910.

SMITH, W. C. & HARLAND, R. M. 1992. Expression cloning of noggin, a new dorsalizing factor localized to the Spemann organizer in Xenopus embryos. *Cell,* 70**,** 829-40.

SOKOL, S. Y. 1999. Wnt signaling and dorso-ventral axis specification in vertebrates. *Curr Opin Genet Dev,* 9**,** 405-10.

SORRE, B., WARMFLASH, A., BRIVANLOU, A. H. & SIGGIA, E. D. 2014. Encoding of temporal signals by the TGF-beta pathway and implications for embryonic patterning. *Dev Cell,* 30**,** 334-42.

ST JOHNSTON, D. & NUSSLEIN-VOLHARD, C. 1992. The origin of pattern and polarity in the Drosophila embryo. *Cell,* 68**,** 201-19.

STRIGINI, M. & COHEN, S. M. 1997. A Hedgehog activity gradient contributes to AP axial patterning of the Drosophila wing. *Development,* 124**,** 4697-705.

STUMPF, H. F. 1966. Mechanism by Which Cells Estimate Their Location within Body. *Nature,* 212**,** 430-&.

SUBTIL, A. & DAUTRY-VARSAT, A. 1997. Microtubule depolymerization inhibits clathrin coated-pit internalization in non-adherent cell lines while interleukin 2 endocytosis is not affected. *J Cell Sci,* 110 (Pt 19)**,** 2441-7.

SUZUKI, A., KANEKO, E., MAEDA, J. & UENO, N. 1997. Mesoderm induction by BMP-4 and -7 heterodimers. *Biochem Biophys Res Commun,* 232**,** 153-6.

TAKEI, Y., OZAWA, Y., SATO, M., WATANABE, A. & TABATA, T. 2004. Three Drosophila EXT genes shape morphogen gradients through synthesis of heparan sulfate proteoglycans. *Development,* 131**,** 73-82.

TELEMAN, A. A. & COHEN, S. M. 2000. Dpp gradient formation in the Drosophila wing imaginal disc. *Cell,* 103**,** 971-80.

TEN BERGE, D., KOOLE, W., FUERER, C., FISH, M., EROGLU, E. & NUSSE, R. 2008. Wnt signaling mediates self-organization and axis formation in embryoid bodies. *Cell Stem Cell,* 3**,** 508-18.

TURING, A. M. 1990. The chemical basis of morphogenesis. 1953. *Bull Math Biol,* 52**,** 153-97; discussion 119-52.

TYSER, R. C. V. M., E.; NAKANOH S.; VALLIER, L.; SCIALDONE, A.; SRINIVAS A. 2020. A spatially resolved single cell atlas of human gastrulation. bioRxiv.

ULLOA, F. & MARTI, E. 2010. Wnt won the war: antagonistic role of Wnt over Shh controls dorso-ventral patterning of the vertebrate neural tube. *Dev Dyn,* 239**,** 69-76.

VALENZUELA, D. M., ECONOMIDES, A. N., ROJAS, E., LAMB, T. M., NUNEZ, L., JONES, P., LP, N. Y., ESPINOSA, R., 3RD, BRANNAN, C. I., GILBERT, D. J. & ET AL. 1995. Identification of mammalian noggin and its expression in the adult nervous system. *J Neurosci,* 15**,** 6077-84.

VAN DEN BRINK, S. C., BAILLIE-JOHNSON, P., BALAYO, T., HADJANTONAKIS, A. K., NOWOTSCHIN, S., TURNER, D. A. & MARTINEZ ARIAS, A. 2014. Symmetry breaking, germ layer specification and axial organisation in aggregates of mouse embryonic stem cells. *Development,* 141**,** 4231-42.

VASQUEZ, R. J., HOWELL, B., YVON, A. M., WADSWORTH, P. & CASSIMERIS, L. 1997. Nanomolar concentrations of nocodazole alter microtubule dynamic instability in vivo and in vitro. *Mol Biol Cell,* 8**,** 973-85.

VERCAUTEREN, D., VANDENBROUCKE, R. E., JONES, A. T., REJMAN, J., DEMEESTER, J., DE SMEDT, S. C., SANDERS, N. N. & BRAECKMANS, K. 2010. The use of inhibitors to study endocytic pathways of gene carriers: optimization and pitfalls. *Mol Ther,* 18**,** 561-9.

VON KLEIST, L., STAHLSCHMIDT, W., BULUT, H., GROMOVA, K., PUCHKOV, D., ROBERTSON, M. J., MACGREGOR, K. A., TOMILIN, N., PECHSTEIN, A., CHAU, N., CHIRCOP, M., SAKOFF, J., VON KRIES, J. P., SAENGER, W., KRAUSSLICH, H. G., SHUPLIAKOV, O., ROBINSON, P. J., MCCLUSKEY, A. & HAUCKE, V. 2011. Role of the clathrin terminal domain in regulating coated pit dynamics revealed by small molecule inhibition. *Cell,* 146**,** 471-84.

WANG, L. H., ROTHBERG, K. G. & ANDERSON, R. G. 1993. Mis-assembly of clathrin lattices on endosomes reveals a regulatory switch for coated pit formation. *J Cell Biol,* 123**,** 1107-17.

WANG, R. N., GREEN, J., WANG, Z., DENG, Y., QIAO, M., PEABODY, M., ZHANG, Q., YE, J., YAN, Z., DENDULURI, S., IDOWU, O., LI, M., SHEN, C., HU, A., HAYDON, R. C., KANG, R., MOK, J., LEE, M. J., LUU, H. L. & SHI, L. L. 2014. Bone Morphogenetic Protein (BMP) signaling in development and human diseases. *Genes Dis,* 1**,** 87-105.

WANG, Y. C. & FERGUSON, E. L. 2005. Spatial bistability of Dpp-receptor interactions during Drosophila dorsal-ventral patterning. *Nature,* 434**,** 229-34.

WARTLICK, O., JULICHER, F. & GONZALEZ-GAITAN, M. 2014. Growth control by a moving morphogen gradient during Drosophila eye development. *Development,* 141**,** 1884-93.

WARTLICK, O., KICHEVA, A. & GONZALEZ-GAITAN, M. 2009. Morphogen gradient formation. *Cold Spring Harb Perspect Biol,* 1**,** a001255.

WHITE, R. J., NIE, Q., LANDER, A. D. & SCHILLING, T. F. 2007. Complex regulation of cyp26a1 creates a robust retinoic acid gradient in the zebrafish embryo. *PLoS Biol,* 5**,** e304.

WILLOX, A. K., SAHRAOUI, Y. M. & ROYLE, S. J. 2014. Non-specificity of Pitstop 2 in clathrin-mediated endocytosis. *Biol Open,* 3**,** 326-31.

WILSON, P. A., LAGNA, G., SUZUKI, A. & HEMMATI-BRIVANLOU, A. 1997. Concentration-dependent patterning of the Xenopus ectoderm by BMP4 and its signal transducer Smad1. *Development,* 124**,** 3177-84.

WITTE, L., LINNEMANNSTONS, K., SCHMIDT, K., HONEMANN-CAPITO, M., GRAWE, F., WODARZ, A. & GROSS, J. C. 2020. The kinesin motor Klp98A mediates apical to basal Wg transport. *Development,* 147.

WOLPERT, L. 1969. Positional information and the spatial pattern of cellular differentiation. *J Theor Biol,* 25**,** 1-47.

WOLPERT, L. 1971. Positional information and pattern formation. *Curr Top Dev Biol,* 6**,** 183-224.

WOLPERT, L. 1986. Citation-Classic - Positional Information and the Spatial Pattern of Cellular-Differentiation. *Current Contents/Life Sciences***,** 19-19.

WU, M. Y. & HILL, C. S. 2009. Tgf-beta superfamily signaling in embryonic development and homeostasis. *Dev Cell,* 16**,** 329-43.

XUE, X., SUN, Y., RESTO-IRIZARRY, A. M., YUAN, Y., AW YONG, K. M., ZHENG, Y., WENG, S., SHAO, Y., CHAI, Y., STUDER, L. & FU, J. 2018. Mechanics-guided embryonic patterning of neuroectoderm tissue from human pluripotent stem cells. *Nat Mater,* 17**,** 633-641.

YAMAZAKI, Y., PALMER, L., ALEXANDRE, C., KAKUGAWA, S., BECKETT, K., GAUGUE, I., PALMER, R. H. & VINCENT, J. P. 2016. Godzilla-dependent transcytosis promotes Wingless signalling in Drosophila wing imaginal discs. *Nat Cell Biol,* 18**,** 451-7.

YAN, D. & LIN, X. 2009. Shaping morphogen gradients by proteoglycans. *Cold Spring Harb Perspect Biol,* 1**,** a002493.

YAO, C. K., LIU, Y. T., LEE, I. C., WANG, Y. T. & WU, P. Y. 2017. A Ca2+ channel differentially regulates Clathrin-mediated and activity-dependent bulk endocytosis. *PLoS Biol,* 15**,** e2000931.

YBOT-GONZALEZ, P., SAVERY, D., GERRELLI, D., SIGNORE, M., MITCHELL, C. E., FAUX, C. H., GREENE, N. D. & COPP, A. J. 2007. Convergent extension, planar-cell-polarity signalling and initiation of mouse neural tube closure. *Development,* 134**,** 789-99.

YONEY, A., ETOC, F., RUZO, A., CARROLL, T., METZGER, J. J., MARTYN, I., LI, S., KIRST, C., SIGGIA, E. D. & BRIVANLOU, A. H. 2018. WNT signaling memory is required for ACTIVIN to function as a morphogen in human gastruloids. *Elife,* 7.

ZECCA, M., BASLER, K. & STRUHL, G. 1996. Direct and long-range action of a wingless morphogen gradient. *Cell,* 87**,** 833-44.

ZHANG, Z., ZWICK, S., LOEW, E., GRIMLEY, J. S. & RAMANATHAN, S. 2019. Mouse embryo geometry drives formation of robust signaling gradients through receptor localization. *Nat Commun,* 10**,** 4516.

ZHENG, Y., XUE, X., SHAO, Y., WANG, S., ESFAHANI, S. N., LI, Z., MUNCIE, J. M., LAKINS, J. N., WEAVER, V. M., GUMUCIO, D. L. & FU, J. 2019. Controlled modelling of human epiblast and amnion development using stem cells. *Nature,* 573**,** 421-425.

ZHOU, S., LO, W. C., SUHALIM, J. L., DIGMAN, M. A., GRATTON, E., NIE, Q. & LANDER, A. D. 2012. Free extracellular diffusion creates the Dpp morphogen gradient of the Drosophila wing disc. *Curr Biol,* 22**,** 668-75.

ZIMMERMAN, L. B., DE JESUS-ESCOBAR, J. M. & HARLAND, R. M. 1996. The Spemann organizer signal noggin binds and inactivates bone morphogenetic protein 4. *Cell,* 86**,** 599-606.